LEVEL

OFFICE OF NAVAL RESEARCH

Contract N00014-75C-0953

Task No. NR 359-451

TECHNICAL REPORT NO. 51

LEED-Auger-Thin-Layer Electrochemical Studies

of the Underpotential Deposition of Lead

onto Gold Single Crystals

by

P. Hagans, A. Homa, W. O'Grady and E. Yeager

Prepared as part of the Ph.D. thesis of P. L. Hagans
in Chemistry at Case Western Reserve University
January 1980

Case Laboratories for Electrochemical Studies
and the Chemistry Department
Case Western Reserve University
Cleveland, Ohio   44106

December 15, 1979

80   4   7   128

REPORT DOCUMENTATION PAGE	READ INSTRUCTIONS BEFORE COMPLETING FORM

1. REPORT NUMBER	2. GOVT ACCESSION NO.	3. RECIPIENT'S CATALOG NUMBER
TR-51		

4. TITLE (and Subtitle)	5. TYPE OF REPORT & PERIOD COVERED
Leed-Auger-Thin-Layer Electrochemical Studies of the Underpotential Deposition of Lead onto Gold Single Crystals	Technical Report, #51
	6. PERFORMING ORG. REPORT NUMBER

7. AUTHOR(s)	8. CONTRACT OR GRANT NUMBER(s)
C. S. Hagans, A. Homa, W. O'Grady and E. Yeager	N00014-75C-0953

9. PERFORMING ORGANIZATION NAME AND ADDRESS	10. PROGRAM ELEMENT, PROJECT, TASK AREA & WORK UNIT NUMBERS
Dept. of Chemistry Case Western Reserve University Cleveland, Ohio 44106	NR 359-451

11. CONTROLLING OFFICE NAME AND ADDRESS	12. REPORT DATE
Office of Naval Research Chemistry Program - Chemistry Code 472 Arlington, Virginia 22217	December 15, 1979
	13. NUMBER OF PAGES
	169

14. MONITORING AGENCY NAME & ADDRESS(if different from Controlling Office)	15. SECURITY CLASS. (of this report)
	Unclassified
	15a. DECLASSIFICATION/DOWNGRADING SCHEDULE

16. DISTRIBUTION STATEMENT (of this Report)

This document has been approved for public release and sale; its distribution unlimited.

17. DISTRIBUTION STATEMENT (of the abstract entered in Block 20, if different from Report)

18. SUPPLEMENTARY NOTES

19. KEY WORDS (Continue on reverse side if necessary and identify by block number)

Underpotential deposition, lead on gold, single crystal electrochemical studies, thin layer cell electrochemistry, LEED and Auger spectroscopy

20. ABSTRACT (Continue on reverse side if necessary and identify by block number)

The underpotential deposition of lead onto very clean and well-ordered single crystal Au samples was studied with linear sweep voltammetry. The single crystal surfaces examined were (100), (110), (111) and (410). The (410) surface is a stepped surface with terraces of (100) orientation four atomic rows in width separated by steps of (100) orientation of monatomic height. The crystals were prepared in an ultra-high vacuum environment ($\sim 10^{-11}$ Torr) by alternate cycles of argon-ion sputtering and annealing until the surfaces were clean within the limits of AES (Auger electron spectroscopy). The surfaces were also examined

DD FORM 1473   EDITION OF 1 NOV 65 IS OBSOLETE
1 JAN 73

S/N 0102-LF-014-6601

Continuation of Block 20 of Report Documentation Page, <u>Abstract</u>

with LEED (low energy electron diffraction) to insure that the clean crystals
gave the expected diffraction pattern. Through use of specially designed transfer
systems the crystals were transferred to a second ultra-high vacuum chamber
and situated above a third chamber capable of high vacuum which contained the
lead counter-reference electrode and solution delivery system. Both of these
chambers were then back-filled to atmospheric pressure with ultra-pure argon.
A drop of electrolyte was placed on the Pb electrode and the electrode was
raised up until formation of the thin-layer cell with a given Au single crystal
was accomplished. Following the voltammetry the crystals were transferred
after pump-down back to the LEED/AES chamber and re-examined with these techniques.

Each of the four gold single crystal surfaces produced a very characteristic
voltammetry curve. The curve for (110) resembled closely that for well-cycled
polycrystalline gold suggesting that the polycrystalline sample was mainly
(110)-like in surface structure. The voltammetry curve for the (100) surface
showed several large, sharp deposition peaks at slow scan rate which represented
both reversible and irreversible processes. The initial large, irreversible
deposition peak was assigned to a process involving the transition of the
reconstructed (5x20) surface to the normal (1x1) surface. Evidence was found
indicating that the sharp, reversible voltammetry peaks found on both the
(100) and (110) surfaces were due to a phase transition which involves the
formation of islands of Pb of metallic-like character from initially adsorbed
Pb in mainly ionic form. The same interpretation has previously been used
to explain the sharp, reversible peaks for polycrystalline Au. The (410)
surface exhibited only broad voltammetry peaks since phase transition and
surface reconstruction phenomena are greatly hindered on this surface due to
the introduction of steps. The (111) surface exhibited sharp, irreversible
voltammetry peak structure. Nearly all of the adsorption and desorption
occurred in a very narrow voltage window (~70 mV). Evidence indicates that
a condensation type of process is occurring on this surface where growth
centers for nucleation are formed from the very small amount initially adsorbed.

TABLE OF CONTENTS

LIST OF TABLES

Accession For

NTIS GRA&I

DDC TAB

Unannounced

Justification

By

Distribution/

Availability Codes

Dist | Avail and/or special

vi

LIST OF FIGURES

LEED-AUGER-THIN-LAYER ELECTROCHEMICAL STUDIES
OF THE UNDERPOTENTIAL DEPOSITION OF LEAD
ONTO GOLD SINGLE CRYSTALS

Abstract

by

PATRICK LEE HAGANS

The underpotential deposition of lead onto very clean and
well-ordered single crystal Au samples was studied with linear
sweep voltammetry. The single crystal surfaces examined were
(100), (110), (111) and (410). The (410) surface is a stepped
surface with terraces of (100) orientation four atomic rows in
width separated by steps of (100) orientation of monatomic height.
The crystals were prepared in an ultra-high vacuum environment
($\sim 10^{-11}$ Torr) by alternate cycles of argon-ion sputtering and
annealing until the surfaces were clean within the limits of AES
(Auger electron spectroscopy). The surfaces were also examined
with LEED (low energy electron diffraction) to insure that the
clean crystals gave the expected diffraction pattern. Through
use of specially designed transfer systems the crystals were
transferred to a second ultra-high vacuum chamber and situated
above a third chamber capable of high vacuum which contained the
lead counter-reference electrode and solution delivery system.
Both of these chambers were then back-filled to atmospheric pressure
with ultra-pure argon. A drop of electrolyte was placed on the

Pb electrode and the electrode was raised up until formation of the thin-layer cell with a given Au single crystal was accomplished. Following the voltammetry the crystals were transferred after pump-down back to the LEED/AES chamber and re-examined with these techniques.

Each of the four gold single crystal surfaces produced a very characteristic voltammetry curve. The curve for (110) resembled closely that for well-cycled polycrystalline gold suggesting that the polycrystalline sample was mainly (110)- like in surface structure. The voltammetry curve for the (100) surface showed several large, sharp deposition peaks at slow scan rate which represented both reversible and irreversible processes. The initial large, irreversible deposition peak was assigned to a process involving the transition of the reconstructed (5x20) surface to the normal (1x1) surface. Evidence was found indicating that the sharp, reversible voltammetry peaks found on both the (100) and (110) surfaces were due to a phase transition which involves the formation of islands of Pb of metallic-like character from initially adsorbed Pb in mainly ionic form. The same interpretation has previously been used to explain the sharp, reversible peaks for polycrystalline Au. The (410) surface exhibited only broad voltammetry peaks since phase transition and surface reconstruction phenomena are greatly hindered on this surface due to the introduction of steps. The (111) surface exhibited sharp, irreversible voltammetry peak structure. Nearly all of the adsorption and desorption occurred in a very

narrow voltage window ($\sim$70 mV). Evidence indicates that a condensation type of process is occurring on this surface where growth centers for nucleation are formed from the very small amount of initially adsorbed.

CHAPTER 1

INTRODUCTION

Mono-and submonolayer amounts of lead can be electrosorbed
onto gold at potentials quite *anodic* (*positive*) to the reversi-
ble potential of bulk lead. These underpotentially deposited
lead layers exhibit a complicated adsorption isotherm as is indi-
cated by the multiple peak structure found in the corresponding
linear sweep voltammetry curve for a polycrystalline gold sub-
strate. Two possible interpretations are used to explain the
shapes and positions of the voltammetry peaks: a smoothly vary-
ing adsorption process where the lead is nearly totally discharged
when it is adsorbed on the gold surface or a two-step process
where the lead is only partially discharged in an initial adsorp-
tion step followed by a phase transition and complete discharge
of the initially adsorbed lead in a later step. These explanations
are often used for many adsorbate/substrate combinations other
than Pb^{2+}/Au. In attempts to understand better the adsorption
process on gold and other polycrystalline substrates, various
laboratories have been studying the effects of using low index,
single crystal substrates. Although these studies have proven
interesting, they as well as those using polycrystalline elect-
rodes, suffer from the effects of potential cycling. In order to
remove impurities from the electrode surface the potential is

-1-

swept progressively anodic until the substrate itself is oxidized and, in the return sweep, reduced. Oxidation and removal of impurities most likely causes the surface to reconstruct which in turn will affect the adsorption isotherm. Since, for the case of single crystal studies, direct examination of the electrode surface structure before and after the electrochemical experiment has not generally been performed, the validity of results obtained must be in question.

In the present work, this problem is alleviated by using ultra-high vacuum, surface sensitive techniques to monitor the composition and orientation of the single crystal electrode. Auger electron spectroscopy (AES) is used to monitor surface composition while low energy electron diffraction (LEED) provides surface structure information. Gold was the chosen substrate, lead the adsorbate. The Au single crystal is cleaned in ultra-high vacuum by alternate cycles of argon-ion sputtering and annealing until the crystal is designated clean by AES and produces the expected LEED diffraction pattern. A specially developed transfer system positions the crystal in the electrochemical cell where linear sweep voltammetry studies are performed. Potential cycling for purposes of removing impurities is eliminated by this procedure making the study of the electrosorption of lead possible for the first time on clean, well-ordered gold single crystals.

Equally as important, changes in the electrode surface structure due to electrochemical treatment can be directly examined with LEED by transfering the crystal back into the ultra-high vacuum environment. LEED patterns obtained as a function of potential at which the gold electrode was removed from the cell should then provide information about the mechanism of lead deposition in the underpotential region.

CHAPTER 2

BACKGROUND ON UPD

Underpotential deposition (UPD) is defined as the deposition of submonolayer and monolayer amounts of a metal on a foreign metal substrate at potentials positive (anodic) to where bulk deposition occurs. The bulk deposition potential corresponds to the reversible Nernst potential given by the Nernst equation:

$$E = E^O + \frac{RT}{zF} \ln a_{M^{z+}} \tag{2-1}$$

for the reaction

$$M^{z+} + ze^- \rightleftharpoons M$$

where E is the electrode potential, E^O the potential at a metal ion activity ($a_{M^{z+}} = 1$) and metal ($a_M = 1$) and R,T, and F are the gas constant, absolute temperature, and Faraday constant, respectively. As will be shown later the Nernst equation must be modified in order to describe the deposition of the first layer onto a foreign substrate.

To date, most UPD studies have been conducted using one electrochemical technique, linear sweep voltammetry. Both faradaic and non-faradaic currents are reflected in the i-E voltammetry curves. A typical curve involving UPD is shown in Figure 2l. The non-faradaic current, due to double layer charging, is superimposed on the faradaic current and is usually assumed to be constant.

-4-
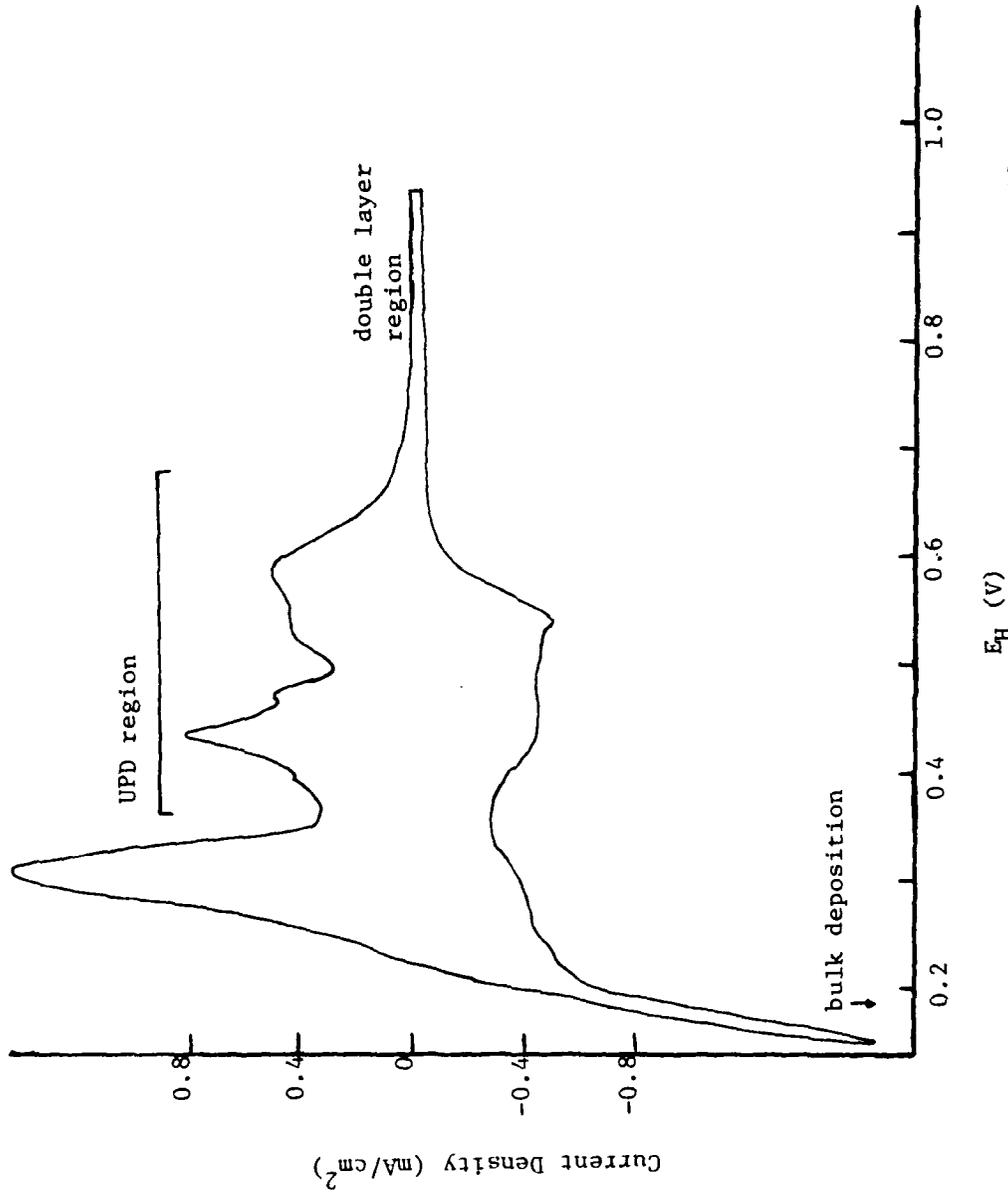
Figure 2.1 Voltammogram for the UPD of Bi onto Au from 2M $HClO_4$ + 2mM Bi^{+3}. Sweep rate: 80 mV/s. Taken from reference (105).

Ordinarily, the amount of metal deposited can be determined from the area under the voltammetry peak. With UPD, however, the species in the mono-and submonolayer can still retain substantial net charge and hence the surface coverage cannot be evaluated in this manner. The dependence of peak potential and shape on sweep rate can provide kinetic information.

There are an extremely large number of papers in the literature describing work on nearly forty different UPD metal/substrate combinations. Four areas have been chosen for review which are now at the forefront of research in the UPD area. Most of the impetus for this work has been the desire for wanting to know details about the nature of the interaction of the metal ion with the metal electrode and what changes occur in this initially adsorbed layer as the potential approaches the Nernst value. Following this discussion, the Pb^{2+}/Au system which was chosen for this work will be reviewed in detail.

2.1 Work Function Correlation

In an effort to obtain some type of macroscopic quantitatative description that would encompass all of the different UPD metal/ substrate combinations in aqueous and nonaqueous solvents Kolb, Przasnyski and Gerisher (1,2) developed a correlation between two parameters: ΔE_p, the peak potential difference between the monolayer stripping peak and the bulk stripping peak obtained with voltammetry and, $\Delta\Phi$, the work function difference between the substrate and adsorbate. When the stripping curve exhibits more than

one peak the peak potential of the more anodic peak is used. The
stripping peak potential chosen for the correlation is indicative
of nearly the same amount of coverage for all the systems studied.

The fact that the UPD phenomena exists indicates that the
chemical potential of the underpotentially deposited layer (μ_{ad})
is different from that of the corresponding bulk metal (μ_{metal}).
This difference in the chemical potential can be obtained from the
following equilibria:

$$Me^{z+}_{solv} + ze^{-}_{metal} \rightleftarrows Me_{metal} \qquad (2\text{-}2)$$

$$Me^{z+}_{solv} + ze^{-}_{substrate} \rightleftarrows Me_{ad} \qquad (2\text{-}3)$$
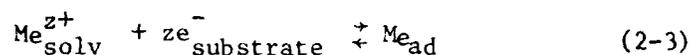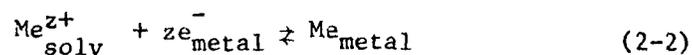
where

$$\bar{\mu}_{Me^{z+}_{solv}} + z\bar{\mu}_{e_{metal}} = \mu_{metal} \qquad (2\text{-}4)$$

$$\bar{\mu}_{Me^{z+}_{solv}} + z\bar{\mu}_{e_{substrate}} = \mu_{ad} \qquad (2\text{-}5)$$

The $\bar{\mu}$'s are the electrochemical potentials defined as $\mu + ze_o\phi$ where
e_o is the electronic charge and ϕ is the inner potential of an ad-
sorbed phase. Comparison of the two equilibria in the same solution
(i.e., equal Me^{z+}_{solv}) yields

$$\mu_{metal} - \mu_{ad} = z \cdot e_o \cdot \Delta E_p \qquad (2\text{-}6)$$

The difference in the chemical potentials of the UPD adsorbed species
and the corresponding bulk metal is a measure of the binding energy
between the adsorbed species and the substrate. Therefore ΔE_p is

also a measure of this binding energy.

The second parameter, $\Delta\Phi$, the difference in work function between the adsorbate and substrate was chosen from consideration that when the metal adatom first becomes adsorbed it probably is only partially discharged. This ionic character imparted to the adatom-substrate bond permits a property such as electronegativity difference as an excellent choice for representing the nature of this interaction. However, from the Mulliken relation (3) for absolute electronegativity

$$\chi_M = \frac{1}{2}(I_A + E_A) \simeq \Phi \qquad (2-7)$$

where I_A and E_A are ionization potential and electron affinity, respectively.

A plot of ΔE_p (in volts) versus $\Delta\Phi$ (in eV) for 21 couples in both aqueous and nonaqueous solutions produced a quite satisfactory linear relationship. Since then more couples have been added (4). The line can be described by the equation $\Delta E_p = 0.5\Delta\Phi$. Three couples, Hg^{2+}/Au, Ag^+/Au and Tl^+/Au were found to deviate quite strongly from the straight line. Kolb et al. have proposed that these differences may be due to specific interactions.

The correlation provides one with a sense, at least qualitatively, of what is occurring during UPD. Microscopically, however, questions such as what is the nature of the interaction of the adatom with the substrate, what is the effect of substrate structure, and what part do the solvent interactions with the surface play still remain unanswered. Further work has been per-

formed to try and quantify the actual amount of charge transferred
during the UPD process. This will be discussed next.

2.2 Electrosorption Valency

The concept of electrosorption valency as first developed
by Vetter and Schultze (5,6) proceeds by representing the electro-
sorption reaction by the following equation

$$S^z_{aq} + \nu M\text{-}OH_2 \rightleftarrows M_\nu\text{-}S^{z+\lambda} + \nu H_2O + \lambda e^-_m \qquad (2\text{-}8)$$
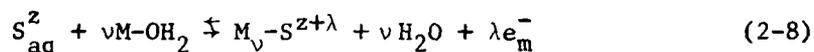
In this reaction scheme a substance S with charge z is specifically
adsorbed on the electrode surface site, M, which is accompanied
by the loss of ν H_2O molecules and a partial charge transfer of λ
electrons. The partial charge transfer coefficient λ is defined by

$$\lambda = z_{ad} - z \qquad (2\text{-}9)$$

where z_{ad} is the actual charge of the adsorbed species with ionic
charge z. A schematic diagram depicting the solution/electrode
interface before and after the establishment of the electrosorption
process for a cation as indicated in equation 2-8 is shown in
figure 2.2. The potential gradient between the electrode surface
and the outer (Helmholtz) layer is shown in the potential distance
plots for each case. The shift of this gradient to larger distances
from the electrode surface is seen to occur in the case of cation
specific adsorption when the conduction band electrons of the metal
interact strongly with the adsorbed cation, compensating its charge.
The potential drop across the diffuse layer $(\phi_h-\phi_e)$ is small since
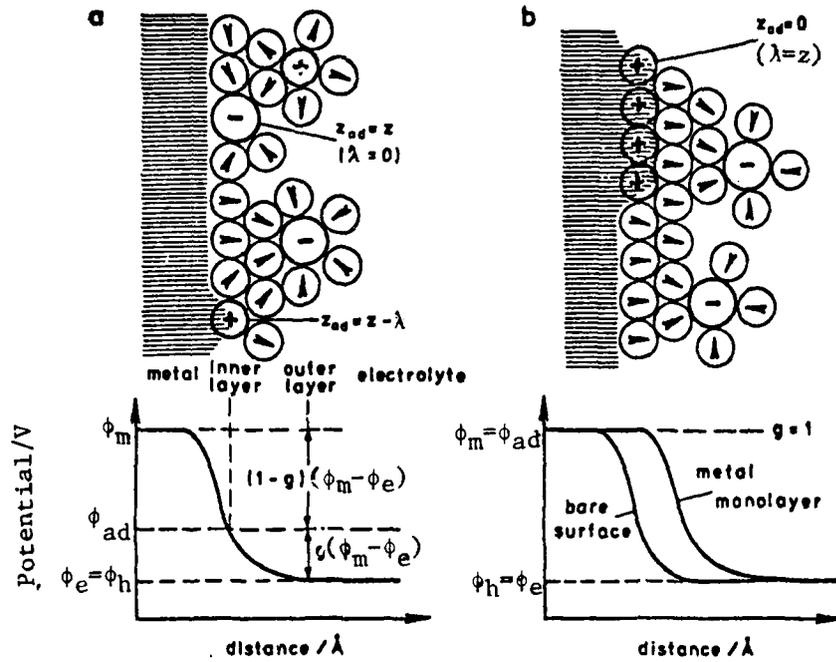
Figure 2.2   Schematic diagram of the double-layer and
corresponding potential distribution in the
presence of a supporting electrolyte: (a)
partially discharged cation and electro-
statically adsorbed anion; (b) completely
discharged cations. Taken from reference
(4).

only the situation involving a high concentration of a supporting

electrolyte is considered. The potential drop between the metal

and bulk electrolyte, $\Delta\phi$, may be expressed as

$$\Delta\phi = \phi_m - \phi_h - \Delta\phi_{pzc} = E - E_{pzc} - \psi_d \qquad (2-10)$$

where $\phi_m - \phi_h$ is the potential difference between the metal and out-

er Helmholtz plane, $\Delta\phi_{pzc}$ is this same difference when the electrode

potential corresponds to E_{pzc} , the potential of zero charge without

specific ionic adsorption and $\psi_d = \phi_h - \phi_e$. With a large concentra-

tion of supporting electrolyte $\psi_d \simeq 0$ and

$$\Delta\phi \simeq E - E_{pzc} \qquad (2-11)$$

To describe the potential dependence of the electrosorption equil-

ibrium Vetter and Schultze have introduced the concept of electro-

sorption valency, γ , defined by

$$\left(\frac{\partial \mu_s}{\partial E}\right)_{\Gamma_{ad}} = \gamma F \qquad (2-12)$$

which for a large concentration of supporting electrolyte becomes

$$\left(\frac{\partial \mu_s}{\partial E}\right)_{\Gamma_{ad}} = \gamma F \qquad (2-13)$$

where μ_s is the chemical potential of S^z in the electrolyte, Γ_{ad}

is the surface excess concentration of the adsorbate and F is the

Faraday. This equation is analogous to that obtained from perform-

---

[1] The pzc is defined as the potential at which the charge on the
electrode surface, q_m , is zero.

ing the above differentiation on the Nernst equation except that γ is replaced by the Nernst valency ν_i/n where ν_i corresponds to the stoichiometric coefficient in the electrode reaction; i.e.,

$$\Sigma \ \nu_i \ S_j + n \ e^- = 0 \qquad (2\text{-}14)$$

The difference between the two is that the Nernst valency is always the ratio of integral values while γ is not so restricted and is dependent on z and λ and other terms to be discussed shortly.

The electrosorption valency can also be used to describe the charge, q_m, transferred through the external circuit to the electrode through use of the equation

$$-\gamma \ F = \left(\frac{\partial q_m}{\partial \Gamma_{ad}} \right)_{\Delta\phi} \approx \left(\frac{\partial q_m}{\partial \Gamma_{ad}} \right)_E \qquad (2\text{-}15)$$

when there is a large concentration of supporting electrolyte. Combining this equation with the adsorption rate, $\upsilon_{ad} = \left(\dfrac{\partial \Gamma_{ad}}{\partial t} \right)_{\Delta\phi}$

and the electrosorption current density, $i = \left(\dfrac{\partial q_m}{\partial t} \right)_{\Delta\phi}$ yields for i the equation

$$i = \left(\frac{\partial q_m}{\partial \Gamma_{ad}} \right)_{\Delta\phi} \left(\frac{\partial \Gamma_{ad}}{\partial t} \right)_{\Delta\phi} = -\gamma \ F \ \upsilon_{ad} \qquad (2\text{-}16)$$

A more sophisticated treatment of the electrosorption process yields (5)

$$\gamma = \gamma_{pzc} - \frac{1}{F} \int_{E_{pzc}}^{E} \left(\frac{\partial C_D}{\partial \Gamma_{ad}} \right)_E \ dE \qquad (2\text{-}17)$$

where the last term describes the change of the double layer cap-

city, (i.e., the capacity $C_D = (\partial qm / \partial \Delta \phi)_{\text{ad}}$, of the outer Helmholtz layer) during electrosorption and γ_{pzc} is γ at the pzc, as given by

$$\gamma_{pzc} = zg - \lambda (1-g) + \kappa_{ad} - \nu \kappa_w \qquad (2-18)$$

The geometrical factor, g, is defined by the equation (see Fig. 2-2)

$$g = \frac{\phi_{ad} - \phi_e}{\phi_m - \phi_e} \qquad (2-19)$$

and is used to describe the geometric position of the adsorbate in the double layer. κ_{ad} and κ_w are dipole energy terms of the adsorbate and water and ν is the number of water molecules displaced by the adsorption of one molecule or atom of adsorbate. If one assumes that a displaced water molecule will re-adsorb onto the foreign monolayer in the same way that it adsorbed onto the substrate then $\nu = 0$. The dipole terms are given by the general equation

$$\kappa_i = \pm \frac{m_i}{e_o \, l_i} \qquad (2-20)$$

where m_i is the dipole moment, e_o is the unit charge, and $l_i = (\phi_m - \phi_e) / (d\phi / dx)$ is the electric field strength at the double layer. $(d\phi/dx)$ is the electric field strength at the adsorption site. Generally the last two terms in equation 2-18 are small in comparison to the charge terms and

$$\gamma_{pzc} \simeq zg - \gamma (1-g) \qquad (2-21)$$

Equations 2-18 or 2-21 cannot be used to obtain γ or γ_{pzc}

since there is no experiment that can determine g, λ or the κ terms.
However, γ can be determined experimentally through use of three
types of methods[1]. The first relies on determining γ from equation
2-15 by measuring the charge flow during the electrosorption pro-
cess. Experiments of special note which determine charge flow are
the thin-layer method of Schmidt and Gygax (Tl$^+$ on Cu, Ag, Au) (8,9)
the rotating ring-disk method of Bruekenstein et al. (Cu^{2+}/Pt, Ag$^+$/
Au, Ag$^+$/Pt) (10,11), measurements of Schultze with large surface
areas (Cu^{2+}/Pt) (12) where the uptake of the adsorbed species can
be measured analytically, and the specular reflectance-potential
step method of Adzic et al. (13).

The second approach involves determining γ from the potential
dependence of the adsorption isotherm using equation 2-13. Tech-
niques used to obtain the adsoption isotherms include the coulomet-
ric measurements of Schultze (Cu^{2+}/Pt) (12) and the radio-tracer
measurements of Bowles (Tl$^+$/Pt) (14). Also, Schultze (7) has made
use of previously published adsorption isotherms $\Gamma_{ad} = f\ (\epsilon,\ \mu_\epsilon)$

The third method relies on kinetic measurements and the re-
lation

$$(\alpha + \beta)\ z = \gamma \qquad (2\text{-}22)$$

to obtain γ. Here α and β are the electrochemical transfer coef-

---

[1] An excellent summary of all of the different types of experiments
encompassed in these methods is given in references 6 and 7. Only
a few will be cited here.

ficients for the adsorption and desorption processes[1]. The gal-
vanostatic method of Schultze (Cu^{2+}/Pt) (12) and the impedance
method of Lorenz and Salie (Tl^{+}/Tl) (15) utilized this relation-
ship.

A compilation of the γ_{pzc} value for over 50 specifically
adsorbed species-substrate combinations is given by Schultze and
Koppitz (7). In general for cation adsorption the γ_{pzc} values are
very close to the z- value for each ion. Exceptions to this exist
for the adsorption of various alkali metal ions on Hg, Ga and Bi
where the γ_{pzc} values are much lower than +1. For anion adsorp-
tion the γ_{pzc} values are for the most part considerably lower
than the corresponding z values. Only for several systems has

the electrosorption valency been determined as a function of
coverage. These include Br^{-}/Au (13), Cu^{2+}/Pt (12) and Ag^{+}/Au
and Ag^{+}/Pt (11).

2.3 Adsorption Isotherms

When the adsorption involves a single type of site and is
nearly ideal (Langmuir behavior) the rate equations for the forward

---

[1] The transfer coefficients, α and β, are empirical parameters de-
fined by the equations

$$\alpha = \frac{RT}{F} \left(\frac{\partial \ln \vec{\upsilon}}{\partial E} \right)_{\mu} \tag{2-23}$$

$$\beta = \frac{RT}{F} \left(\frac{\partial \ln \overleftarrow{\upsilon}}{\partial E} \right)_{\mu} \tag{2-24}$$

where $\vec{\upsilon}$ and $\overleftarrow{\upsilon}$ are the rates of adsorption and desorption, respect-
ively.

and reverse reactions are

$$\overrightarrow{i} = k_1 \, C_{S^z} \, (1-\theta) \, \exp \frac{\alpha z F \Delta \phi}{RT} \qquad (2\text{-}25)$$

$$\overleftarrow{i} = k_{-1} \, \theta \, \exp - \frac{\beta z F \Delta \phi}{RT} \qquad (2\text{-}26)$$

where k_1 and k_{-1} are the rate constants for the forward and reverse
steps, respectively, z is the formal charge of the ionic speices,
and C_{S^z} is the concentration of S^z in the solution. The fraction-
al coverage θ of the surface by the adsorbate is proportional to
the surface concentration, Γ_{ad} provided the contribution to Γ_{ad}
from the non-specifically adsorbed species in the outer Helmholtz
and diffuse layer is negligible. This is a good approximation
with a large excess of non-specifically adsorbed supporting elect-
rolyte. The term $(1-\theta)$ is proportional to the concentration of
free sites left on the surface. If the system is at equilibrium
$\overrightarrow{i} = \overleftarrow{i}$ and

$$\frac{\theta}{1-\theta} = K \, C_{S^z} \, \exp \frac{(\alpha+\beta)zF\Delta\phi}{RT} \qquad (2\text{-}27)$$

where $K = {}^{k_1}/{}_{k_{-1}}$. According to equation 2-22, the $(\alpha+\beta)z$ term in
the exponent can be replaced with γ. The above equation relating
the potential difference $\Delta\phi$ to the fractional surface coverage θ
corresponds to the Langmuir adsorption isotherm modified for the
special case of adsorption accompanied by charge transfer. This
equation is only applicable for low or high coverages ($\theta < 0.2$ or
> 0.8) where the interaction of adsorbed species on the electrode
surface can be considered negligible for low coverage or has ap-

proached a constant value for high coverages.

For the case where interaction between adsorbed species cannot be considered negligible, the equilibrium constant, K, is assumed to decrease exponentially with increasing coverage

$$K = K^O \exp\left(-\frac{r\Theta}{RT}\right) \qquad (2\text{-}28)$$

where r is known as the interaction parameter and is found to experimentally vary, depending on the adsorption process, from +5 to -5. Substitution of equation (2-28) into equation (2-27) yields

$$\frac{\Theta}{1-\Theta} \exp\left(\frac{r\Theta}{RT}\right) = K^O \ C_S z \ \exp\frac{(\alpha+\beta)z \ F\Delta\phi}{RT} \qquad (2\text{-}29)$$

This equation corresponds to the Frumkin adsorption equation with $(\alpha+\beta)z=z$. Frumkin differed from Schultze and Vetter in that he did not introduce the electrosorption valence into the adsorption isotherm. The Langmuir isotherm is a special case of the Frumkin isotherm for r=0.

Another special case is the Temkin isotherm valid for intermediate coverages, $0.2 < \Theta < 0.8$. It is arrived at by assuming that the exponential term $\frac{r\Theta}{RT}$ predominates and that the $\frac{\Theta}{1-\Theta}$ term is approximately unity. Taking the logarithm of each side of equation (2-29) with this assumption yields the Temkin isotherm plus a potential term

$$\Theta = \frac{1}{r} \ (R \ T -\ln K^O \ C_S z + (\alpha+\beta)z \ F\Delta\phi \qquad (2\text{-}30)$$

Here the coverage Θ varies directly with the potential $\Delta\phi$ and

logarithimetically with concentration C of the adsorbate S_z.

Several techniques have been employed for measuring adsorption isotherms for the UPD process. Most workers have measured the charge passed to reach a certain state of coverage and thus assumed that this charge was directly proportional to coverage. This, however, is not necessarily a safe assumption: the electrosorption valence is not generally independent of coverage. Further, there is the problem of a priori separation of the charge involved in the UPD layer formation from the overall double layer charging in methods involving potential steps or sweeps. A further complication is that the number of sites and the saturation coverage are usually not known experimentally and cannot be calculated theoretically for polycrystalline electrodes even with a given model for the adsorption.

The most commonly used technique is linear sweep voltammetry where an estimate of the charge is determined by direct integration of the current-potential profiles. This charge, however, is the sum of charges for two or more processes. There is the faradaic contribution which is due to the UPD process and any other faradaic process (alloying, O_2 and H_2 adsorption, etc.) which may be occuring simultaneously. Superimposed on this is the non-faradaic component due to charging of the double layer. To insure that the only faradaic process occuring is UPD the voltage limits for the voltammetry are set carefully for each system so that excursions

into regions where unwanted side-reactions occur is avoided. The
double layer charge is estimated from the current flowing in either
a blank run without the UPD species present or from the double
layer region of the voltammetry curve anodic to the UPD potential
region. This approach assumes that the double layer capacitance
is constant with respect to potential over the UPD range - often
a questionable assumption.

Along with measurement of charge voltammetry also provides
some qualitative insights into the adsorption process. The width
at half height,δ, of the UPD peaks found in the current-voltage
profile, indicates whether there is a strong interaction between
the adsorbate atoms on the surface. Generally a half-width of
approximately 90 mV/z is found for the case of Langmuir adsorption.
Peaks with much larger half-widths ($r > 0$ in equation 2-29) in-
dicate there is a repulsion among adsorbate atoms while much lower
half-widths ($r < 0$) show that there is a net attraction. Peaks
with r values of -4 or less generally are thought to involve a
two-dimensional phase transition among the adsorbate atoms which
had been adsorbed at a more anodic potential. Most systems with
polycrystalline substrates exhibit broad adsorption regions which
follow Langmuir isotherms. Exceptions to this include Pb on Ag
and Au (1) and Tl on Ag (16) which have multiple peak structure
involving quite narrow peaks in their voltammetry curves.

A second method used for measuring the charge is the fast

galvanostatic transient technique. Here a constant anodic current is applied and the variation of potential with time is followed on an oscilloscope. This method has the advantage that both the faradaic and double layer charge can be determined directly from the time-potential curves for each current density used. Schultze (12) has used this technique for the Cu^{2+}/ Pt system where the adsorption equilibrium was found to be closely approximated with a Temkin isotherm (i.e., a plot of potential versus charge is linear).

The opposite of this method, the potentiostatic technique, has also been used. Here the potential is stepped from a potential anodic to where UPD occurs and the resulting current-time transient is recorded. Integration of the current data provides charge-time or potential plots. The deposition of Tl^{+} onto Ag single crystals (16) has been studied by this method.

Both the fast galvanostatic transient - charge and the potentiostatic pulse - charge methods rely on the charge being proportional to the surface concentration. This is not a good approximation if the electrosorption valency depends on coverage. This assumption is avoided with the twin-electrode thin-layer cell (17, 18), rotating ring-disc technique (11) and certain optical methods (13, 19).

Optical reflectance data can be used to determine adsorption isotherms. In the instance of halide ion adsorption (13) and Pb^{2+} adsorption on Au (19), the change in relative specular

reflectance ($\Delta R/R_0$) has been shown to be a linear function of the excess surface concentration Γ_{ad} at wavelengths near the inter-band (5d-6s) transition edge (i.e., 2.3 eV). This was demonstrated by stepping the potential from a value where the surface was free of adsorbed species to a value corresponding to a particular coverage. During the time period where the adsorption process was under diffusion control the flux of the adsorbed species was calculated from the concentration and diffusion coefficient using the Sand equation. The surface concentration could then be determined and correlated with the reflectance changes. Temkin behavior was found for both Br^- and Pb^{2+} adsorption on Au.

Another interesting method for measuring UPD isotherms has been developed by Bruckenstein et al. using the rotating ring-disc electrode (RRDE) technique (11). With this technique the flux of the UPD species to and from the substrate disc electrode can be monitored by the ring electode at the same time the current at the disc electrode is being measured. The isotherm for the adsorption of Ag^+ on Au was constructed by potentiostating the gold disc electrode at a potential 50 mV anodic to the reversible Nernst potential for a specified time. Following this, the Ag was anodically stripped from the Au surface at a given sweep rate. During this process the change in the ring current level is constantly monitored with the ring potential set at a value so that all of the Ag^+ reaching the ring is reduced to Ag. Integration

of the change in the ring current level with respect to time provide values for the coverage Θ. An isotherm of Θ versus potential at which the disc electrode was potentiostated was then constructed.

The last technique commonly used by Schmidt's group to obtain adsorption isotherms is linear sweep voltammetry used in conjunction with a twin-electrode thin-layer cell (17,18). The cell consists of four electrodes. The working electrode and the "generator" electrode are situated parallel to each other at a distance of 50 μ. Electrolyte between these two electrodes forms the thin-layer cell. The reference and counter electrodes used to complete the cell are located external to the thin-layer cell with a restricted solution path to minimize mass transport in or out of the cell. The generator electrode in the case of UPD studies is a reversible metal/metal ion electrode where the metal is the same as that being underpotentially deposited onto the working electrode surface. The potentials of the working and generator electrodes are controlled independently. Thus by monitoring the charge through the generator electrode precise quantities of the metal ions to be deposited can be introduced into the electrolyte and subsequently quantitatively deposited on the working electrode.

Schmidt et al. use the equation

$$\Gamma_M (E, C_M z+) = \lim_{E \to \infty}_a (2F)^{-1} \int_{E_a}^{E} i_g \, dt$$

$$(2\text{-}31)$$

where E_a is the starting potential of a particular scan and i_g is

the generator current. Plots of Γ (or Θ) versus potential have

been determined for several systems. These include Pb^{2+}/ Au (20)

Pb^{2+}/Ag (17) and Pb^{2+}/Ag(100), (111) and (110) (18). The single

crystal electrode studies, however, are in doubt since it is un-

likely that the surface has the structure corresponding to the

macroscopic orientation.

2.4 Single Crystal Results

Of particular interest are the effects of surface morphology

in the UPD phenomena and the question of whether ordered adsorbate

structures can be produced on single crystal surfaces. Several

groups have studied UPD on single crystal substrates. All of the

systems studied are shown in Table 2.1 along with the techniques

used. With the exception of recent Cu single crystal work (25),

all of the results reported to date have been obtained on Ag and

Au low index planes. Presumably these two metals have been chosen

for the bulk of the studies because the voltammetry curves for the

UPD of many metal cations on polycrystalline Au and Ag contain much

structure not found in other systems. This suggests, as in the

case of hydrogen adsorbed on Pt, that the structure may be due to

the UPD of the metal on various exposed single crystal planes of

the polycrystalline substrate. Also none of the systems listed

in Table 2.1 have been reported to form surface alloys in the UPD

region of potentials. Linear sweep voltammetry has been the pre-

Table 2.1 List of UPD Studies on Single Crystal Electrode Surfaces

Ion	Substrate	Technique	Reference
Tl^+	Ag (100), (111), (110)	LSV, Reflectance, Potential Pulse	16, 21
Pb^{2+1}	Ag (100), (111), (110)	LSV, Reflectance, Potential Pulse	21, 22, 23, 24
Pb^{2+}	Au (100), (111), (110)	LSV, Reflectance, Ellipsometry	19
Pb^{2+}	Ag (111), 100)	LSV (twin-electrode thin-layer cell), potential pulse	18
Pb^{2+}	Cu (111), (100), (110)	LSV, Potential pulse	25
Bi^{3+}	Au (111)	LSV, potential pulse	26, 27
Cu^{2+}	Au (111), (110), (100)	LSV	24
Cu^{2+}	Au (111), (100)	LSV, RHEED	28
Cu^{2+}, Bi^{3+}, Pb^{2+}, Tl^+, Sb^{3+}	Au (111), (100), (110)	LSV	29
Pb^{2+}	Ag (111)	LSV	30

LSV = Linear Sweep Voltammetry

RHEED = Reflected High Energy Electron Diffraction

dominate technique used for single crystal studies. Optical and
potentiostatic methods were also occasionally employed.

The deposition of Pb^{2+} on single crystals of Au will be
reviewed in detail in the next section. However, as an example
of the pronounced effect surface orientation has on UPD consider
the voltammetry curves shown in Fig. 2.3 for the deposition of
Tl^+ on the Ag(100), (111), and (110) surfaces (16). The curve
for polycrystalline Ag is shown for comparison. Increased fine
structure over that found on the polycrystalline sample especial-
ly in the case of the Tl^+/Ag(111), is clearly evident. The Ag(110)
surface exhibits a voltammetry curve very similar to that for the
polycrystalline sample suggesting that the polycrystalline sample
used in this work was predominantly of (110) orientation. There
are similarities between all three single crystal curves as is in-
dicated by the peak rotation (A_1, A_2, etc). Peak potentials, ampli-
tudes and shapes, however, are very different for each surface.
Through charge and optical considerations the authors, Bewick and
Thomas, have concluded that the UPD process for this case involves
the deposition of one monolayer of Tl^+ ions followed by a phase
transition. This, in turn, is followed by deposition of a "second
monolayer" followed by a second phase transition just prior to the
onset of bulk deposition.

The examination of the UPD of Cu^{2+} onto Au (111) and (100)
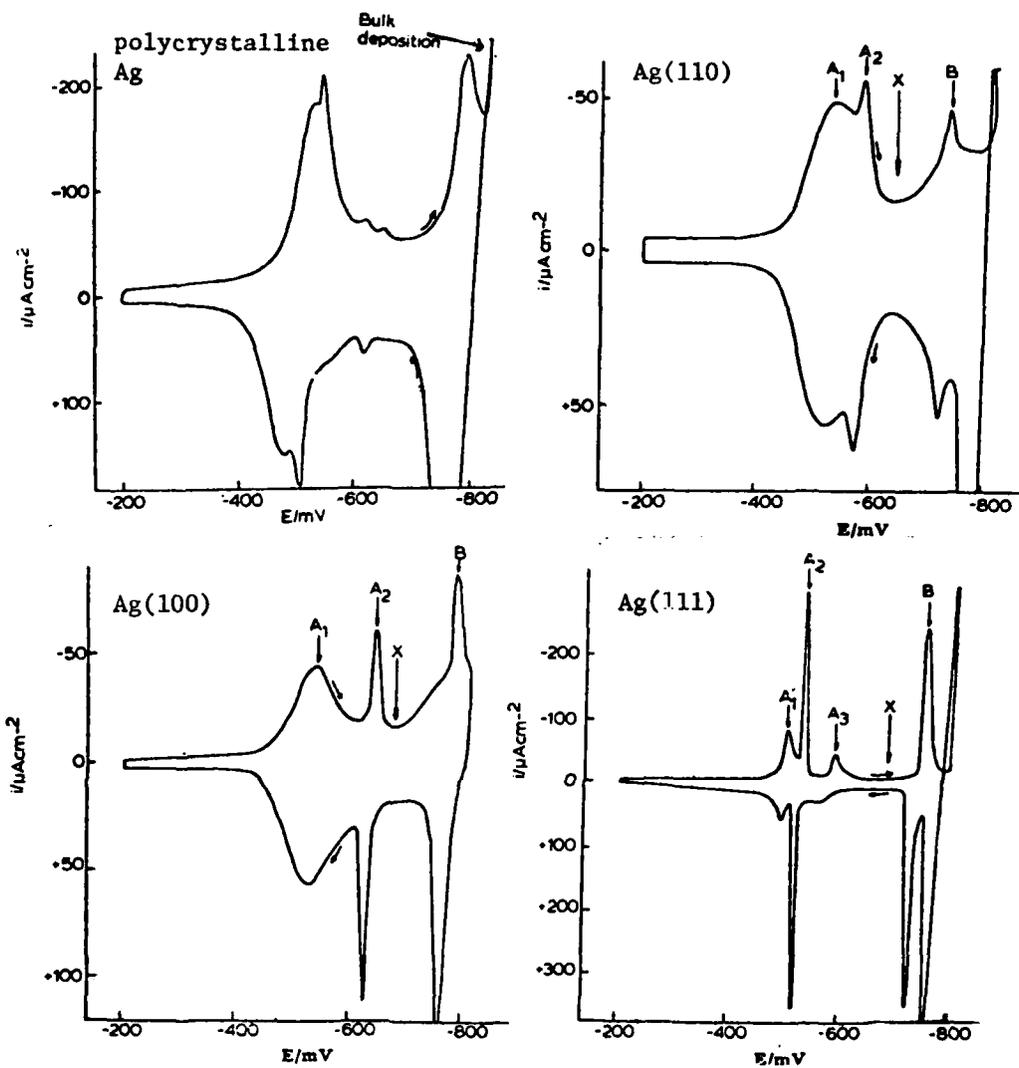
Figure 2.3   Linear sweep voltammograms for the UPD of Tl^+ on
polycrystalline and low index single crystals of
Ag. Electrolyte: 0.75 mM Tl_2SO_4 + 0.5 M Na_2SO_4
+ 1 mM $HClO_4$. Sweep rate for polycrystalline
sample: 100 mV/s. Others recorded at 30 mV/s.
Taken from reference (16).

by Beckmann et al. (28) deserves special mention as this has
been the only experiment to date where the structure of the ad-
sorbate was examined directly. The technique chosen in this
work was reflectance high energy electron diffraction (RHEED)
which produces diffraction patterns from ordered substrates which
are indicative of the atomic structure of the surface. Grazing
incidence of the electron beam is used to insure that only the
first few atom layers are sampled. Results for the Cu^{2+}/Au(111)
system indicate that the deposition of approximately 2/3 of a
monolayer of Cu^{2+} causes a ($\sqrt{3}$ x $\sqrt{3}$) R30 overlayer structure
to appear in RHEED. This nomenclature, due to Wood (31), indi-
cates that the unit cell vectors of the overlayer are $\sqrt{3}$ in mag-
nitude of the Au(111) vectors in both directions and that the
vectors for the ordered overlayer are rotated 30° with respect to
those for the Au(111) surface. Potential excursions into bulk
deposition of Cu^{2+} and subsequent stripping produced a (2x2)
RHEED pattern on the (111) substrate. This rearrangement of the
Au(111) surface was assigned to the formation of ordered domains
of an Au_3Cu alloy.

2.5 Pb^{2+}/Au System

Several reasons can be given as to why the underpotential
deposition of Pb^{2+} onto Au single crystals was chosen for this
work. First, as mentioned in the last section, this is one of
the few systems which exhibits considerable structure in the volt-

ammetry scan. In fact, as many as seven peaks are discernible
as shown in Figure 2.4. Second, the electrochemistry laboratory here
at Case Western Reserve University has had considerable prior
experience working with this system. Both voltammetry and opti-
cal measurements using polycrystalline and single crystal Au were
used (19,32). Lastly, in comparison with other systems the UPD
of Pb^{2+} onto Au has been the object of much study in the liter-
ature. Several groups have contributed a fair amount of experiment-
al effort in an attempt to decipher the mechanism by which Pb is
adsorbed onto the Au surface.

A list of all the studies involving the Pb^{2+}/Au system are
given in Table 2.2. The bulk of the experimental work to date
has been directed toward unraveling the complex adsorption iso-
therm found for this system. An idea of this complexity is
given in Figure 2.4. The voltammetry curve for the Pb^{2+}/Au
system shows two principle peaks, the first at $\sim$ 0.30V and the
second at $\sim$ 0.05V. The first peak is much broader than that ex-
pected for Langmuir behavior. This indicates that there is a
net repulsion between the Pb initially adsorbed onto the surface.
The possibility exists, however, that this broad peak may actual-
ly be composed of two or more peaks, each exhibiting nearly Lang-
muir behavior. The second peak is extremely narrow with the width
at half-height being as small as $\sim$ 10mV. The extreme narrowness
indicates that there is an attraction between adsorbed Pb atoms
which may involve a two-dimensional phase transition.
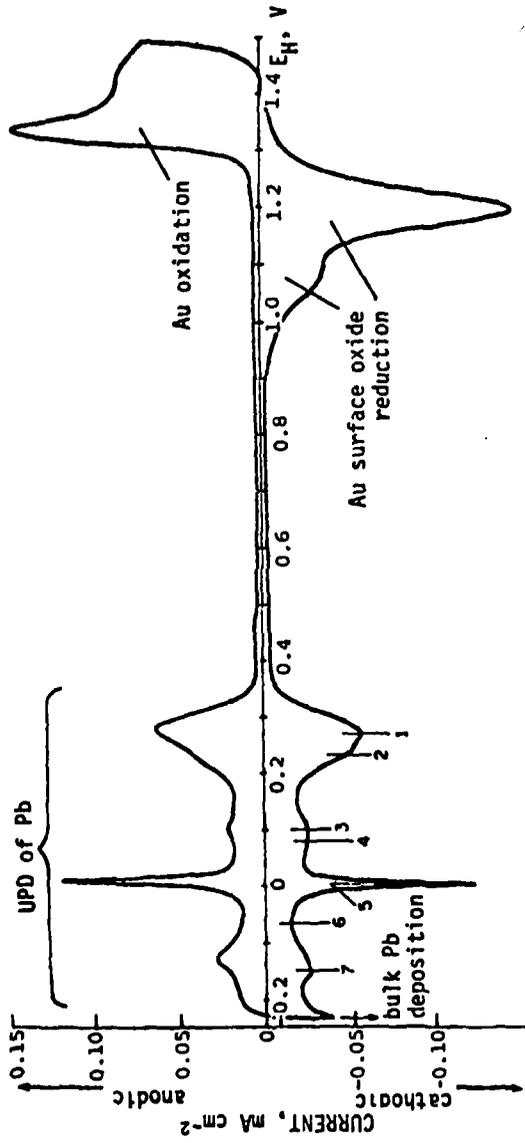
Figure 2.4   Voltammogram for the UPD of Pb^{2+} on polycrys-
talline Au. No electrolyte composition or
sweep rate given. Taken from reference (102).

An adsorption isotherm for this process has been determined independently by two different groups. The Θ-E isotherm determined from measurements using a twin-electrode thin-layer cell is a continuous line with only slight deviations from Temkin linearity at the potentials where the two priciple peaks occur (20). Estimation of the interaction paramater, r, from the half-widths of each peak provides values of r≃+5 for the broad peak and r≃ -2 for the narrow peak. The authors use these r values along with the perfectly continuous transition in the Θ-E curve from one coverage level to another to argue that a two-dimensional phase transition does not occur with this system. Instead they interpret the adsorption process as being due to a discontinuous decrease of the free energy of desorption with increasing coverage which results in a steplike shape of the Θ-E isotherm. They also comment that evidence exists indicating that the second voltammetry peak may be due to the build-up of a second layer of Pb on the Au surface. Other evidence supporting their view is found in the determination of the electrosorption valency. At a coverage $\Theta \simeq 0.1$, γ was found to be 1.95 indicating that the Pb was almost totally discharged when initially adsorbed at $\sim 0.3V$. Ring-disc measurements also verified this view (36).

At variance with the above is the adsorption isotherm obtained from reflectance measurements (19). Plots of the normalized reflectance charge versus Pb^{2+} concentration obtained by stepping

Table 2.2   List of Studies of the UPD of Pb^{2+} on Au

Technique	Reference
Galvanostatic	33
Chronoamperometry	34,35
Rotating Ring-Disc	36
LSV (Twin-electrode thin-layer cell)	20
LSV, Reflectance (Also studied low index single crytal Au planes)	19
LSV, Ellipsometry	32
LSV (Single crystals only)	29

LSV = Linear Sweep Voltammetry

the potential from a region where no UPD occurs to potentials
between the two predominate peaks yield straight lines for the
concentration range 3×10^{-6} to $5 \times 10^{-4} M$, as was expected for Temkin
behavior. However, at concentrations above $5 \times 10^{-4} M$ there was a
large break in the curve indicating that the adsorption of Pb was
not occuring by a continuous, smoothly varying process. The
authors also found that at conditions where the broad voltammetry
peak is under diffusion control the sharp spike is not, suggest-
ing that the spike does not involve the further adsorption of Pb.
Reflectance and ellipsometric data (32) indicate that at the
potential where the spike occurs a marked change in the state of
the surface occurs and that this change is accompanied by a shift
of the previously adsorbed Pb layer toward more metallic proper-
ties. Combination of the above experimental evidence has led the
authors to postulate a two-step mechanism for the UPD of Pb^{2+} on
Au. The first step commencing at $\sim 0.3V$ in the adsorption of Pb^{2+}
mainly is ionic form

$$Pb^{2+}(soln) + (2-y)\ e^- \rightleftharpoons Pb^{y+}\ (ads)$$
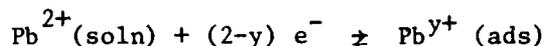
The second step is a phase transition in the previously adsorbed
Pb layer which is accompanied by further discharge of the Pb
(probably to 0 valency)

$$Pb^{y+}(ads) + ye^- \rightleftharpoons Pb\ (ads)$$
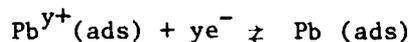
Subsequent discussions have appeared in the literature by
both groups of authors in an attempt to further prove their claims

(37,38). As of yet, however, the problem remains unresolved since
no new experiemental results have been published for this system
which either prove or disprove either groups of authors contentions.

2.5.1 Single Crystal Results

The effect of changing substrate structure has been examined
by two groups (19,29). Both used linear sweep voltammetry to ex-
amine Pb^{2+} adsorption on the Au(111), (110) and (100) surfaces.
Both sets of results are reproduced in Figure 2.5. Only the anod-
ic stripping portions were published by one group (29). Qualita-
tively the curves are very similar. Quantitative differences are
expected in results of this type as neither group used techniques
such as LEED to guarantee that the surface structure was that
expected from exposing a given plane. Also, the surface structure
can be disturbed by electrochemical cleaning which involves alter-
nate cycles of oxidizing and reducing the Au surface. Neverthe-
less, both sets of curves demonstrate the strong influence that
crystal structure has on UPD. Plots of charge density versus
potential for each surface also show characteristic profiles (19).

Comparison of single crystal results with that on polycrystal-
line Au yield several interesting facts. The broad adsorption
region seen at $\sim$ 0.3V for polycrystalline Au is also found on the
(110) surface and to some extent on the (100) surface. The sharp
spike at $\sim$ 0.05V, however, is predominantly found on the (111)
surface. A fairly sharp spike is also seen for the (100) surface

a)
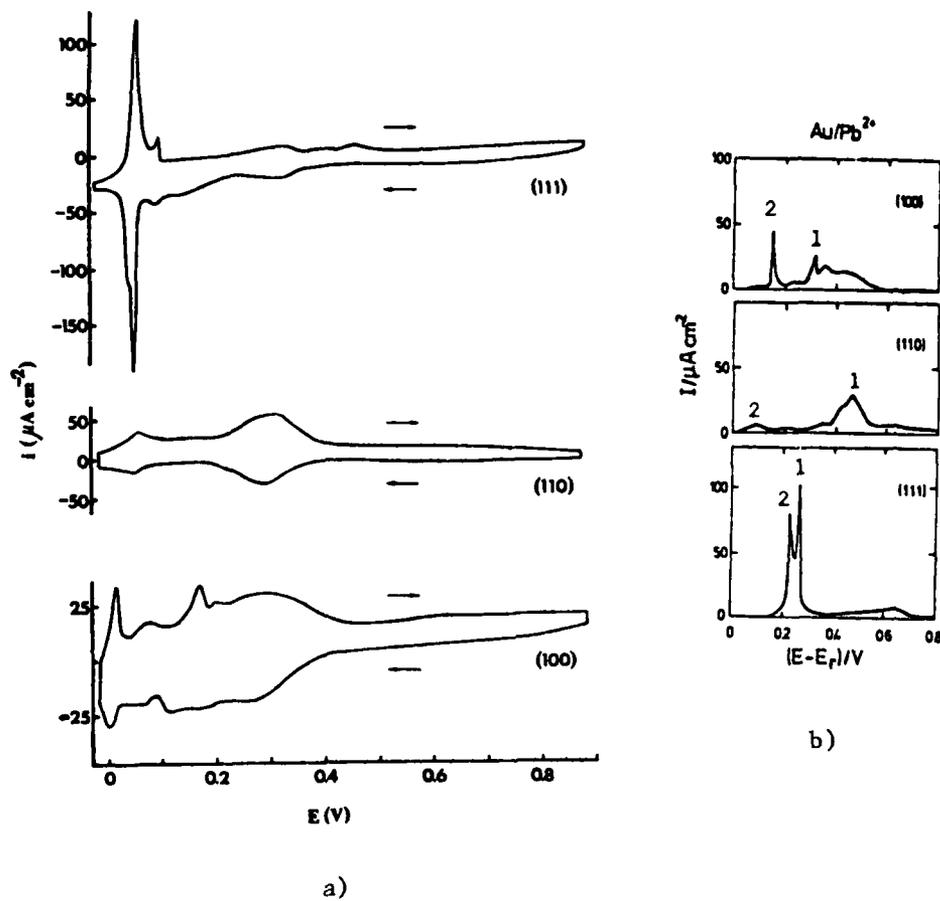
Figure 2.5   a.   Voltammetry curves for single-crystal gold
                  electrodes with (100), (110), and (111) orient-
                  ations in 1 mM $Pb(NO_3)_2$ + 1M $HClO_4$. Sweep rate:
                  20 mV/s. Taken from reference (19).

            b.   Anodic stripping curves for the same single
                  crystals as a in 1mM PbO + 1 M $HClO_4$. Sweep
                  rate: 20 mV/s. $E_r = E - E_{Pb}$. Taken from refer-
                  ence (29)

but it is shifted some 50mV cathodic from that found on Au(111).
These results may indicate that the bulk of the Pb initially ad-
sorbed on polycrystalline Au is done so on (110) and possibly
(100) exposed planes. The small amount of Pb initially adsorbed
on the exposed (111) planes, however, appears to result in the
sharp spike at $\sim$ 0.05V. The voltammetry curve for the (100) sur-
face is quite different than that for the polycrystalline sample,
suggesting that very few (100) planes are exposed.

One group attempted to correlate the charge associated with
the two predominate peaks of each voltammetry curve shown in Fig-
ure 2.5 with LEED structures found in gas phase studies of Pb on
Au single crystals (39,40). The charge values were first convert-
ed to surface concentration. Then they were compared to surface
concentrations calculated from proposed structures which had been
postulated from the LEED patterns taken at various Pb coverages.
The results are shown in Table 2.3 for the peaks as numbered in
Figure 2.5. Fairly good evidence is provided for an epitaxial
type growth at low coverages followed by the formation of a close-
packed monolayer at high coverages. Of course, verification that
these structures existed at the electrochemical interface could
not be made and the use of charge as an indication of surface con-
centration carries with it dubious assumptions mentioned earlier.

Table 2.3   Proposed Structures for Pb^{2+} at Various Coverages on Single Crystal Au Substrates

Orient.	No. of Peak	E_{pk}(mV)	$\delta_{1/2}$(mV)	$\delta_{1/2}/\delta_L$	Q_{exp} (μC/cm^2)	Γ_{exp} (10^{-4}cm^{-2})	Γ_{calc} (10^{-4}cm^{-2})	Proposed Structure
111	1	262 $\pm$ 5	14 $\pm$ 2	0.3	160* $\pm$ 30	5.0*	4.63	p ($\sqrt{3} \times \sqrt{3}$) R30°
111	2	221 $\pm$ 5	13 $\pm$ 2	0.3	290 $\pm$ 15	9.1	9.53	h.m.
100	1	314 $\pm$ 5	33 $\pm$ 3	0.7	206 $\pm$ 10	6.4	6.05	c (2x2)
100	2	146 $\pm$ 5	18 $\pm$ 2	0.4	305 $\pm$ 15	9.6	9.53	h.m.
110	1	456 $\pm$ 6	90 $\pm$ 10	2.0	227 $\pm$ 10	7.1	7.28 7.08	p (7x1) p (6x1)
110	2	98 $\pm$ 5	$\approx$ 100	2.2	285 $\pm$ 15	8.9	9.53	h.m.

Taken from reference 29; Peaks as numbered in Figure 2.4; E_{pk} = relative peak potential; $\delta_{1/2}$ = half width of peak; δ_L = 90mV/$_z$ = 45mV = half width of a Langmuir peak; Q_{exp} = experimental charge of peak; Γ_{exp} = corresponding surface concentration = $\frac{Q_{exp}}{zF}$; Γ_{calc} = surface concentration calculated from proposed structure; h.m. = hexagonal or distorted hexagonal monolayer; * = dependent on sweep rate.

CHAPTER 3

BACKGROUND OF METHODS

3.1 Thin-Layer Electrochemical Measurements

Thin-layer electrochemistry involves the confinement of the reactant within a layer of 10^{-3} cm at the working electrode surface. This cell design is particularly advantageous for several reasons. First, this arrangement is extremely insensitive to relatively high levels of impurities due to the large ratio of electrode surface to volume of electrolyte. For example, an electrolyte with 10^{-4} M impurity confined in a thin layer of 10^{-3} cm would provide 0.1 monolayer of impurity on an electrode. This assumes all the impurity would adsorb on the electrode surface and that the surface atom concentration is 10^{15} atoms/cm^2. Second, current-potential behavior (as measured in voltammetry) is relatively easy to understand since the thin layer is kept smaller than the diffusion layer, alleviating the need for considering most mass transport phenomena. In the simplest cases, combination of the Nernst equation with Faraday's law serves to reproduce the current-voltage curves. Third, very small volumes of solution are needed since the thin-layer contains only approximately 1 μl of solution

As a direct consequence of the reasons listed above a thin-layer cell was chosen for this work. Since the electrochemistry was to be performed in an ultra-high vacuum chamber (back-filled

to atmospheric pressure), as little electrolyte as possible should
be used. Introduction of large amounts of solution would make
pump-down extremely difficult due to adsorption of the solvent
and possibly other components of the electrolyte on the chamber
walls. The normal three-electrode cell arrangement was replaced
with a system in which one electrode was used for both the count-
er and reference. Examples include the α - Pd-H electrode used in
studies of H_2 adsorption on Pt (41,42) and the Pb electrode used
in this work to study the UPD of Pb on Au.

The thin-layer method has been extensively reviewed by Hubbard
(43), and Anson and Hubbard (44). Equations are derived for both
reversible and irreversible reactions where the thin-layer cell is
used in conjunction with various methods (i.e. voltammetry, chrono-
potentiometry, etc.). For the case of UPD, equations are derived
to describe the voltammetric current-potential curve for the case
of one or more reversible voltammetry peaks in the UPD region.
Types of instrumentation including descriptions of various cell
designs, and applications of the thin-layer method are also given
ample consideration.

3.2 Ultra-high Vacuum Surface-Sensitive Techniques

For this work, LEED (low energy electron diffraction) and
AES (Auger electron spectroscopy) were the chosen techniques for
examining the electrodes before and after the electrochemical ex-

periment. LEED was an obvious choice since single crystal electrodes would be used to examine the effect of surface orientation on certain electrochemical reactions. LEED provides a check as to whether the orientation of a particular single crystal was correct and whether the electrochemical experiments had changed the structure of the surface. AES was chosen as the qualitative tool for identifying elements on the electrode surface. This would be used to insure cleanliness of the surface before the electrochemical experiment and to monitor adsorbed species on the surface after the experiment was completed. AES has excellent surface sensitivity ($\sim$ 0.01 monolayer, 20 $\overset{\circ}{A}$ maximum electron beam penetration depth) and uses overlapping components for the detection system with LEED. Background on each of these techniques is given below.

3.2.1 AES

Bombardment of a specimen with a monoenergetic beam of electrons produces a secondary electron distibution similar to that shown in Figure 3.1 for W(110) contaminated with carbon (45). Four regions can be seen in the curve. Region I represents the elastically scattered electrons. If these electrons are coherent, they contribute to the LEED pattern. Incoherent electrons would form the diffuse background of the diffraction pattern. Region II is composed of primary electrons which have suffered discrete energy losses. These may be due to losses arising from electron-
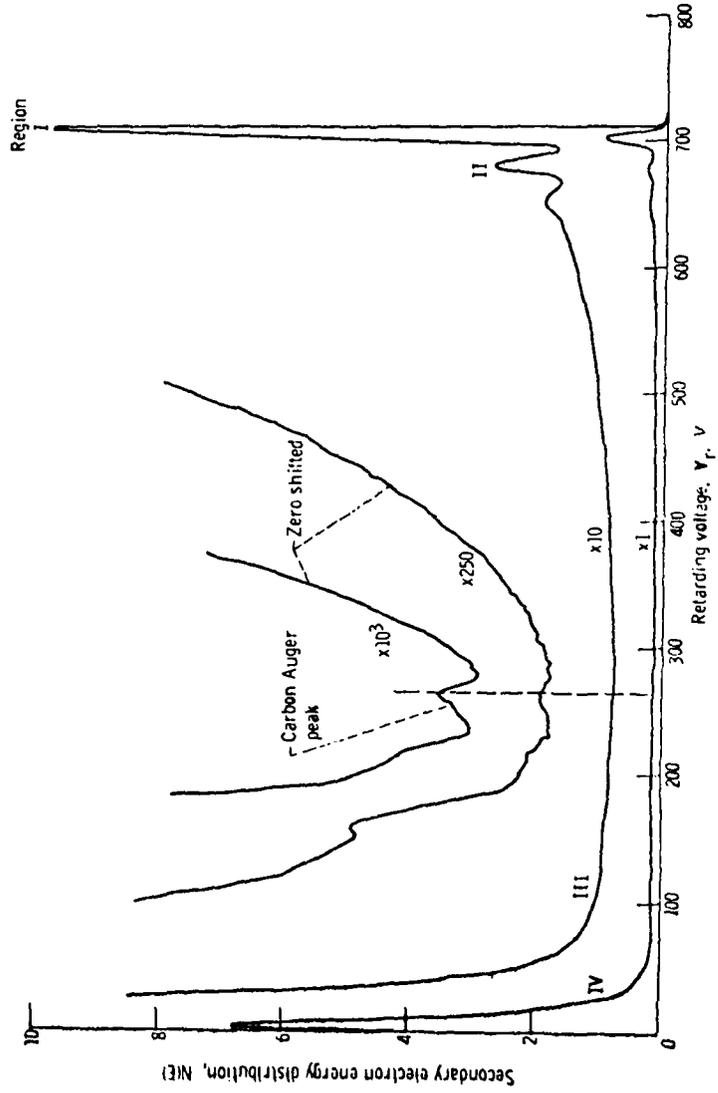
Figure 3.1 Secondary electron energy distribution for carbon-contaminated W(100). Primary beam energy E_o = 698 eV. Taken from reference (45).

ic interband transitions and surface plasmon oscillations. In
Region III are found the Auger electrons. Typical energies can
range from 50 eV to over 1000 eV, depending on the incident elect-
ron energy and the element being examined. Region IV is composed
of the true secondary electrons. The primary electrons make many
collisions inside the solid, creating energetic secondary elect-
rons. This process continues where more secondaries are formed
with ever decreasing energies. The peak at near zero volts would
continue to infinity if it were not for the fact that the elect-
rons must overcome the work function of the material to escape.

The Auger process is initiated by bombardment of a sample
with electrons of energy 2-5 keV typically. The Auger process
is shown for a singly ionized Si atom in Figure 3.2 (46). In this
figure bombardment by a primary electron forces the ejection of a
K-shell electron. The Auger process is initiated when an electron
drops from the L_1 level to fill the K-shell vacancy. The energy
released from this transition can either be emitted as a photon or
through the release of another electron. Most often the process
results in a second electron being emitted, in this case from the
$L_{2,3}$ level. Taking the events in sequence, a $KL_1L_{2,3}$ Auger process
is illustrated in Figure 3.2.

From the diagram in Figure 3.2 the energy of the second emit-
ted electron (Auger electron) can be estimated (46,47). The ener-
gy, E, would be simply $E_K - E_L$ if it were not for the fact that the
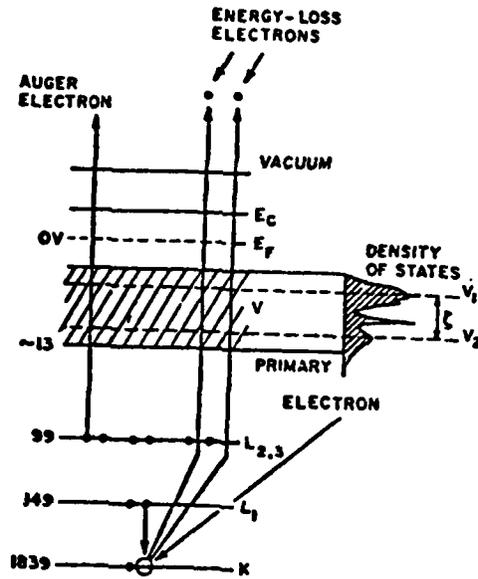
Figure 3.2   The singly ionized Si atom. The electronic energy
             levels are listed on the left (in eV) with the zero
             of energy at the Fermi level E_r; E_c is the bottom
             of the conduction band. The x-ray nomenclature is
             given on the right, and the density of states has
             been drawn into the valence band. A $KL_1L_{2,3}$ Auger
             process is depicted, after primary electron ioniza-
             tion. Taken from reference (46).

ejected electron must use up the energy $(E'_{L_{2,3}} + \phi)$ to escape

the atom, where ϕ is the work function of Si and $E'_{L_{2,3}} \neq E_{L_{2,3}}$.

The energy $E'_{L_{2,3}}$ is the energy of the $L_{2,3}$ level in a singly

ionized Si atom and can be approximated by the relationship

$E'_{L_{2,3}}(Z) = E_{L_{2,3}}(Z+\Delta)$, where Z is the atomic number and $\Delta \approx 1$ to

account for the extra charge caused by the initial ionization.

Thus, the energy of the Auger electron in Figure 3.2 is given by

$$E(Z) = E_K(Z) - E_{L_1}(Z) - E_{L_{2,3}}(Z+\Delta) - \phi \qquad (3-1)$$

Generalization of this equation for the Auger process from levels

$W_o\ X_p\ Y_q$ gives

$$E_{WXY}(Z) = E_W(Z) - E_X(Z) - E_Y(Z+\Delta) - \phi_A \qquad (3-2)$$

where ϕ_A is the work function of the analyzer. The term ϕ_A was

introduced by addition of the extra energy term $-(\phi_A - \phi)$ to equa-

tion 3-1. Calculation of E for values of Z shows that most el-

ements should be uniquely identifiable, even if several different

elements co-exist on the surface at one time. This has been ex-

perimentally verified. Of course, Auger transitions are not pos-

sible for hydrogen and helium.

As is indicated in Figure 3.1 by the Auger energy distri-

bution N(E) for W(110), the sensitivity for detection of Auger

electrons is very poor. The spreading out of Auger peaks can be

due to lifetime broadening caused by short transition times and

energy losses suffered by the escaping electrons. Harris (48),

however, using an electrostatic analyzer showed that the Auger
spectrum detectability is greatly enhanced by electronic differ-
entiation of the energy function distribution. An example of this
enhancement is demonstrated in the Auger spectrum for V(100) shown
in Figure 3.3 (49). Plots of both N (E) = dI/dE and $dN(E)/dE$ =
d^2I/dE^2 versus E are shown, where I is the Auger electron current.
Most Auger spectra reported are obtained in this way.

Several types of analyzers, including magnetic and electro-
static, can be used to obtain Auger spectra. The discussion here
will be restricted to one type, the retarding-field analyzer (RFA)
which was used in this work. This analyzer may not have quite
the sensitivity and resolution as magnetic or other types of
electrostatic analyzers {e.g., double-pass cylindrical mirror
analyzer (CMA)}. It does, however, have the advantage of also
being used for obtaining LEED diffraction patterns. Its expense
is also much less than the others.

A schematic diagram of a typical 4-grid RFA is shown in Figure
3.4a. The retarding potential along with a small modulation volt-
age k sin ωt is applied to the two inner grids. The inner and out-
er grids are held at ground to shield the sample and the fluores-
cent screen collector from the ac perturbation applied to the
analyzing grids. To measure dI/dE versus E, the lock-in ampli-
fier (LIA) is tuned to the frequency of the modulating voltage,
and the retarding potential and LIA output are fed to a X-Y re-
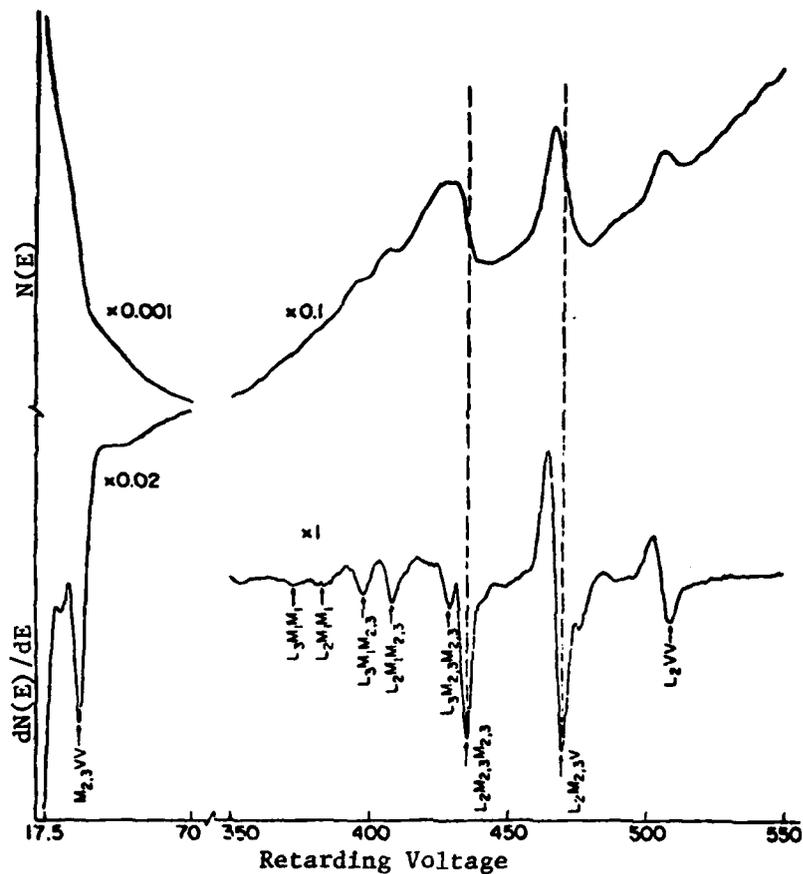
Figure 3.3 N(E) and N'(E) Auger spectron of a vanadium
(100) metal surface. Primary electron energy:
1000eV. Peak-to-peak modulation: 6.0V. Taken
from reference (49)

(a)

(b)
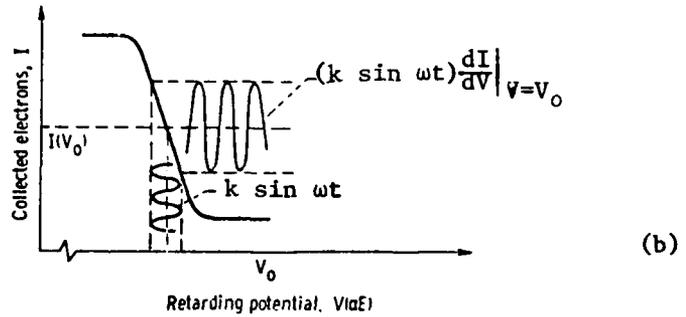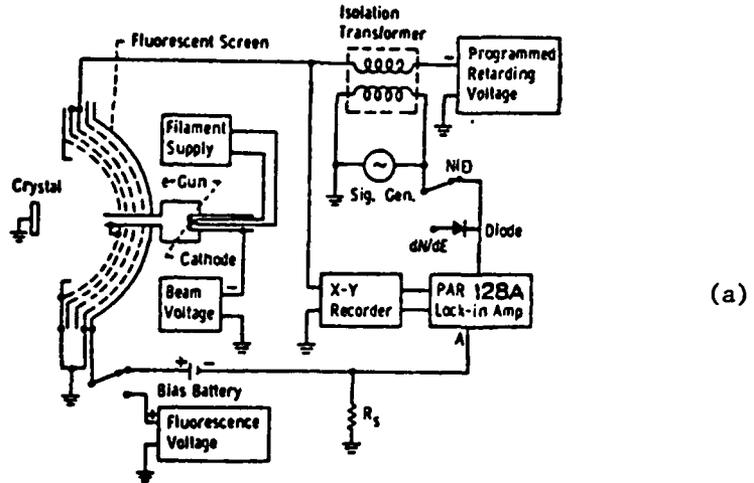
Figure 3.4   a.   A detailed schematic drawing
                   of a combined LEED/AES analyzer
                   and its associated electrons
                   Taken from reference (45).

          b.   Illustration of the retarding
               potential-modulation technique
               used in AES. Taken from reference
               (45).

corder. To measure d^2I/dE^2, the signal channel of the LIA is tuned to a frequency double that applied to the analyzer grids. This double frequency is also applied to the reference channel of the LIA.

The detected current for Auger electrons of energy E can be derived in the following way (47,50). When only a dc retarding potential V is applied to the analyzing grids, electrons with energy less than $E=eV$ will be repelled. The collector therefore receives an electron current

$$I(E) \propto \int_{E_o}^{\infty} N(E) \ dE \tag{3-3}$$

For this case the electron current reaching the fluorescent screen will decrease as the retarding potential V is increased (see Figure 3.4b). If a modulation voltage $k \sin \omega t$ is applied for a fixed value V_o of the retarding potential, the current will contain an ac component with an amplitude proportional to $(dI/dV)_{V=V_o}$ (Figure 3.4b). The electron current I(E) can now be expanded in a Taylor series about the energy E_o since V is proportional to the electron energy E,

$$I(E) = I(E_o) + (E-E_o) \left(\frac{dI}{dE}\right)_{E=E_o} + \frac{(E-E_o)^2}{2!} \left(\frac{d^2I}{dE^2}\right)_{E=E_o} + \ldots \tag{3-4}$$

Applying the modulation voltage $E-E_o = k \sin \omega t$ to E_o gives

$$I(E) = I(E_o) + k \ N(E_o) \sin \omega t + \frac{k^2}{4} \left(\frac{dN}{dE}\right)_{E=E_o} (1-\cos 2\omega t) + \ldots \tag{3-5}$$

$$\simeq I(E_o) + k \left(\frac{dN}{dE}\right)_{E=E_o} \sin \omega t - \frac{k^2}{4}\left(\frac{dN}{dE}\right)_{E=E_o} \cos \omega t + \dots \quad (3\text{-}6)$$

The amplitude of the fundamental harmonic (ω) is

$$A_1(E_o) = k\,N(E_o) + \frac{k^3}{8} \frac{d^2N}{d E^2}\bigg|_{E=E_o} + \frac{k^5}{195} \frac{d^4N}{dE^4}\bigg|_{E=E_o} + \dots \quad (3\text{-}7)$$

The amplitude of the first harmonic (2ω) is

$$A_2(E_o) = \frac{k^2}{4}\left(\frac{dN}{dE}\right)_{E=E_o} + \frac{k^4}{48}\left(\frac{d^3N}{dE^3}\right)_{E=E_o} + \frac{k^6}{1536}\left(\frac{d^5N}{dE^5}\right)_{E=E_o} + \dots \quad (3\text{-}8)$$

Taylor (51) has shown by assuming the Auger peak with amplitude A_1 has a Gaussion distribution that

$$A_1(E_o) = k\,N(E_o) \quad (3\text{-}9)$$

$$A_2(E_o) = \frac{k^2}{4}\left(\frac{dN}{dE}\right)_{E=E_o} \quad (3\text{-}10)$$

provided the peak-to-peak modulation amplitude is less than ½ of the width at half-amplitude of the Gaussion peak. This would result in errors at the peaks of the amplitudes of less than 6%.

AES can be used to obtain several types of information regarding surfaces. Besides the qualitative aspect mentioned earlier AES can also provide quantitative information and, in a few cases, chemical bonding information. Three approaches are available for quantitative analysis: 1) Comparison with standards, 2) Absolute measurement of the number of atoms on the surface, and 3) Relative ratio measurements. All the methods are discussed by Chang (46,52). The third approach as developed by Chang appears to be the most accurate with errors of less than ± 20% being pos-

sible.

Generally chemical bonding information obtained from peak shifts and changes in peak structure cannot be obtained with AES. Chemical shifts are difficult to obtain because if Δ_W, Δ_X, Δ_Y are the shifts for the WXY levels, the measured shift will be

$$\Delta E = E_W - E_X - E_Y - (E_W + \Delta_W - E_X - \Delta_Y) = -\Delta_W - \Delta_X - \Delta_Y$$

$$(3-11)$$

This requires that all three Δ's must be known while only ΔE is measured directly. Also, since most chemical shifts are ≤ 1 eV the relatively broad Auger peaks cannot be used as an accurate measure of this shift. Exceptions, however, do exist (e.g., vanadium oxide study by Somorjai, et al. (49)). The possibility also exists that peak shapes may reveal binding information. Of particular interest are the studies of various metal carbides (46) and the different types of adsorbed carbon (46).

A particularly interesting use of Auger has been to study the growth mechanism of metal films vapor deposited on metal substrates. By constructing AST (Auger special-time) plots for both the substrate and adsorbate, different types of film growth mechanisms are possible as shown in Figure 3.5. Rhead et al. (39,40, 55-7) have made use of this technique to study the vapor deposition of various metals on single crystals of gold and copper. This technique can also be used to calibrate a particular Auger instrument so that quantitative measurements can be performed.
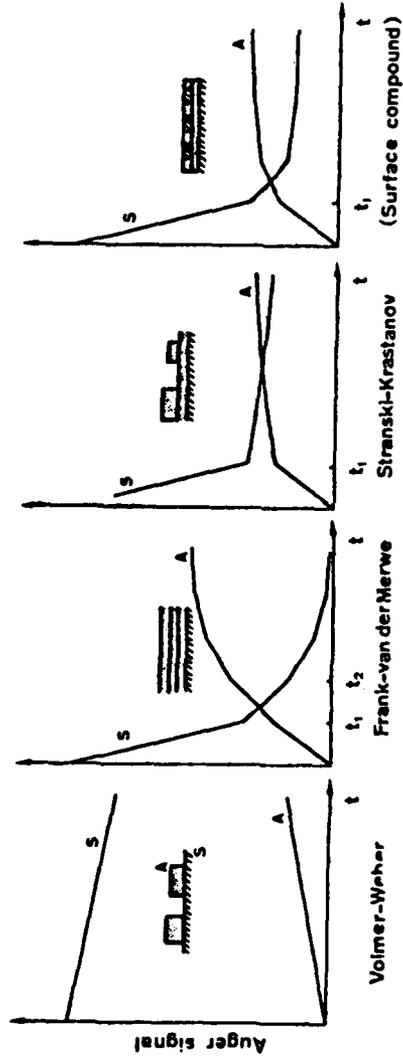
Figure 3.5   Variations of Auger signals for the substrate S and the adsorbate A during film growth by different mechanisms. t_1:time to complete the first monolayer (t_2 the second monolayer). Volmer-Weber: Formation of crystallites without the monolayer stage. Frank-van der Merwe: monolayer by monolayer. Stranski-Krastanov: monolayer followed by crystallites. Surface compound: monolayer followed by insertion of substrate atoms in the adsorbate layer. Taken from reference (54).

3.2.2 LEED[1]

In a typical LEED experiment an electron gun directs a mono-
energetic beam of electrons in the 10 to 500eV range to a single
crystal sample. The electrons which are elastically diffracted
by the surface are detected either by a Faraday cup or, as is used
most often, displayed onto a fluorescent screen. The RFA grid
system used in Auger analysis (see Figure 3.4a) is adaptible for
LEED studies by applying a negative potential to the inner grids
that is a few volts below that of the incident beam to repell the
inelastically scattered electrons. The fluorescent screen is held
at a positive potential of several kV to accelerate the diffracted
electrons to sufficient energy to excite the phospher. The pen-
etration depth of the electron beam is typically 3-10 $\overset{o}{A}$ and the
coherence width of the beam at the crystal is $\sim$200-500 $\overset{o}{A}$. These
data imply that LEED samples only 1 to 3 atom layers and can see
only features which measure less than 200 $\overset{o}{A}$ in any direction.
Non-coherent elastically scattered electrons from gross imperfec-
tions will not interfere with the diffraction of electrons from
surface structures but instead, manifest themselves as diffuse
background. The wavelength of the incident electrons is given
by the deBroglie relation

$$\lambda = \frac{h}{P} = \frac{h}{(2mE)^{\frac{1}{2}}} \simeq \frac{150.4^{\frac{1}{2}}}{E} \quad \overset{o}{A} \qquad (3-12)$$

---

[1] Many excellent reviews exist for LEED. A representative
example can be found in references (58) to (65) from which the
following discussion was taken.

where h is Planck's constant, p is the momentum, m is the mass of the electron and E is the kinetic energy in eV. At a typical LEED energy of 150V λ is of the order of 1 $\overset{o}{A}$.

If a surface has sufficient long-range order, the elastically scattered electrons form a diffraction spot pattern on the fluorescent screen which is a projection of the reciprocal lattice of the two-dimensional surface structure. Diffraction will occur when the Bragg grating equation

$$n\lambda = a (\sin \Theta - \sin \Theta_o) \tag{3-13}$$

is satisfied where a is the two dimensional lattice spacing, Θ and Θ_o are the diffracted and incidence angle of the electrons with respect to the surface normal and n is an integer. The diffraction process is illustrated in Figure 3.6. The wave vector $\vec{k}$ of the incident electron is separated into components parallel $(\vec{k}_{||})$ and perpendicular $(\vec{k}_\perp)$ to the surface, where $\vec{k} = \vec{k}_\perp + \vec{k}_{||}$. The elastically scattered electron is assigned wave vector $\vec{k}' = \vec{k}'_{||} + \vec{k}'_\perp$. Designation of the position of each diffracted beam with respect to the translational symmetry of the surface mesh leads to the momentum conservation law

$$\vec{k}'_{||} = \vec{k}_{||} + \vec{g}(hk) \tag{3-14}$$

where $\vec{g}$ (hk) is reciprocal lattice vector associated with the two dimensional Miller indices, h and k. The reciprocal lattice vector $\vec{g}(hk)$ is defined in terms of the unit cell vectors $\vec{b}_1$ and $\vec{b}_2$ of the reciprocal lattice as

$$\vec{g}(hk) = 2 \pi (h\vec{b}_1 + k \vec{b}_2) \tag{3-15}$$

The real space unit cell vectors $\vec{a}_1$ and $\vec{a}_2$ can be used to gener-

KINEMATICS OF ELASTIC LOW-ENERGY
ELECTRON DIFFRACTION

$$\vec{g}(hk) = 2\pi \left[h\vec{b}_1 + k\vec{b}_2 \right]$$

$$\vec{b}_1 = \vec{a}_2 \times \vec{a}_3 / \left[\vec{a}_1 \cdot \vec{a}_2 \times \vec{a}_3 \right]$$
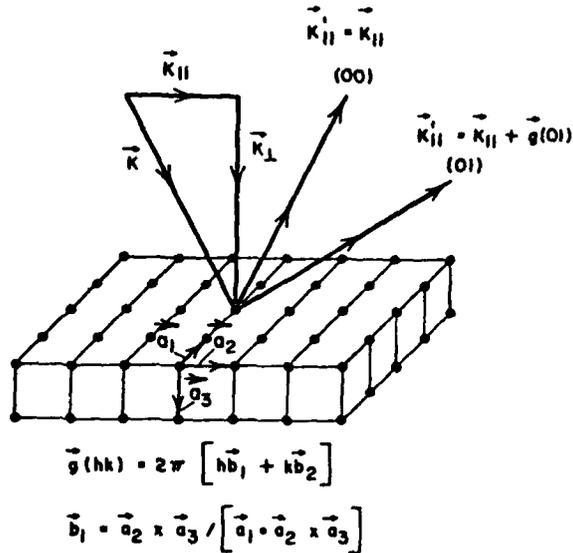
Figure 3.6   Schematic illustration of an incident
electron beam of wave-vector $k = k_\perp + k_\parallel$,
scattered elastically from a single
crystal into a state characterized by
the wave-vector $k' = k'_\perp + k'_\parallel$. The con-
struction of the reciprocal lattice
associated with the single-crystal sur-
face also is shown. The vectors g(hk)
designate the reciprocal lattice vectors
associated with the lowest-symmetry
bravais net parallel to the surface.
Taken from reference (58).

ate the reciprocal space unit cell vectors by the relations

$$\vec{b}_1 = 2\pi \frac{\vec{a}_2 \times \vec{a}_3}{\vec{a}_1 \cdot (\vec{a}_2 \times \vec{a}_3)} \tag{3-16}$$

$$\vec{b}_2 = 2\pi \frac{\vec{a}_3 \times \vec{a}_1}{\vec{a}_1 \cdot (\vec{a}_2 \times \vec{a}_3)} \tag{3-17}$$

with

$$\vec{b}_1 \cdot \vec{a}_1 = 2\pi \qquad\qquad \vec{b}_1 \cdot \vec{a}_2 = 0$$

$$\vec{b}_2 \cdot \vec{a}_2 = 2\pi \qquad\qquad \vec{b}_2 \cdot \vec{a}_1 = 0 \tag{3-18}$$

where $\vec{a}_3$ is the unit cell vector perpendicular to the surface unit mesh. Examples of real and the corresponding reciprocal space mesh is shown in Figure 3.7.

For most clean, unreconstructed metal surfaces the relatively simple LEED patterns can by inspection be related to the periodicity of the real space lattice. Quite often, however, adsorbed overlayers and reconstructed surfaces produce spot patterns which are complex. To determine the periodicity of the real space lattice from these spot patterns a system has been developed which involves the superposition of two-dimensional ordered structures. For example, consider a clean substrate with unit cell B onto which is adsorbed a species forming a lattice with unit cell A. Nets A and B both can be described by unit cell vectors $\vec{a}_B$, $\vec{b}_B$ and $\vec{a}_A$, $\vec{b}_A$. The vectors for each mesh are interrelated through the equations
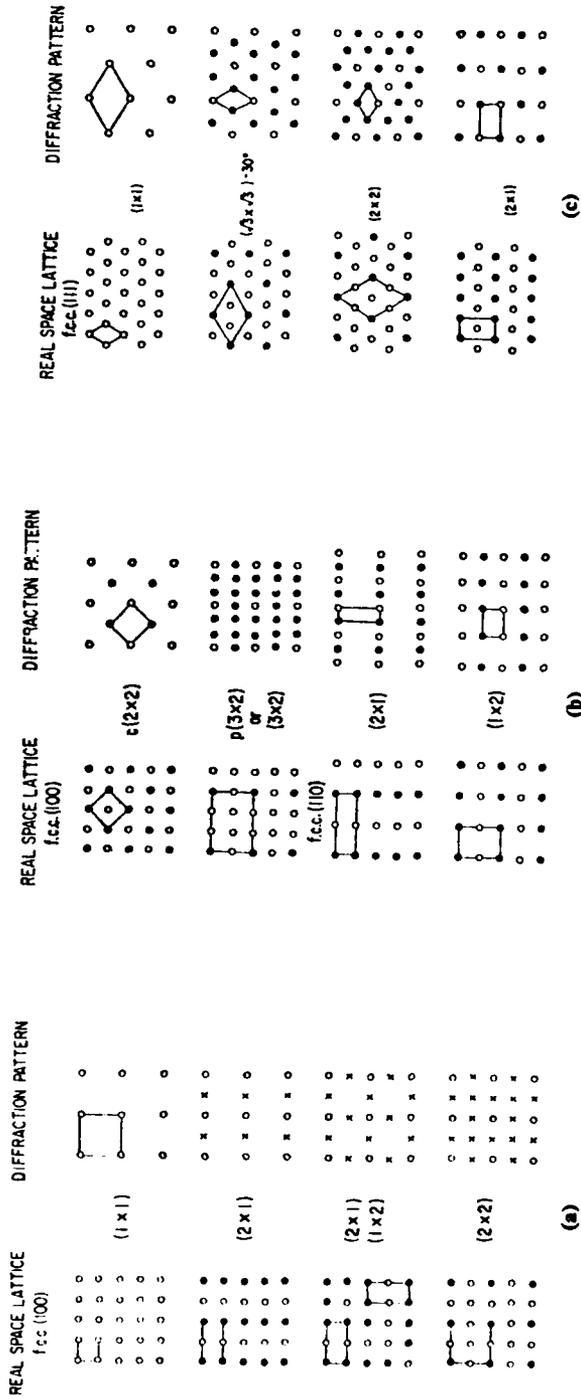
Figure 3.7 Possible surface structures and their corresponding LEED diffraction pattern for the low index planes of a face centered cubic crystal. Taken from reference (59).

$$\vec{a}_A = G'_{11} \vec{a}_B + G_{12} \vec{b}_B \qquad\qquad (3\text{-}19)$$

$$\vec{b}_A = G_{21} \vec{a}_B + G_{22} \vec{b}_B \qquad\qquad (3\text{-}20)$$

The areas of each net, $B = | \vec{a}_B \times \vec{b}_B |$ and $A = | \vec{a}_A \times \vec{b}_A |$, are related by

$$\frac{A}{B} = \det G \qquad\qquad (3\text{-}21)$$

where B is the 2x2 matrix $\begin{vmatrix} G_{11} & G_{12} \\ G_{21} & G_{22} \end{vmatrix}$ connecting the two nets.

Three types of classifications of surface structures are possible depending on the value of det G:

> a. If det G is an interger the nets are simply related. In this case, every point in the lattice with the larger unit cell (usually the adsorbate lattice) is also a point in the smaller lattice. A shorthand notation due to Wood(31) for a surface structure of this type is
>
> $$R \{hkl\} \frac{|\vec{a}_A|}{|\vec{a}_B|} \times \frac{|\vec{b}_A|}{|\vec{b}_B|} -\alpha-D \qquad\qquad (3\text{-}22)$$
>
> where R {hkl} is the symbol for the substrate material and its surface plane, D is the chemical symbol of the overlayer or deposit and α is the angle through which the adsorbate unit mesh is rotated with respect to the substrate's.
>
> b. If det G is a rational fraction, the nets are rationally related. Superposition of two nets A and B in this way give rise to a third "coincidence" net, C which has unit cell vectors a_c and b_c. These are simply related to the vectors for the substrate and adsorbate nets by the expressions
>
> $$\vec{a}_C = P_{11} \vec{a}_B + P_{12} \vec{b}_B = Q_{11} \vec{a}_A + Q_{12} \vec{b}_A \qquad\qquad (3\text{-}23)$$

$$\vec{b}_C = P_{21} \vec{a}_B + P_{22} \vec{b}_B = Q_{21} \vec{a}_A + Q_{22} \vec{b}_A \qquad (3-24)$$

where det P and det Q are integers with no common factor. Here det P is the number of substrate meshes and det Q the number of substrate meshes in the coincidence mesh. Wood rotation for structure of this type is

$$R \{hkl\} \frac{|\vec{a}_C|}{|\vec{a}_B|} \times \frac{|\vec{b}_C|}{|\vec{b}_B|} - \alpha-D \qquad (3-25)$$

c. If det G is an irrational number, the nets are irrationally related. In this case the system no two-dimensional translational symmetry.

Examples of each of the three possibilities are shown in Figure 3.8. The operations expressed above can easily be transformed to reciprocal space by relations of the type shown below where * indicates reciprocal lattice.

$$\begin{pmatrix} \vec{a}_A^* \\ \vec{b}_A^* \end{pmatrix} (\vec{a}_A \ \vec{b}_A) = \begin{pmatrix} \vec{a}_B^* \\ \vec{b}_B^* \end{pmatrix} (\vec{a}_B \ \vec{b}_B) = \begin{pmatrix} 10 \\ 01 \end{pmatrix} \qquad (3-26)$$

$$\begin{pmatrix} \vec{a}_A^* \\ \vec{b}_A^* \end{pmatrix} = \tilde{G}^{-1} \begin{pmatrix} \vec{a}_B^* \\ \vec{b}_B^* \end{pmatrix} \qquad (3-27)$$

$$\begin{pmatrix} \vec{a}_C^* \\ \vec{b}_C^* \end{pmatrix} = \tilde{P}^{-1} \begin{pmatrix} \vec{a}_B^* \\ \vec{b}_B^* \end{pmatrix} = \tilde{Q}^{-1} \begin{pmatrix} \vec{a}_A^* \\ \vec{b}_B^* \end{pmatrix} \qquad (3-28)$$

where the tilde denotes a transpose.

It is interesting to note that the process described above only describes the periodicity of the overlayer in relation to that of the substrate. The position of the individual atoms
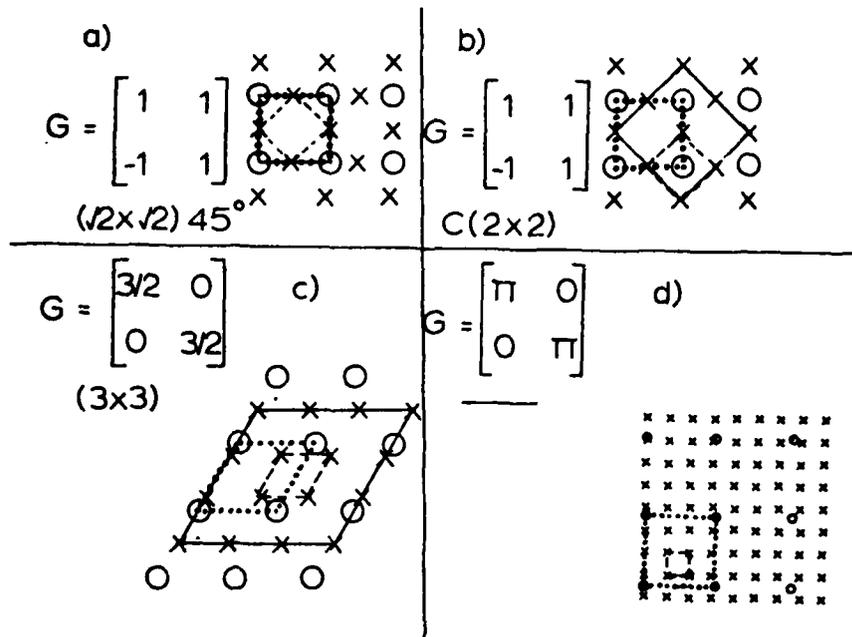
Figure 3.8   Examples of some lattices- - -unit cell of B,....
unit cell of A,————unit cell of C. (a) an ex-
ample of simply related structures, (b) the same
structure but a non-primitive unit cell is used
for C, (c) rationally related structures, (d) ir-
rationally related structures. Taken from refer-
ence (60).

in most instances cannot be inferred from the LEED pattern alone. An example of the ambiquity that can arise is demonstrated in Figure 3.9. Only a vigorous analysis of the spot intensities obtained as a function of beam energy (I-V curve) will produce actual positions of the atoms. I-V curves should be obtained with the gun at normal incidence to the sample and with the sample rotated and tilted through several different numbers of degrees. Unfortunately, the theory used to compute a surface structure from intensity date has not evolved to the routine stage as found for the case of bulk structure determination from X-ray intensity data. Each surface structure determination is the result of much experimental and computational effort. Many problems need to be solved with the most perplexing probably being the lack of a quantitative description of the multiple scattering events which the incident electron undergoes due to penetration below the top atom layer.

3.3 Gas Phase Studies of Pb Adsorbed on Au Single Crystals

Although this work deals with the electrosorption of Pb onto Au single crystals it is advantageous to review the literature for gas phase studies on these same single crystals. Analogies have been shown to exist between electrochemical studies and work on gas phase adsorption. Examples include the work function correlation of Gerisher, et al. (1) and the attempt by Dickertmann
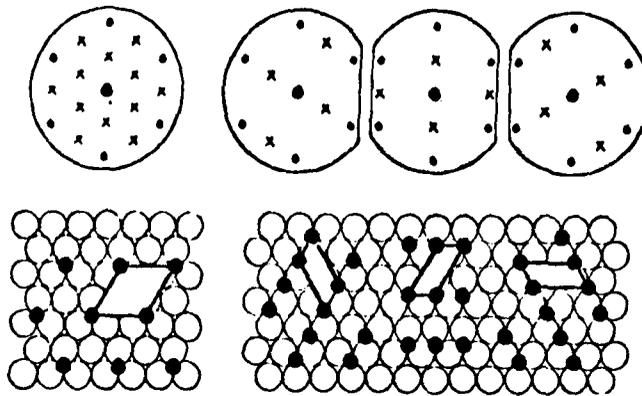
Figure 3.9   Example of ambiguity that can arise in pattern in-
              terpretation. At left, a (2x2) structure on a (111)
              plane of an fcc lattice, with corresponding schematic
              LEED pattern drawn above it. Half-orders are shown
              as crosses. At right, a (2x1) adlayer having three
              rotational orientations. Pattern that arises from
              separately scattering patches will be a superposition
              whose synthesis gives the same spot pattern as at
              left. Taken from reference (62).

and Schultze to correlate the voltammetry peaks found in the UPD

of certain metals onto Au single crytals with LEED patterns ob-

tained by gas phase adsorption of the same metals onto gold (29).

The recent electrochemical results from this laboratory for the

adsorption of H_2 onto Pt single crystals (41,42,66) show certain

analogies with the gas phase data. Before describing the gas

phase results LEED results for clean, low index planes of Au will

be reviewed.

3.3.1 Structure of Au Single Crystals

Models of the Au (111), (100) and (110) surfaces assuming

ideal termination of the bulk crystal lattice are shown in Figure

3.10. The reciprocal lattice for each of these surfaces has been

previously shown in Figure 3.7. The LEED pattern, however, found

for each surface is not that shown in Figure 3.7 suggesting that

all of these surfaces are reconstructed.

Four groups have used LEED to examine the Au (111) surface.

Both Fedak and Gjostein (67), and Chesters and Somorjai(68) found the

hexagonal (1x1) pattern expected from termination of the bulk

lattice. The other groups (69,40) found essentially the (1x1)

pattern but each spot was surrounded by several satellite spots.

Zehner (69) obtained a sharp hexagonal array of satellite spots

around each principle spot in the (1x1) pattern. Perdereau et

al. (40) have used the designation $p(\sim 20 \times \sim 20)R30^o$ to describe the

reconstructed pattern. The interpretation is much the same as
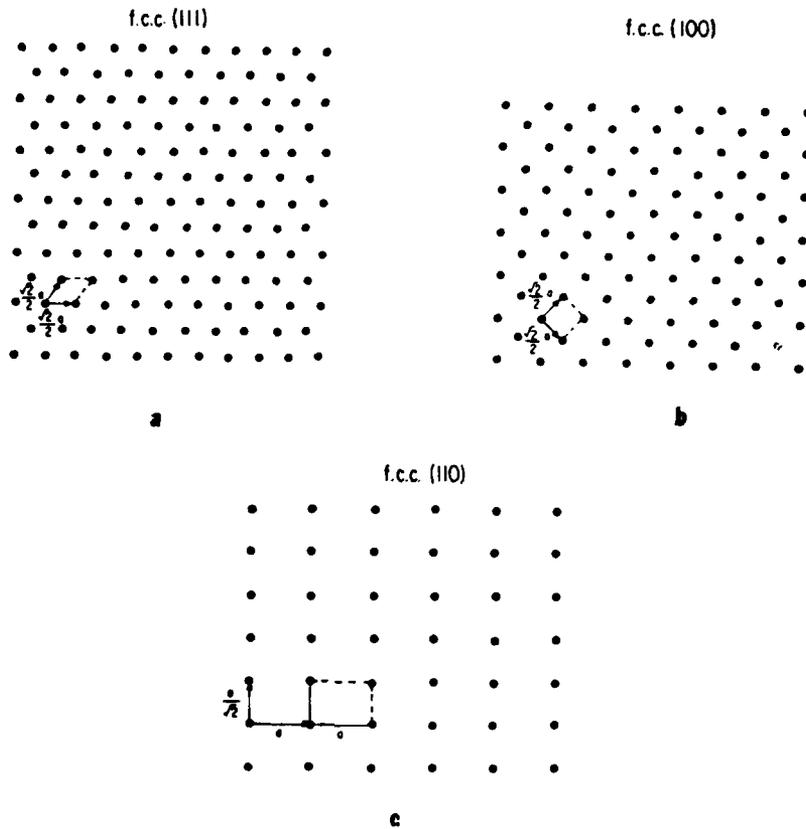
Figure 3.10   Atom orientation of the low index planes
               for a face centered cubic crystal assuming
               ideal termination of the bulk lattice.
               The unit cell vectors are shown for each
               surface. The lattice parameter, a, for
               Au is equal to 4.09 Å.   Taken from refer-
               ence (59).

that used for the reconstructed (100) surface: a hexagonal over-
layer of Au with a lattice parameter contracted by about 5%.
This interpretation is unverified as no LEED intensity analyis
has been perfomed.

The Au (100) surface has been the object of much work and
discussion in the literature. A representation of a particular-
ly well-resolved reconstructed LEED pattern for this surface is
shown in Figure 3.11a. The square spots are those that would a-
rise from the normal (1x1) mesh. The earlier interpretation of
this pattern (70) suggested that a twinning effect was involved
where (221) planes are parallel to the (100) surface. These (221)
planes then either reconstruct or the electronic charge redistri-
butes on this surface. Better resolved LEED patterns (71) and
RHEED results (72) however, gave support to the suggestion by
Palmberg and Rhodin(73) that a reordered hexagonal array of sur-
face atoms with an interatomic spacing 5% smaller than that found
in bulk Au was responsible for the reconstructed pattern (see fig-
ure 3.11b). Use of the above interpretation enables the LEED
pattern shown in Figure 3.11a to be designated (5x20) assuming
the existance of the above structure in two mutually perpendicul-
ar domains. The same explanation is used for the reconstructed
Pt(100)(74) and Ir(100) (75) surfaces. Studies of this surface
with positive ion channeling spectroscopy (PICS) support the hex-
agonal overlayer explanation and indicate that this layer is only
one monolayer in depth superimposed on the (100) substrate (76).

(001)

[010]

[010]

○ REORDERED LAYER
• NORMAL LAYER

(a)

(b)
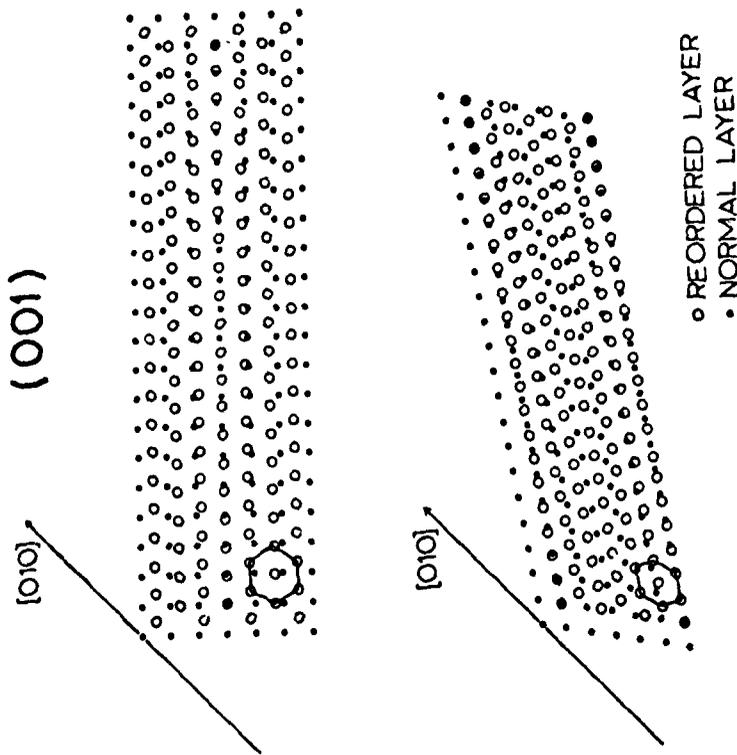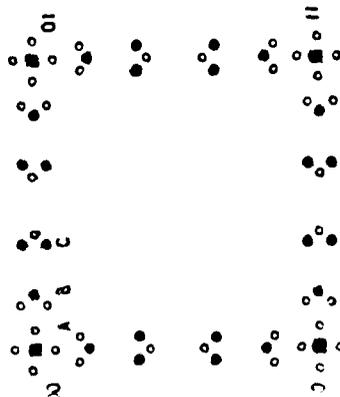
3.11 a. Schematic representation of a well-resolved LEED pattern from the reconstructed Au (100) surface. Singlet spots near substrate reflections are designated by A. B and C are triplet spot configurations. Taken from reference (103).

b. Schematic representation of a normal (001) surface (open circles) with a superimposed hexagonal layer (solid circles) with a 5% contraction in the Au interatomic spacing. The upper view is along the [001] direction, and the lower is along the [101] direction. Taken from reference (76)

The exact interatomic spacing and the suggested (5x20) unit cell have been argued in the literature as no LEED intensity analysis has been performed for this surface. From a RHEED study Grønlund and Nielsen (72) concluded that exact coincidence with the underlying square mesh only came in the fivefold direction and not in the approximately twentyfold direction. Rhead (103), however, using the measured spot splittings in Figure 3.11a has concluded that there is no simple coincidence in any direction. Thus, the designation ($\sim$5x$\sim$20) is probably more correct but awaits verification by a LEED intensity analysis.

The ($\sim$5x$\sim$20) structure remains very stable as long as the surface remains clean. The adsorption of approximately 0.05 monolayer of an impurity substance causes the overlayer to revert to the (1x1) structure (40). A temperature of 800°C also produces the same transformation (67). A metastable (1x1) surface can be prepared by O_2, N_2 or CO ion bombardment which is nearly completely impurity-free (77). The Pt(100)-(1x1) (78) and Ir(100)-(1x1) (79) surfaces can also be prepared in this manner. Use of energy loss spectroscopy (ELS) shows that the electronic structure of the Au(100)-(1x1) surface is different from that of the reordered surface.

The LEED pattern for the clean Au(110) surface shows half-order spots in the <001> direction (67). From this (1x2) LEED pattern one can be inferred that the unit cell has doubled in length

in the <001> direction with respect to that expected for the (1x1)
surface and is unchanged in the <110> direction. Such is the
case for both the Pt(110) (80) and Ir(110)(81) surfaces.

The model usually proposed to explain the reconstructed
(1x2) pattern is shown in Figure 3.12. This "missing-row model"
depicts the surface as having every other close-packed row miss-
ing from the (1x1) structure. Analysis of LEED intensity data
for Pt(110)-(1x2) (referenced by private communication in refer-
ence 83) and Ir(110)-(1x2) (82) has found reasonable agreement
with the missing row model. LEED intensity analysis of the Au
(110)-(1x2) surface by Noonan and Davis (83) however, is not in
agreement with this model or any other "simple" model which could
be used to explain the reconstructed LEED pattern. Further models
are being tested which involve movement of an increasing number
of atoms but progress may be very slow due to the apparent com-
plexity of the reconstruction.

Another separate LEED intensity analysis was performed on
the Au(110)-(1x2) surface by Wolf et al. (84). Distinct broaden-
ing of the LEED spots in the reciprocal < 010> direction was
attributed to statistical faults of the reconstructed layer.
This spot broadening was not found in the intensity analysis re-
ported above. A statistical one-dimensional disorder theory was
presented and used to analyze the LEED intensities. A roughened
surface model was used where the missing row model is considered
valid except that the rows perpendicular to the < 001> direction

f.c.c.(110)

[1̄10]

[001]
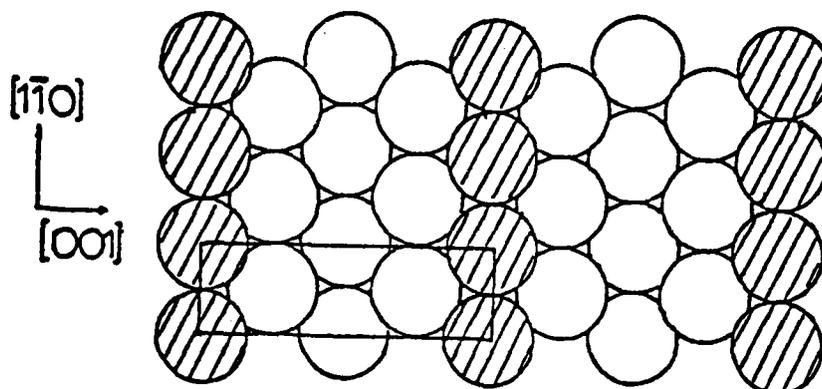
Top view
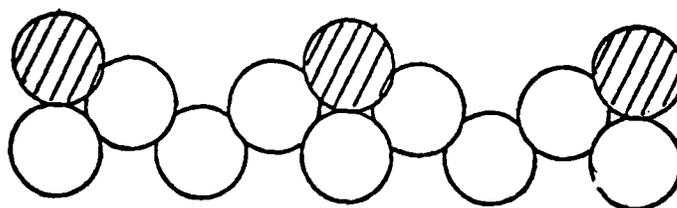
Side view

Figure 3.12 Missing row model for the reconstructed Au(110)
-(1x2) surface structure. Hatched circles repre-
sent reconstructed Au atoms. Taken from reference
(83).

are treated as having different heights. Results indicate that
even at room temperature there are a considerable number of defects
which destroy the long-range order of the rows. These defects
must be very small as spot-splitting should occur if defects ap-
proaching atomic dimensions of an ordered stepped-or kinked-sur-
face were present.

The stability of the Au(110)-(1-2) surface has not been
studied to any great extent. Wolf et al.(84) reported the trans-
formation from a (1x2) to a (1x1) structure to occur at $\sim420^{\circ}C$
while another reported this process to occur at $\sim600^{\circ}C$ (67).
Rhead et al.(40) have shown that the adsorption of a small amount
of Pb also initiated this change but a (1x3) structure was ob-
served before the (1x1) structure appeared. Further annealing of
the clean (1x2) surface produced fractional order spots on hex-
agonal positions suggesting, as in the case of the reconstructed
Au(111) and Au(100) surfaces, that a hexogonal overlayer with a
contracted lattice parameter may also describe the Au(110) sur-
face layer (84).

3.3.2 Pb Vapor-Deposited onto Au Single Crystals

Rhead et al. (39,40) have made a LEED/AES study of the vapor
deposition of Pb from a Knudsen cell in monolayer and sub- onolay-
er amounts onto the three low index planes of Au. The sequence
of LEED patterns found for all three surfaces is summarized in
Table 3.1. The process of Pb deposition occurs in a similar way

Table 3.1 LEED Patterns Found for Vapor Deposition of Pb onto Au Single Crystals

Deposition Time	(100)	(111)	(110)
0	p($\sim$5x $\sim$20)	p($\sim$20x $\sim$20)R30°	p(1x2)
0.5		p(1x1)	p(1x3)
0.75	p(1x1)	p($\sqrt{3}$ x $\sqrt{3}$) R30°	
1.25	c(2x2)	p($\sim$20 x $\sim$20)R30°	p(1x1)
1.50	c(7$\sqrt{2}$ x $\sqrt{2}$)R45°		p(7x1)
1.75	c(3$\sqrt{2}$ x $\sqrt{2}$)R45°		
2.00	c(6x6)		p(7x3)
2.25			p(4x4)
3.00	hexagonal `12 spots'	hexagonal `6 spots'	hexagonal `12 spots'
4.00		hexagonal `12 spots'	

From Reference 40

on all three surfaces. First, the reconstructed surface is transformed into that expected from truncation of the bulk low index plane. This is followed by a series of ordered low packing density configurations at the submonolayer level followed by formation of a compact hexagonal monolayer. Further deposition results in another hexagonal arrangement noted by the formation of a `12 spot´ pattern (i.e., concentric rings, each of twelve spots, produced by two perpendicular hexagonal nets).

The sequence of diffraction patterns enables Rhead et al(40), to make certain deductions about what the actual surface atom configuration is without the benefit of intensity data. Models of all surface structures are presented which are so constructed as to permit a smooth transformation to the next structure with the addition of more Pb. After formation of the hexagonal close-packed monolayer a second hexagonal layer is formed upon further deposition which is attributed to the formation of a surface Pb-Au alloy. Reasons for this deduction are that Auger signals from both Pb and Au are still quite strong and the relatively large size of the unit mesh is difficult to explain with atoms of only one type. Although LEED intensity analysis is needed to accurately determine the composition of the alloy, it is given a preliminary designation as $AuPb_2$. This was arrived at from previous alloy formation studies by other authors, e.g.(85).

The Auger results were used to support the above-mentioned conclusions. The AST plots for both Pb and Au follow the surface

compound type plot shown in Figure 3.5. For the Pb signal there is a sharp knee right before the `12 spot´ hexagonal LEED pattern. At the same time a change in slope occurs for the Au signal. Both of these inflexions indicate that formation of the compact mono-layer is complete. The shape of the signals (especially the non-zero plateau of the Au signal) past this point correspond to a layer-by-layer growth of the alloy.

3.4 Studies of Electrode Surfaces with Surface-Sensitive Tech-niques

Several groups have made use of surface-sensitive techniques to study electrode surfaces. These are summarized in Table 3.2. Two types of equipment arrangements are used for the experiments. Either the electrode is transferred from the vacuum chamber to an electrochemical cell inside an inert glove box and vice versa or it is transferred to a separate compartment that is part of the vacuum system where vacuum integrity can be maintained. For the case of the Mössbauer work the electrode was frozen in the cell and removed to the spectrometer(95). Only two groups Revie et al. (94) and O'Grady et al.(41-2,66), have used the second technique. Hubbard's initial experiments where electrolyte adsorption was studied also used this technique (92). Electrochemical measure-ments, however, had to be conducted in at external cell due to difficulties in performing electrochemistry with his internal cell arrangement (87). All other work listed in Table 3.2 was per-

Table 3.2 Electrochemical Studies Involving Surface-Sensitive Techniques

Electrochemical System Studied	Techniques Used	Reference
UPD of Cu^{2+} and Ag^+ on Pb	XPS	86
UPD of Cu^{2+} on Au(111) and Au (100)	RHEED	28
H_2 adsorption on low index and stepped Pt surfaces	AES, LEED	Low index planes: 41,42,87-90; electrolyte adsorption only: 92 Stepped surfaces: 90
Oxide formation on Pt surfaces	XPS	93
Oxide formation on low index Pt surfaces	LEED/Auger	87,90
Fe passivation	AES	94
Fe passivation	Mossbauer	95

Note: Optical studies are omitted here as their use with electrochemical studies has been well-documented in the literature.

formed using the external glove box arrangement. A serious short-coming of the glove box technique is the probability of contamination of the electrode surface due to the inability of keeping the atmosphere in the glove box clean. This has been well-documented in the H_2/Pt studies by Ross (90).

CHAPTER 4

EXPERIMENTAL

This chapter deals with all aspects of the experimental pro-
cedure used in this work. Basically, three phases were involved
in the experiment. The first involved the preparation of the
Au single crystal surfaces which included slicing the particular
orientation from a single crystal rod and cleaning and character-
izing with LEED and AES these samples in the ultra-high vacuum
environment. After the crystals were cleaned the second phase
was initiated. Included in this phase was the transfer of the
samples into a thin-layer cell type of electrochemical arrange-
ment and the study of the adsorption of Pb on these surfaces with
linear sweep voltammetry. Following completion of the electro-
chemical measurements the third phase was undertaken in which the
samples were transfered back into the ultra-high vacuum environ-
ment and re-examined with LEED and AES. Each of these phases
will be dealt with in detail in the following sections.

4.1 Description of Equipment

In Figure 4.1 is shown a schematic diagram of the experiment-
al apparatus. The system is composed of three interconnected but
isolatable chambers. The LEED/AES and thin-layer electrochemical
chambers were capable of ultra-high vacuums (10^{-10} - 10^{-11} torr)
while the third, the solution delivery chamber, was capable of
10^{-8} torr vacuum. All three chambers were constructed of 316
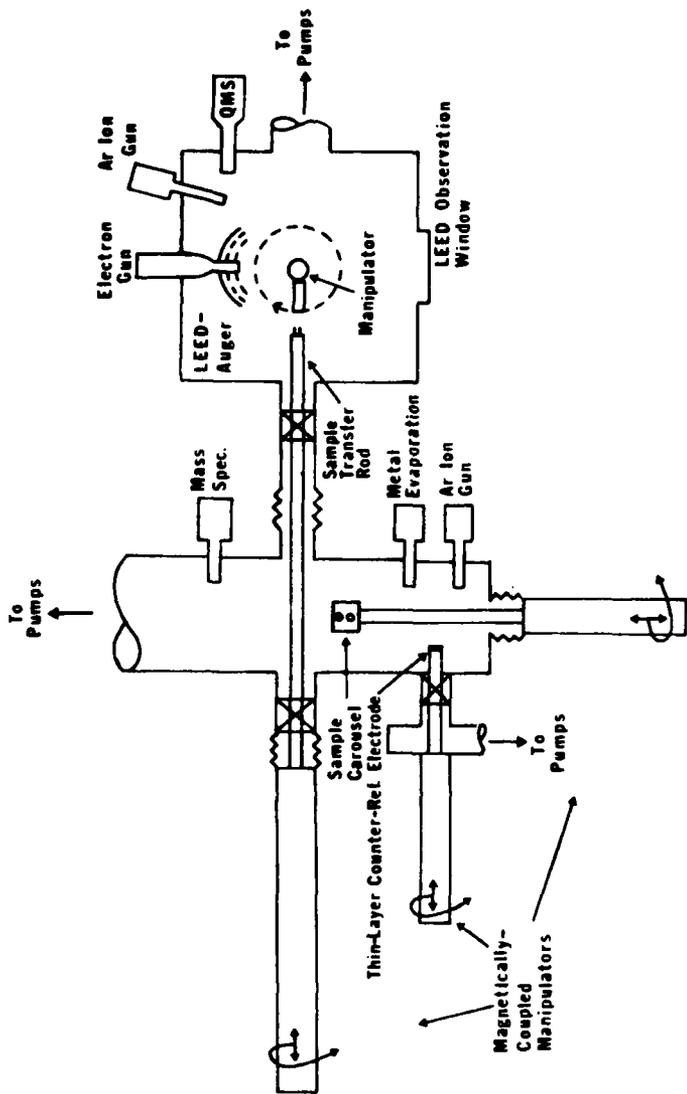
Figure 4.1 Schematic of the entire LEED-AES-Electrochemical System.

stainless steel.

Reduction of the pressure to the ultra-high vacuum level in each chamber was accomplished in several stages. Rough pumping of the system to 100 torr was accomplished with an oil-less carbon vane pump followed by further pumping down to 10^{-2} torr with sorption pumps using 4 $\overset{o}{A}$ molecular sieves cooled to liquid nitrogen temperature. The ion pump was then slowly opened to the chamber and allowed to pump until a pressure of $10^{-6} - 10^{-7}$ torr was reached. The titanium sublimation pump was also cycled on for about 30 s. every 5 m. during this time. The system was then heated using a number of heating tapes and strip heaters for 8-12 h. at approximately 100°C. After cooling for 6-8 h. the base pressure of the chamber was reached (e.g. for the LEED-Auger chamber, $3x10^{-11}$torr). At 10^{-10} torr the principle residual gases left in the chamber were found by a mass spectrometer to be H_2 (mass 2) H_2O (mass 18), N_2 and CO (mass 28) and CO_2 (mass 44) , as is shown in the mass spectrum of the LEED-AES chamber presented in Figure 4.2. This spectrum was taken with a quadrupole mass spectrometer from EAI (Electronic Associates Inc).

4.1.1 LEED/AES Chamber

This chamber housed the normal incident electron gun and the grid optics and flourescent screen detector for the LEED and AES
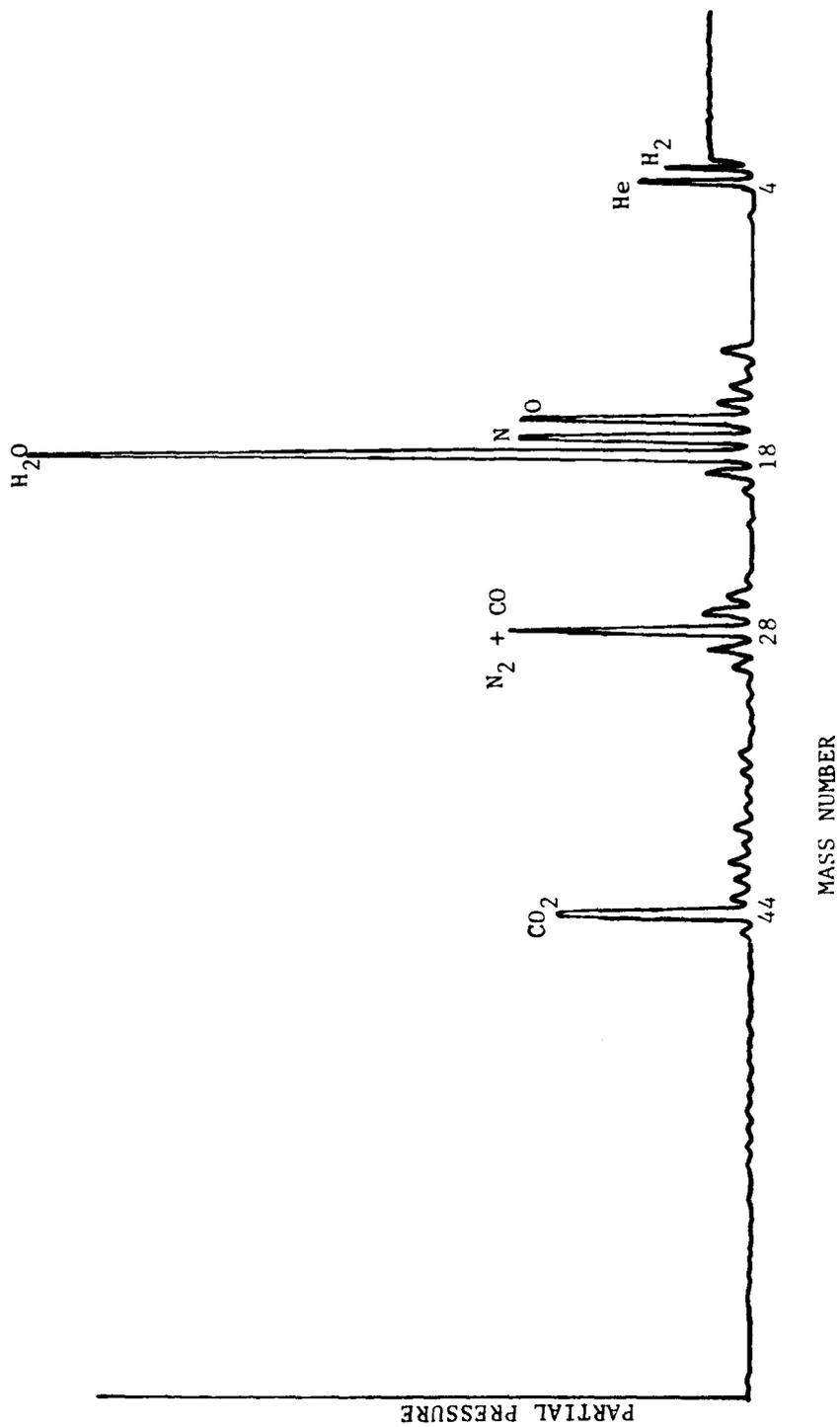
Figure 4.2 Mass spectrum of the LEED-AES chamber at a pressure of 1×10^{-10} Torr taken with the quadrupole mass spectrometer. Multiplier voltage: 3000eV. Filament current: 0.8 mA.

spectroscopy[1]. Details concerning LEED and AES have already been given in Chapter 3. This chamber also contained a quadrupole mass spectrometer for residual gas analysis and a Varian 3000 eV argon-ion sputtering gun used to clean the Au samples.

A precision Varian manipulator was used to direct the sample through all of the motions needed for alignment in the electron and ion-gun beams and positioning to facilitate transfer of the sample to the electrochemical chamber. This manipulator enabled the sample to be precisely moved in the x, y, and z directions. It also contained a tilt mechanism for adjusting the sample in the z plane (perpendicular to the crystal surface) and liquid nitrogen sample cooling capability. In order to anneal the sample a specially designed heater was constructed on the end of the manipulator. Details are shown in Figure 4.3. The sample was heated radiatively by being enclosed along with the tungsten filament in a tantalum shroud. The filament was positioned in back of the sample holder so that there was no direct line-of-sight between it and the sample. This prevented any tungsten which may evaporate from the filament from depositing onto the sample. Temperatures in excess of 1200°C were possible with this arrangement. The temperature was monitored by a Pt/Pt-10% Rh thermocouple wire spot-welded in such a position so that it came in con-

---

[1] All of this equipment was obtained from Varian with the exception of the lock-in amplifier which was the PARC 128A.
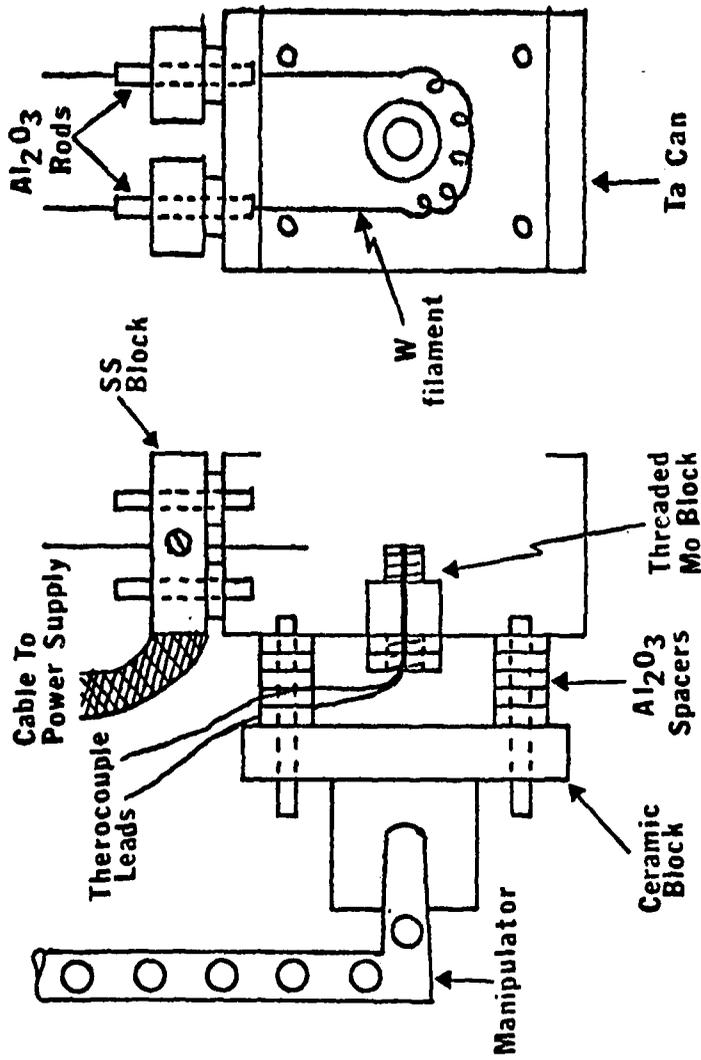
Figure 4.3 Detailed drawing of the heater system used to anneal samples in the LEED-Auger chamber.

tact with the sample holder directly behind the sample.

This chamber contained its own independent system of pumps which included two sorption roughing pumps, a titanium sublimation pump (TSP) and a 140 1/s Varian diode ion pump[1]. The ion pump could be valved off from the rest of the system alleviating the problem of having to start it up when the system was to be pumped back down to ultra-high vacuum. A liquid nitrogen cryo-panel situated just above the TSP filaments was used when a very low vacuum ($\sim 3 \times 10^{-11}$ torr was desired. It mainly pumps water. The pressure during rough-pumping was read by a Hastings thermocouple guage while a Varian dual filament ion-guage was used to read pressures below 10^{-4} torr.

4.1.2 Thin-layer Electrochemical Chamber

All of the electrochemical measurements were performed in this chamber. The principle components were the two magnetically-coupled manipulators which enabled the sample to be transferred inside the chambers while maintaining ultra-high vacuum conditions. These manipulators were capable of both rotational and translation-al movement. One manipulator was 5 feet in length and was used to transfer the single-crystal sample to and from the LEED/AES cham-

---

[1] A triode pump or possibly a diffusion or turbomolecular pump may have been more suited for this chamber. Availability, however was the prime factor for using the diode pump.

ber.[1] Details of the sample holder and the end of this manipula-
tor are shown in Figure 4.4. The second manipulator approximately
one foot in length was coupled to a copper sample carrousel capable
of holding six samples. Each sample holder was treaded onto a
corresponding mounting on the carrousel. This manupulator was
used to accept the sample from the longer manipulator and to
hold the single crystal electrode in the thin-layer cell. This
manipulator was also capable of x and y motion through the use
of a bellows and a micrometer controlled support manufactured
by Huntington. A side-view of this chamber is shown in Figure 4.5.

Other accessories on this chamber were a Varian 600 eV
argon-ion gun for sample and counter electrode cleaning and a
Veeco mass spectrometer for residual gas analysis. A Knudsen
cell for evaporating foreign layers onto the electrode surface was
included but not used in the present study. The pumps for this
chamber were similar to those for the LEED-Auger chamber except
that the ion pump was a 110 l/s triode pump. Care must be taken
when using either diode or triode pumps as they are known to have
memory affects and may release unwanted contaminants (96), par-
ticularly CO.

_____

[1] This manipulator was purchased from Huntington Mechanical
Laboratories. The long manipulator was constructed in the mac-
hine shop at Case Western Reserve University.

glass plate

resin

(c)

Au crystal — Au foil

holes

Top View

Au foil

Stainless Steel holder

Side View

(b)

pin crystal

sample holder

spring clip

transfer wand

(a)
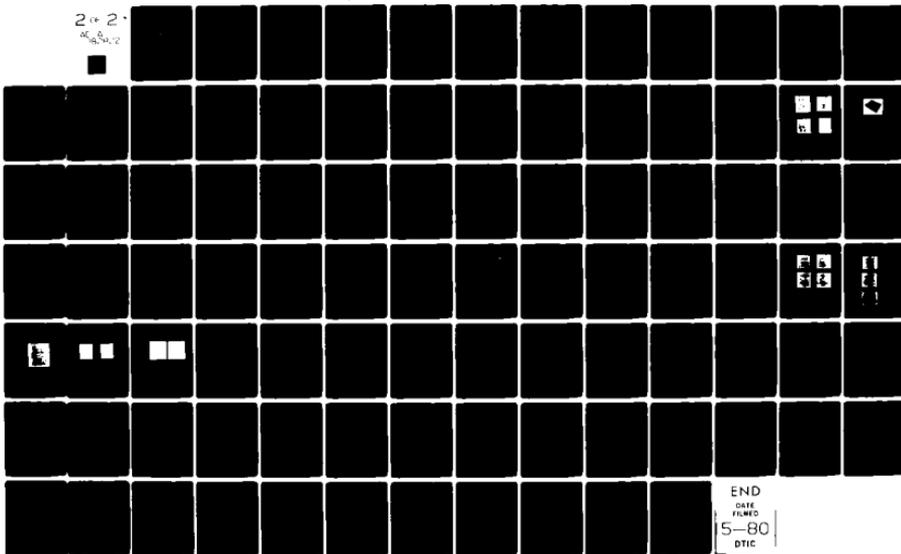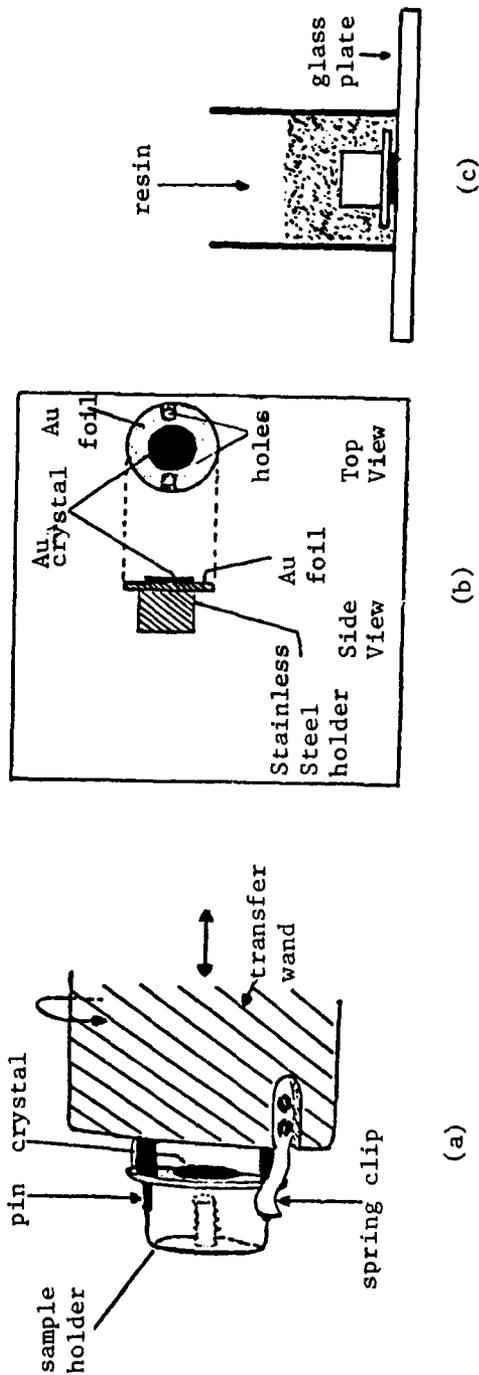
Figure 4.4 a. Details of the end of the transfer wand used to transfer a sample from the heater (Figure 4.3) in the LEED –AES chamber to the sample carrousel (Figure 4.5) and vice-versa.

b. Sample holder with single crystal mounted on it.

c. Method for casting sample and sample holder in resin for polishing.
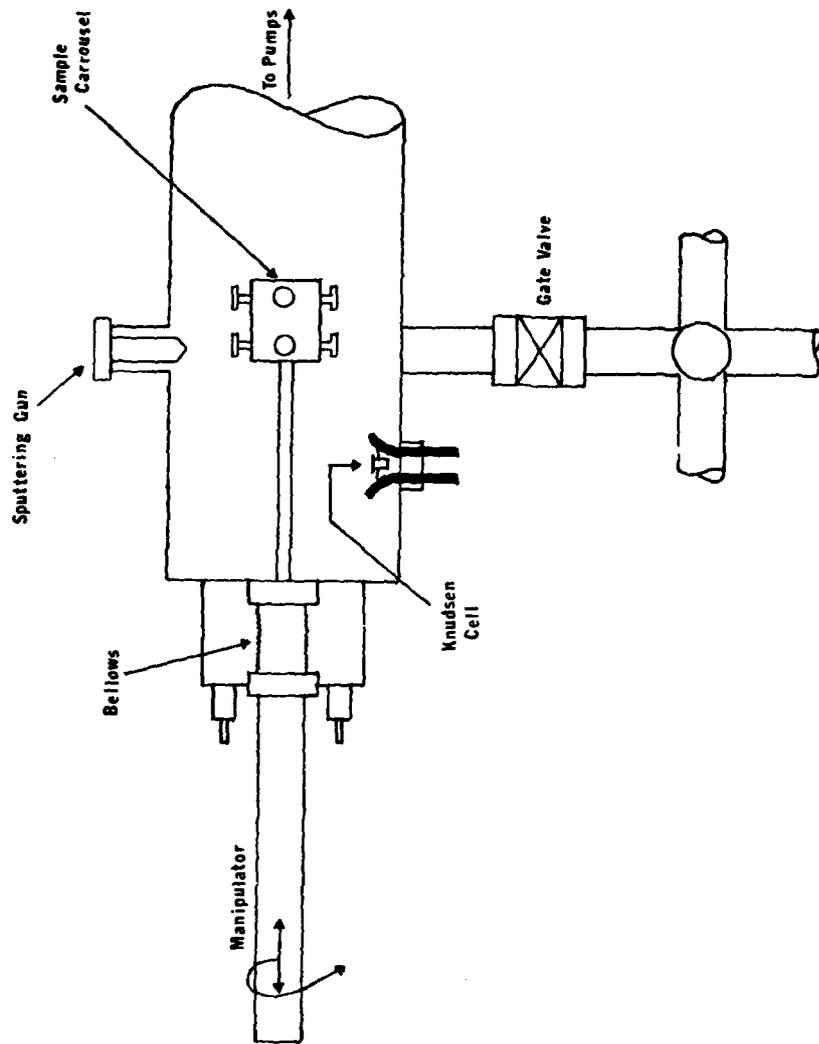
Figure 4.5 Side view of the electrochemical chamber.

4.1.3 Solution Delivery Chamber

Details of this chamber are shown in Figure 4.6. The cham-
ber was a 6-way stainless steel tee connected directly underneath
the electrochemical chamber. Connected to the tee was another
magnetically-coupled manipulator on which was mounted a Teflon
block which contained the Pb counter and reference electrode press-
fitted into it. The solution was delivered to the Pb electrode
by way of an all Teflon valve and tubing system. The use of
Teflon was dictated by the electrolyte, dilute HF. The valves
(from Hamilton) are those commonly used in gas chromatography
and thus were not designed for use in ultra-high vacuum. How-
ever, they do seal very well and a modest vacuum of 10^{-8} torr
was easily reached. The valve and tubing system was constructed
in such a way as to allow for rinsing the Pb electrode with either
electrolyte or H_2O through the use of sorption pumps.

Also attached to the 6-way tee was an electrical feedthrough
carrying the connection between the potentiostat and the counter-
reference electrode. This feedthrough also had an auxilliary Pt
or Au working electrode connected to it which could be used to
check the reference potential of the counter-reference electrode.
In the present work the reference potential established by the re-
versible Pb/Pb^{2+} couple was a function of the concentration of
Pb^{2+} ions in the HF electrolyte and did not have to be checked.

The same sorption pumps that were used for the electrochem-
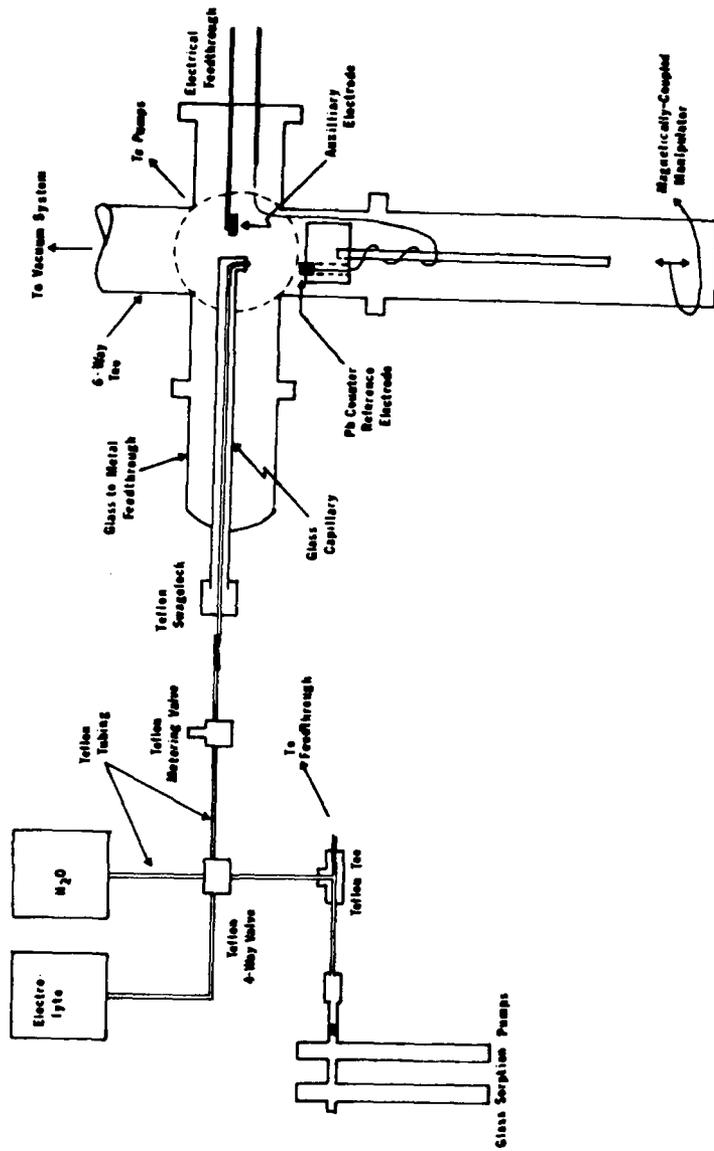
Figure 4.6 Details of the solution delivery system.

ical chamber were also used here as the two chambers were inter-connected. Both chambers could be valved off from each other and from the high-vacuum line common to each.[1] Due to this chamber's small size no TSP could be used. However, added pumping capability was achieved through the use of a Varian 500 1/sec ion pump. The large size of this pump compared to the small volume being pumped enabled very rapid pump-down times to be obtained.

4.2 Preparation and Cleaning of Au Single Crystals

The process of going from a single crystal rod of gold to clean single crystal surfaces was the most time-consuming and tedious part of this experiment. The procedure that was followed is described in the sections below.

4.2.1 Alignment and Spark Cutting

Four Au single crystal surfaces were cut from a high purity (Marz Grade; 99.999% purity) single crystal Au rod from Materials Reseach Corp. The four surfaces were (111), (110), (100) and (410). Au (410) is a stepped surface and in stepped-surface notation (64)

---

[1] Connected also to this common vacuum line was a line made of stainless steel ¼" tubing and Swagelock connectors used to deliver the ultra-pure argon gas (Scott Enviromental Technology, 99.9999% pure; Total hydrocarbons <0.5 ppm and oxygen <1 ppm) to each of the three chambers. The gas line was connected through Granville-Phillips leak valves to both the LEED/AES chamber and the electrochemical chamber for precise gas leak control for sputtering purposes. The gas was delivered through an Airco ultra-pure stainless steel regulator.

designated as Au-S-{4(100)x(100)}. The S indicates a stepped

surface which in this case is composed of terraces of (100) orient-

ation four atomic units wide, separated by steps of (100) orient-

ation one atomic unit high. The relationship between all of

these planes on a stereographic triangle for a face-centered cubic

crystal is shown in Figure 4.7. The (111) surface is $54^\circ 44'$ and

$35^\circ 16'$ from the (100) and (110) surfaces, respectively, while the

(100) is 45° away from the (110) surface. The Au(410) surface lies

15° from the (100) surface towards the (110) plane.

Before cutting it was necessary to orient the single crystal

rod to facilitate cutting the desired plane. To accomplish this

the crystal was mounted on a Supper goniometer and back-reflect-

ance Laue X-ray measurements were undertaken. The symmetry of the

resulting diffraction spots are used to align the crystal along

the desired plane. The goniometer has provisions for orienting

the sample about three rotational axes. Once the initial diffrac-

tion pattern is obtained and its symmetry deciphered, the crystal

can be rotated through the use of a Greninger net to within about

2° of the desired plane. After this, trial and error goniometer

movements are used to get the spot pattern from the desired plane

aligned exactly on the film. An excellent review of the experiment-

al aspects of this technique is given by Wood (97).

Once the desired plane was aligned perpendicular to the X-ray

beam the goniometer with the sample was mounted on a Servoimet

spark-cutting apparatus. The cutting blade was a piece of stain-
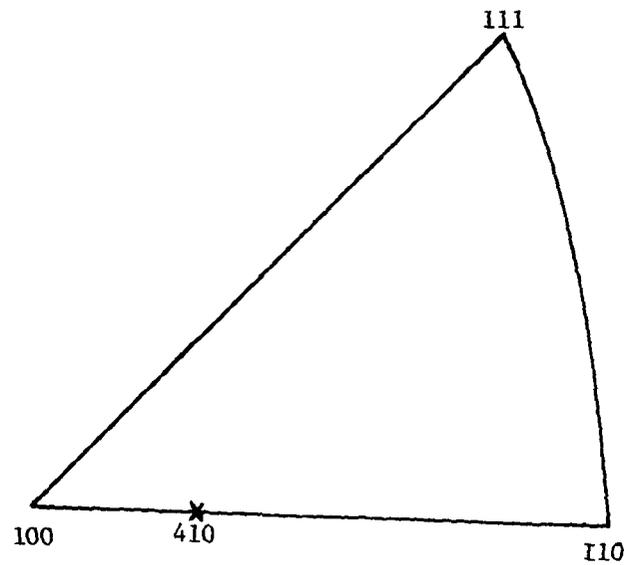
Figure 4.7   Stereographic triangle showing the angular
             relationship between the low index planes
             of a face-centered cubic crystal.   The (410)
             plane is located 12° from the (100) towards
             the (110) plane.

less steel sheet aligned paralled to the plane to be cut. The cutting was achieved with a spark discharge from a capacitor each time the cutting tool came in contact with the crystal. The cutting pressure was controlled by a solenoid connected to the spark source. The sample was kept cool by being bathed with a continuous stream of oil. Each slice was approximately 1mm thick.

Since the slices for each of the planes obtained by spark-cutting were of unusual shape, it was necessary to cut a round piece from the sample to facitiltate the electrochemical measurements on these surfaces (this is called trepanning). When performing electrochemical measurements with the thin-layer technique using, e.g. linear sweep voltammetry it is desireable and usually necessary to have the paralled electrode surfaces of the same geometry to achieve uniform current distribution. This is most easily achieved with circular electrodes. The spark-cutter was again used with the tool being a stainless-steel tube with an inside diameter of approximately 0.6 cm. The tool was aligned perpendicular to the sample which was mounted on a flat aluminum block using a heat-sensitive resin. The sample was then etched in a warm solution composed of 5 parts H_2O, 1 part concentrated HNO_3 and 5 parts concentrated HCl to remove all the disturbed surface layer.

4.2.2 Polishing

The samples were polished already mounted on the stain-less steel sample holders used in the final measurements. Mounting was

achieved by first spot-welding the sample to a piece of ½" diameter, 0.002 inc. thick Au foil of the same purity as the sample. Spot-welding was accomplished with two specially made Mo electrodes: one was a flat block with one side highly polished while the other was a standard-sized tip. The sample was placed face-down on the block and the foil was spot-welded to it from the back with the use of the tip. This prevented any large surface deformations to occur. The foil with the single crystal attached was then spot-welded to the stainless steel sample holder(see Figure 4.4b).

For polishing, the whole sample holder was cast sample down in a resin manufactured by Buehler (see Figure 4.4c). After the resin had set, the single crystal surface sample was polished on a wheel using the following sequence of Buehler polishing materials.

Abrasive	Extender	Polishing Cloth
9μ diamond paste	oil	nylon
6μ diamond paste	oil	nylon
1μ diamond paste	oil	nylon
0.05μ alumina	H_2O	microcloth

Occasionally 1μ and 5μ alumina were substituted for 1μ and 6μ diamond paste. After each polish the sample and polishing wheels were washed repeatedly with distilled water to ensure removal of all the polishing compound. Under magnification the surface still contained very fine scratches after the final polish. These result from scratching the "soft" Au surface with 0.05μ alumina. However, they are of no problem as it is known that scratches resulting from a final polish using 0.3μ alumina can be annealed out in

in ultra-high vacuum (69).

Following the final polish the resin was removed by immersal in CH_2Cl_2. Before being placed in the vacuum system the sample and holder were immersed in a ultrasonic cleaner to insure removal of all resin and polishing compound. The sample was then rinsed several times with concentrated (15M)HNO_3 followed by triply distilled H_2O and degreased by refluxing iso-propyl alcohol over the sample-holder system in the vapor.

4.2.3 Cleaning in Ultra-High Vacuum

The samples were subjected to cycles of Ar-ion sputtering and annealing until the surface was clean within the limits of AES ($\sim$ 1% of a monolayer). Then a sharp LEED pattern was obtained with no diffuse background. The samples were introduced into the vacuum system through a port on the electrochemical chamber. In the early work only one argon ion gun was available and this was installed on the electrochemical chamber in order that the counter electrode surface as well as the working electrode could be cleaned. The high temperature furnace used for annealing the single crystals, however, was mounted on the manipulator in the LEED-Auger vacuum chamber. This necessitated frequent transfer of the sample between the chambers. Typically 5 to 7 sputtering-annealing cycles were required. In the later work, a second Ar^+ sputtering gun was installed in the LEED-Auger chamber to avoid the many transfers between the chambers. Ion energies ranged from 500 eV in the

electrochemical chamber where the sample could be placed within a centimeter directly in front of the ion gun to 1500 eV in the LEED/ AES chamber where the sample could only be situated within 15cm of the gun. Sputtering time for each cycle was generally 30 m for an argon pressure of $5x10^{-5}$ torr. The annealing part of the cycle ranged from 1 h for a sample that had previously been cleaned to several hours for a newly polished sample. Long annealing times were necessary for new samples to promote segragation of impurities at the surface and to anneal out the surface damage caused by polishing and etching.

Principle contaminants found in the Au samples were C, O and Ca with major Auger peaks at 272 eV, 510 eV and 291 eV, respectively. Removal of these impurities produces and Auger spectrum as shown in Figure 4.8. The major Au transitions marked in the figure and their probable designations (47) are shown below

Auger Peak Energy	Designation of Transition
141	N_V N_{VI} N_{VI}
150	N_V N_{VII} N_{VII}
160	N_{IV} N_{VI} N_{VI}
184	N_V O_{II} O_{II}
200	N_{IV} O_{II} O_{II}
239	N_{IV} N_{III} O_{III}
255	N_{IV} N_{VII} V

Once a Au sample was clean, it could be left several days in ultra-high vacuum without fear of contamination from contact with the residual gases. This apparently is due to gold's inertness to-
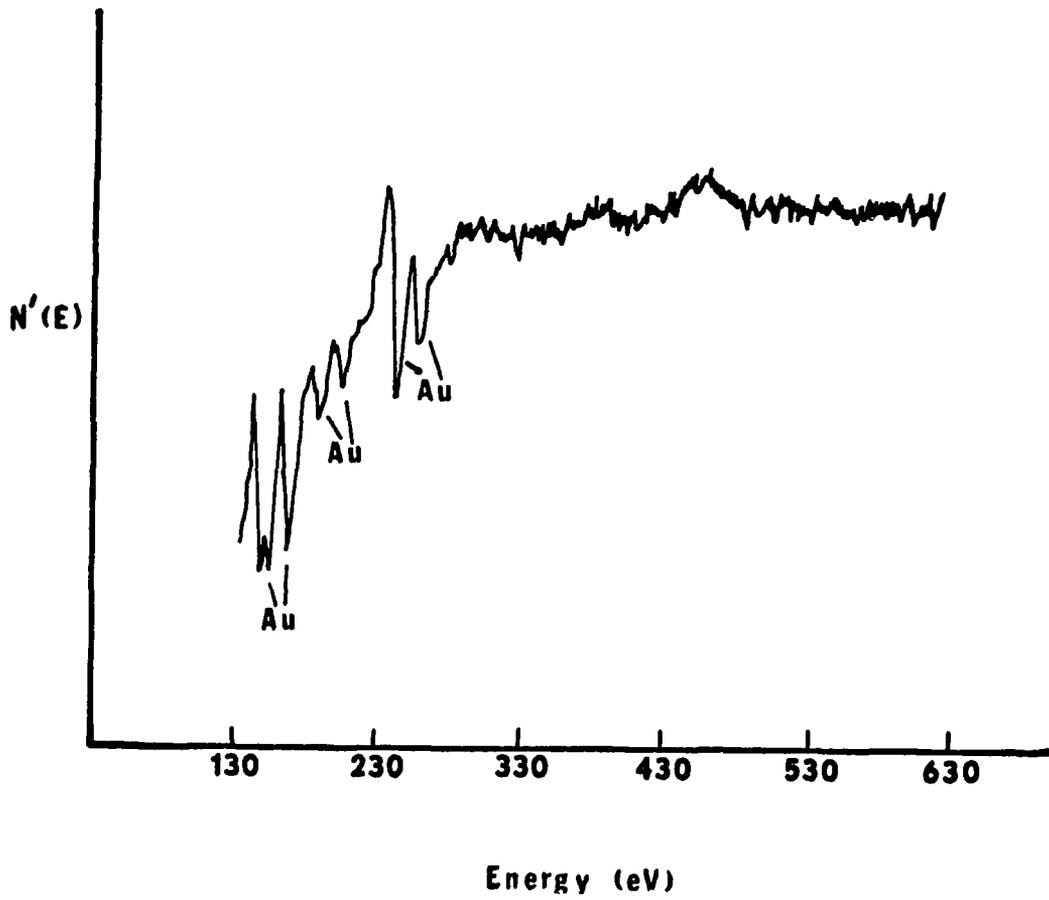
Figure 4.8 Auger spectrum of a clean Au (111) single crystal. Beam energy:
1800 eV. Beam current: 13 μA. Modulation Voltage: 10V.

ward adsorption with the common residual gases which are found in ul-tra-high vacuum. A clean sample could be left in the chamber for 1-2 days without fear of contamination while another sample was being cleaned. This permitted an electrochemical experiment to be run with more than one clean sample in the vacuum system at the same time. If a clean sample was left for more than 1 day however, it was always given a quick 15 m sputter and 30 m anneal just to ensure its cleanliness before an experiment was run.

After an electrochemical experiment and subsequent LEED-Auger examination, a particular sample had to be recleaned. This en-tailed removing the sample from the chamber and rinsing with di-lute HNO_3. Otherwise a simple sputter might not remove all of any Pb that might have been on the surface, particularly since the surface temperature may become sufficiently high to promote dif-fusion of the Pb into the Au. In the subsequent anneal the pos-sibility of forming an Au-Pb alloy is also highly probable making recleaning of the sample all the more necessary.

4.3 Solution Preparation

The electrolyte used in this work was 0.1M HF into which was dissolved 1mM $Pb(NO_3)_2$. The HF was J.T.Baker Ultrex Grade with the principle contaminants being Cl^- (1ppm) and NO_3^- (< 1ppm). Dilution of this acid reduces the impurity level by nearly 1/250 of its original value. The ultra-pure $Pb(NO_3)_2$ (anhydrous) was obtained from Research Inorganic. Pyrolyzed water was used for dilution. It is prepared by refluxing distilled water vapor

along with a stream of O_2 over a heated Pt/Pt-10% Rh gauze at $900^\circ C$ to remove organic contaminants. The distillate is then collected and re-distilled in a nitrogen atmosphere to remove dissolved O_2.

In external thin-layer cell measurements, this electrolyte showed no detectable impurity in the voltage range -0.12 to 1.9 V vs. RHE. Sweeps as slow as 1mV/s. were used to allow ample time for any impurity to diffuse to the electrode surface.

4.4 Pb Counter/Reference Electrode Preparation

The Pb counter/reference electrode mounted in the Teflon block has already been shown in Figure 4.6. The Pb electrode (purity, 99.999+%) measured ¼" in diameter and 1/8" in length and was cut from a rod obtained from Research Inorganic.

Before placing the electrode into the vacuum chamber it was rinsed several times with dilute HNO_3 to remove the oxide layer followed by pyrolyzed water. Occasionally inside the vacuum system the Pb electrode was sputtered for several minutes to remove any surface contaminants. Pb foil was placed over any exposed Teflon to prevent the sputtering of carbonaceous substances. It should be pointed out, however, that no difference was seen in the voltammetry between the sputtered and the only HNO_3 washed electrode. The electrode always remained stored in an argon atmosphere until just before an experiment was to be run. Then it was quickly removed, washed with HNO_3, and water to remove any salts left on the surface from the previous experiment placed

back in the chamber and the chamber pumped back down. After the chamber was back-filled with Ar to run the experiment the Pb electrode was rinsed several times with fresh electrolyte. This procedure apparently enabled the Pb electrode to remain contamination free.

4.5 Experimental Sequence Followed

Once one or more Au samples were clean, the following procedure was followed to perform the electrochemical experiments.

1. After the electrode surface was designated clean by LEED and AES it was transferred from the LEED/AES chamber to the electrochemical chamber.

2. The valve was closed between the two chambers and the electrode was positioned over the solution delivery chamber. All filaments were shut off at this time.

3. The 500 l/s ion pump was isolated by closing the valve and the solution delivery chamber was back-filled with high -purity argon. The chamber was usually back-filled slightly above atmospheric pressure and then allowed to return to atmospheric pressure by bleeding through the solution. This insures complete purging of the solution delivery tubes.

4. The valve separating the 110 l/s ion pump and the electrochemical chamber was closed and the chamber back-filled

to atmospheric pressure with Ar.

5. The valve separating the electrochemical and solution delivery chamber was opened.

6. The Pb electrode was rinsed several times with fresh electrolyte.

7. A small drop of electrolyte was placed on the Pb electrode and the electrode raised into the electrochemical chamber.

8. The Au single crystal electrode and the Pb electrode were brought together at a potential preset on the potentiostat to form a thin-layer cell with an approximate 10^{-2} cm gap.

9. Linear sweep voltammetry studies were then conducted.

10. The potential sweeping was stopped at the desired separation potential and the Pb electrode moved back into the solution delivery chamber.

11. If another single crystal was to be examined, steps 5-10 were repeated.

12. After the electrochemistry was completed the solution delivery chamber was valved-off and the electrochemical chamber pumped back down.

13. When a pressure of $\sim 5 \times 10^{-7}$ torr was reached (30-45 min.), the sample was transferred back into the LEED/AES chamber for examination. The pressure in the LEED-Auger chamber remained in the $10^{-9} - 10^{-10}$ torr range even during the transfer because of the low conductance between the

two chambers.

4.6 Ex-situ Thin-Layer Cell

Many electrochemical experiments were conducted in a separate thin-layer cell outside the vacuum chamber primarilly for comparison with the measurements made in the cell in the vacuum chamber and to test new counter-reference electrodes. These experiments were performed in a thin-layer cell constructed using a Mitutoyo Co. micrometer which could be read to 1/10,000 of an inch. On the end of the spindle was mounted the electrode sealed in a Teflon cylinder. The spindle was attached to one arm of a U-shaped aluminum block. On the arm opposite the spindle was mounted the other electrode also sealed in a Teflon cylinder. The whole arrangement was covered by a sterile, clear polyethylene glove. Tubes for solution delivery and purge gas and wires for the electrical connections were sealed in the fingers of the glove. A pinhole was put into the bottom finger to allow used solution and purge gas to escape.

CHAPTER 5

RESULTS

In this section will be presented the LEED/AES and linear
sweep voltammetry results for the underpotential deposition of
Pb onto four different Au single crystals: Au(111), (100), (110)
and (410) or {4(100) x (100)}. LEED and AES results for the Au
surfaces before and after the electrochemical measurements will
be reported. Before proceeding to the data obtained inside the
ultra-high vacuum chambers, some preliminary work in the external
thin-layer cell will be presented.

5.1 Preliminary Thin-Layer Results

A voltammetry curve for the UPD of Pb on polycrystalline Au
is shown in Figure 5.1. Excellent agreement is found between this
curve and that presented previously in Figure 2.4 and with that
obtained by previous work in this laboratory (32). In the cathoic
(deposition) sweep there is a broad region commencing at ∿0.45V
versus reversible Pb followed by a sharp spike at ∿0.22V. Some
substructure in each of these regions is also evident as well as
further structure at ∿0.1V near bulk deposition. Anodic to the
UPD region are found peaks due to the oxidation of the Au surface
and reduction of the oxide layer. The peak shapes in this region
agree very well with those found in earlier work by Arvia et al.

-99-
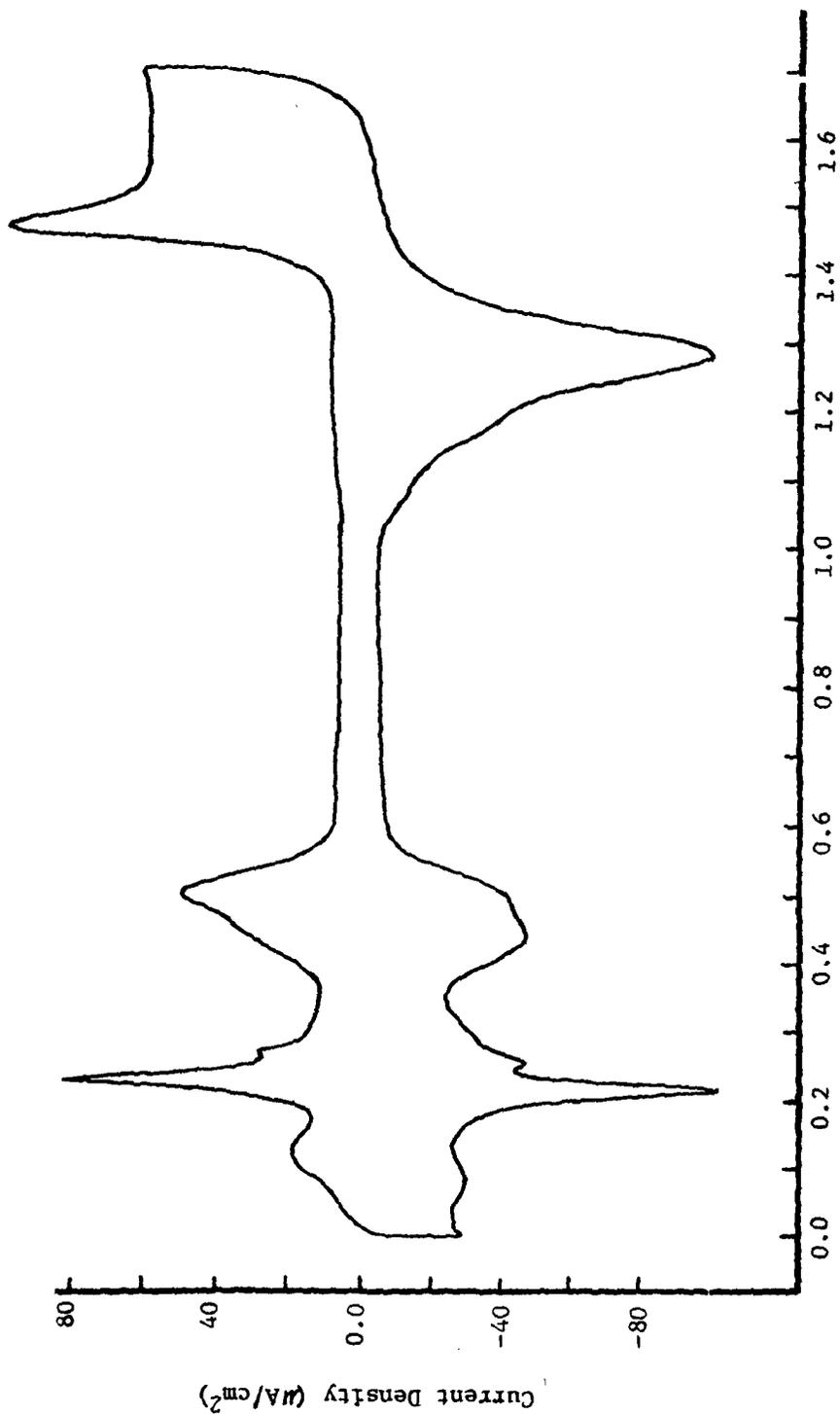
Figure 5.1 Voltammogram for the UPD of Pb on polycrystalline Au in 0.1 M HF obtained by the thin-layer technique in an external cell. Gap: 5×10^{-3} cm. Pb was generated from the Pb counter-reference electrode by holding the electrodes at the Pb/Pb^{2+} reversible potential for 1 m. Sweep rate: 50 mV/s.

(98) using a $HClO_4$ electrolyte. Both $HClO_4$ and HF are not specifically adsorbed on the electrode surface and thus exhibit very similar oxide regions when examined with voltammetry.

Sweep rate studies were also conducted on this surface. At a sweep rate of 1mV/s the process indicated by the sharp spike is completely reversible. At higher sweep rates the process becomes progressively irreversible as is indicated by a $\sim$50mV separation between the anodic and cathodic sharp spikes at a sweep rate of 200mV/s. Peak width also varies with sweep rate. The width at half-height at s=1mV/s is $\sim$10mV while at s=200mV/s it is $\sim$50mV. The broad deposition region at $\sim$0.45 V also shifts with sweep rate but the process indicated by this peak is not reversible in the region s=1 - 1000mV/s. At fast sweep rates both the anodic and cathodic portions of this broad peak become larger in height than the sharp spike. This is due to broadening of the spike at the faster sweep rates.

The dependency of peak position on sweep rate was also used to obtain information on the mechanism of UPD. Srinivasan and Gileadi (99) have shown that for an irreversible adsorption reaction where the net rate can be taken as nearly equal to the forward rate, the peak potential E_p should vary with the sweep rate (s) according to the equation

$$E_p = \frac{RT}{\gamma \beta F} \ln \frac{k \gamma \beta F}{k_1 RT} + \frac{RT}{\gamma \beta F} \ln s \qquad (5-1)$$

where k is the charge needed to form a monolayer of adsorbate.
Plots of E_p versus $\ln \beta$ for the peaks at ~ 0.45V and ~ 0.22V for the
cathodic sweep are shown in Figures 5.2 and 5.3. The linear re-
gion of the sloping portion of the curve should have a Tafel
slope $= RT/\gamma \beta F$ if an adsorption process is at work. Using
these Tafel slopes and assuming β, the transfer coefficient, is
equal to 0.5, the charges transferred through the external cir-
cuit per Pb ion that is adsorbed (γ) is calculated to be 1.4
for the first, large adsorption peak and ~ 2 for the sharp spike.
The assumption that $\beta = \frac{1}{2}$ is open to question and hence the values
of the apparent charge transferred are provisional. Nonetheless,
if the rate controlling step for the first adsorption peak is
simply the ion adsorption step with the simultaneous removal of
a single water molecule, then perhaps the value of 1.4 does have
some significance in view of the earlier discussed mechanism
proposed that this peak corresponds to partial charge transfer
to form an adion of intermediated charge. The sharp peak, cor-
responding to the proposed phase change, probably has kinetics
too complex for the apparent charge value to have direct sig-
nificance.

The intercept of the linear region of the plots in Figures
5.2 and 5.3 with the reversible peak potential is a measure of
the exchange current density. A comparison of these intercepts
indicates that the apparent exchange currents for both peaks are
relatively close in value (within a factor of ~ 2 of each other).
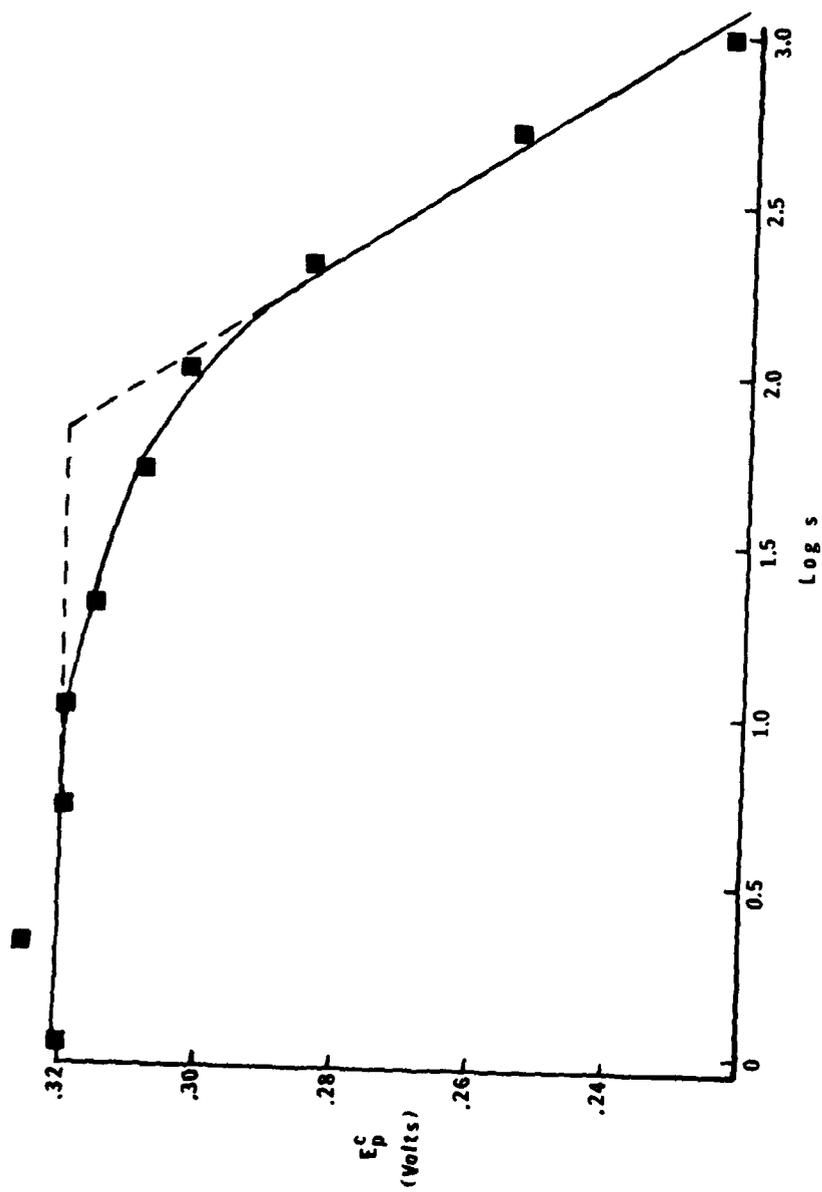
Figure 5.2 Plot of the logarithm of the sweep rate (s) versus the peak potential of the initial cathodic Pb adsorption peak in Figure 5.1. The voltages are referenced to the reversible hydrogen electrode.
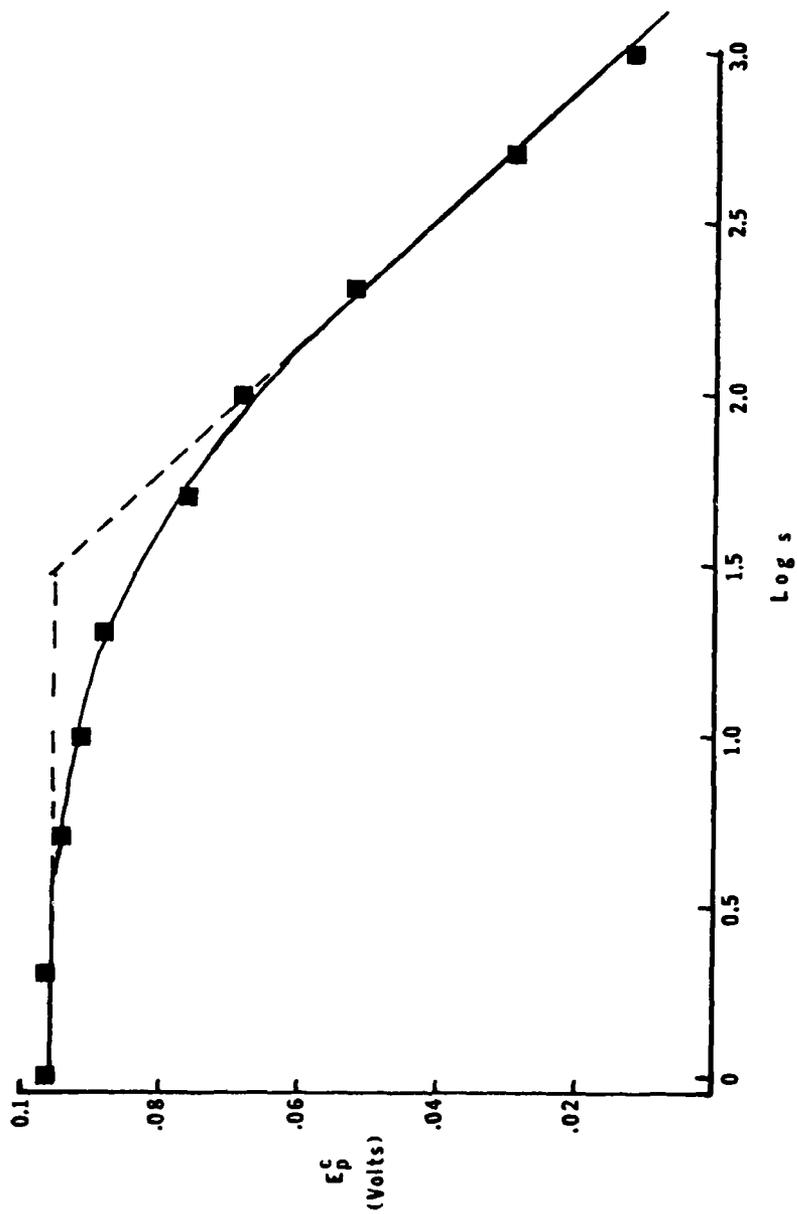
Figure 5.3 Plot of the logarithm of the sweep rate (s) versus the peak potential of the sharp cathodic Pb adsorption peak in Figure 5.1. The voltages are referenced to the reversible hydrogen electrode.

This is somewhat surprising.

5.2 LEED/AES Results for Clean Au Single Crystals

An Auger spectrum of a clean Au sample has already been shown in Figure 4.8   Typical LEED patterns for each of the four clean single crystal are shown in Figure 5.4. The patterns for Au(100), (110) and (111) are those expected for the clean crystal. These have been described previously in Chapter 3. The spots for Au (111) are broad and some splitting is evident but not quite as pronounced as has been reported earlier (40,69). The splitting is probably a function of surface preparation as two other groups have reported simple hexagonal patterns for this surface (67,68). There is very little diffuse scatter indicating that the surfaces are perfect, at least within 100-200 $\overset{o}{A}$, the coherence width of the electron beam.

To this author's knowledge, this is the first time the Au (410) surface has been studied with LEED. As previously mentioned this surface is composed of terraces of (100) orientation four atoms in width separated by steps of (100) orientation one atom in width. In stepped-surface notation, this surface is called Au - S - {4(100)x(100)}. Models showing top and side views are shown in Figure 5.5. The LEED pattern for this surface contains the same spot orientation as that found for Cu(410) obtained by Perdereau and Rhead (100). Copper, like gold, is also face-centered cubic. The spot pattern for Cu(410) is interpreted
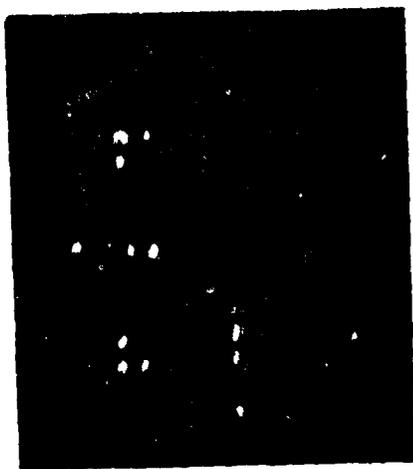
Au(100) - (5x20), 54 eV
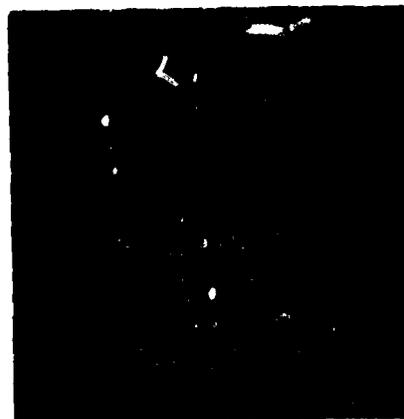
Au(110) - (1x2), 68 eV

Au(111) - (1x1), 58 eV
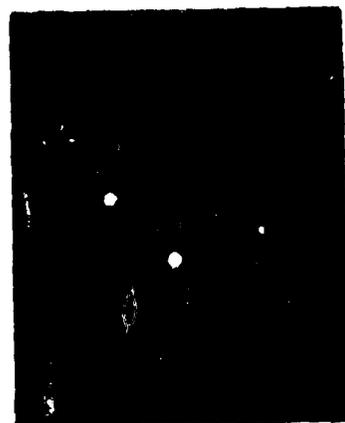
Au(410) - (1x1), 48 eV

Figure 5.4. LEED Patterns for Clean Au Single Crystals.
            Film: Polaroid 107. f-setting: 4.7. Exposure
            time: 3 m.
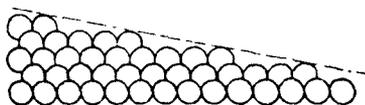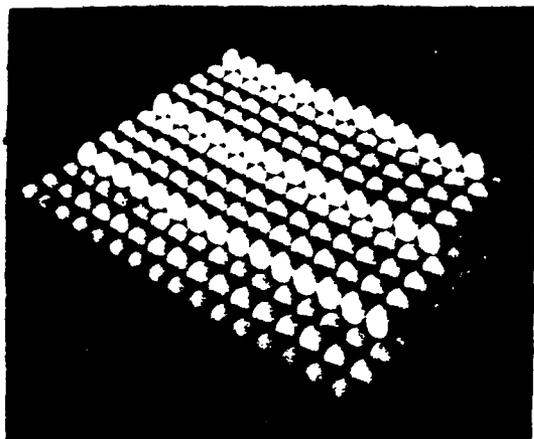
Figure 5.5 Top and side views of the
stepped Au-S-[4(100)x(100)]
surface. Taken from refer-
ence (100).

as that expected from a clean, unreconstructed surface. The origin of the LEED pattern, particularly the pairs of spots or doublets found in every other vertical row of spots, was described by kinematic analysis. The doublets always found in the diffraction patterns for stepped surfaces are aligned in a direction corresponding to the normal to the step direction and the distance between the spots in a given doublet is inversely proportional to the average internal between atomic steps in the crystal.

5.3 Voltammetry Curves for the UPD of Pb onto Au Single Crystals

In nearly all the voltammetry curves presented below, the Au single crystal and Pb counter-reference electrode were brought together at a potential of either +0.6 or +0.7 V versus Pb_{rev}[1]. In this region no other process occurs except charging of the double layer. In a few instances the electrodes were brought together at 0.0V which corresponds to the Pb bulk deposition potential. The initial potential will be noted on all figures. For none of the curves shown here will the electrodes have seen a potential more positive than 0.7V. For all curves the electrolyte was 0.1 M HF and 10^{-3} M $Pb(NO_3)_2$.

---

[1] All potentials reported in this work are those set on the potentiostat. A setting of 0.00V was designated as the Pb/Pb^{2+} reversible potential since this potential marked the beginning of bulk Pb deposition.

5.3.1 Au(110)

Shown in Figure 5.6 is the voltammetry curve for the Au(110) surface. The initial potential was 0.0V and the sweep rate 50mV/s. Besides the difference in current density the similiarity between the curve and that for polycrystalline Au (Figure5.1) is quite striking. Changing the initial potential to 0.7V does very little to alter the curve as shown in Figure 5.7 for a sweep rate of 20mV/s. The potential was increased in the cathodic direction in 0.1 V intervals to a final potential of 0.1 V vs. Pb_{rev}. Some shift is seen in the first deposition peak; otherwise there is very little change.

5.3.2 Au(100)

In Figure 5.8 is shown the curve for Au(100) with s=50mV/s and the initial potential set at 0.0 V. This extremely interesting curve has three principle regions in the cathodic sweep: a small, broad deposition peak at $\sim$0.42 V (Peak 1) which may or may not have a reversible counterpart; a very large, sharp spike at $\sim$0.25 V (Peak 2) which appears to be indicative of a highly irreversible process; and another smaller spike at $\sim$0.15 V (Peak 3) which has a nearly reversible counterpart (Peak 3').

The extreme difference between the Au(100) and Au(110) surfaces is indicated in Figure 5.9. The shape and arrangement of Peak 3 and 3' appear to be the same as the spikes seen on the (110) surface except their potential is shifted some 100 mV anodic.
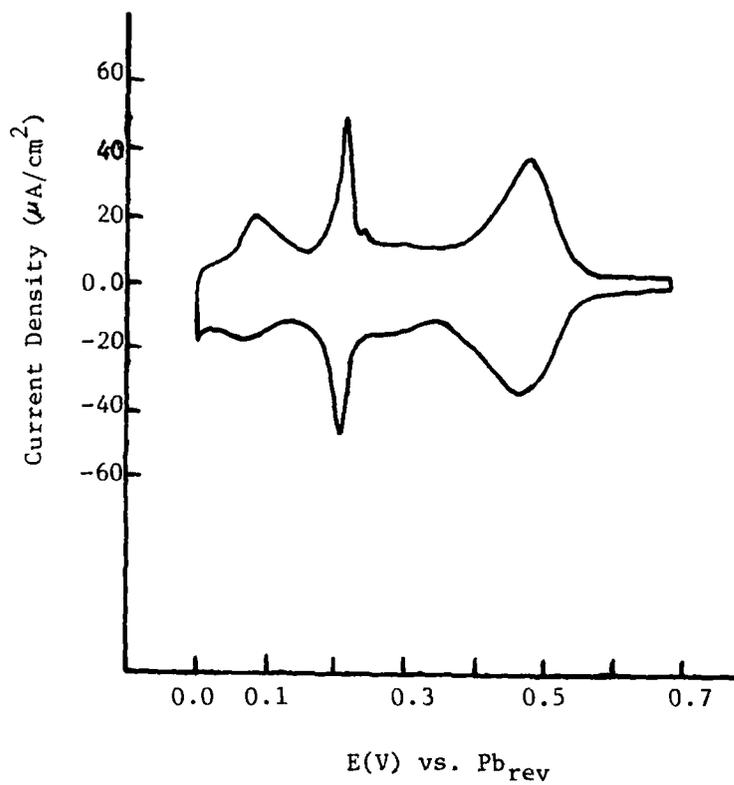
Figure 5.6   Voltammogram for the UPD of Pb on Au(110)-
(1×2) in 0.1 M HF + 1 mM $Pb(NO_3)_2$. Sweep
rate: 50 mV/s. Initial potential: 0.0V.

Figure 5.7 Voltammograms for the UPD of Pb on Au (110)-(1x2)
in 0.1M HF + 1 mM Pb (NO$_3$)$_2$. Sweep rate: 20 mV/s.

Initial potential: 0.7 V. Electrode cycled cathod-
ic in 0.1 V steps.
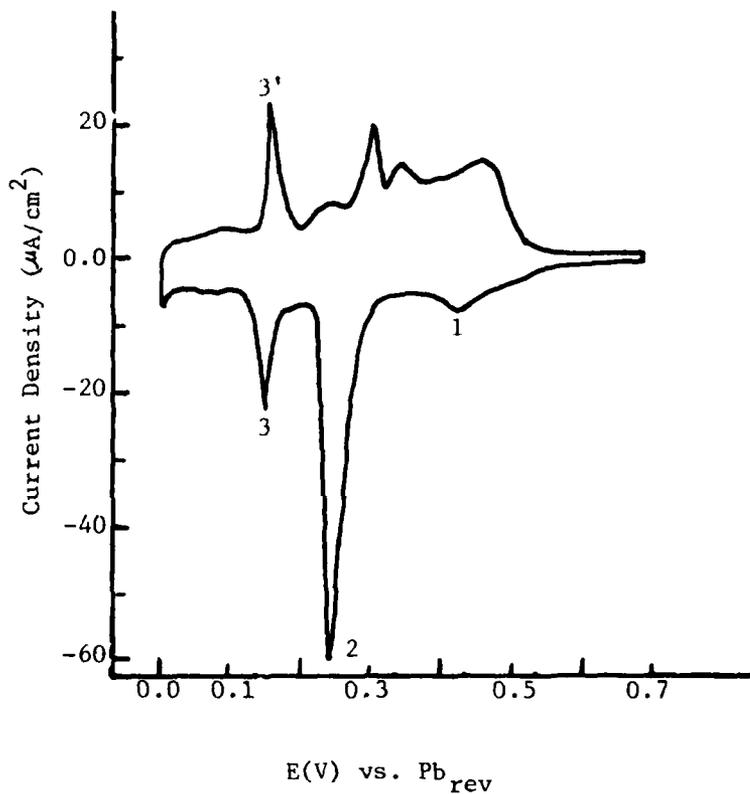
Figure 5.8 Voltammogram for the UPD of Pb on Au(100)-(5x20) in 0.1 M HF + 1mM Pb(NO$_3$)$_2$. Sweep rate: 50mV/s. Initial potential: 0.0 V.
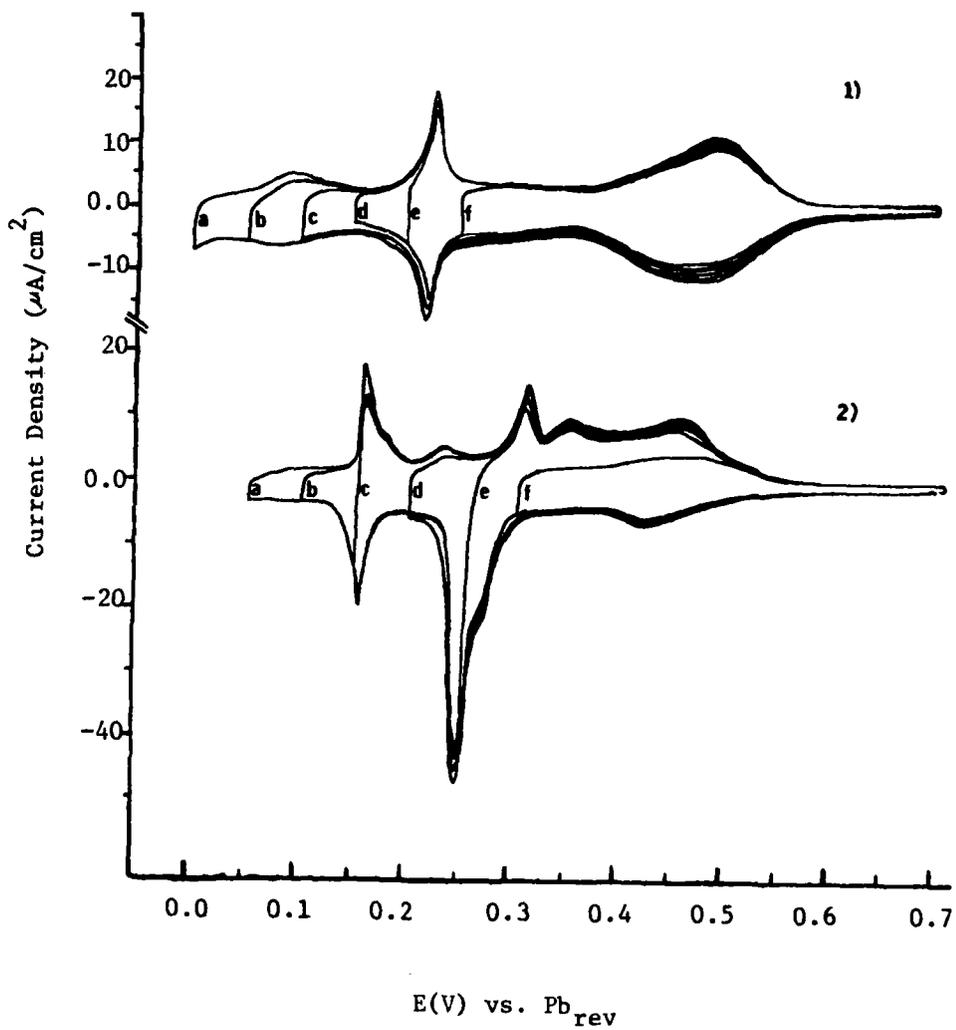
Figure 5.9 Voltammograms for the UPD of Pb on 1) Au (110)-(1x2) and 2) Au (100)-(5x20) in 0.1 M HF + 1mM Pb(NO$_3$)$_2$.

Sweep rate: 20 mV/s. Both electrodes initially at 0.0 V.

Otherwise, the curves are quite dissimilar. The expanded curve in Figure 5.9 also indicates some substructure in both Peak 2 and Peak 3'. Also, from changing the potential limits, the anodic counterpart to Peak 2 is manifested in three, separate, extremely irreversible peaks (compare sweeps e and f).

Reduction of the sweep rate to 2mV/s for the (100) surface produces the curve shown in Figure 5.10. The substructure in Peak 2 and 3' is now quite evident. Peak 2 is seen to be composed of two sharp spikes while Peak 3' is the composite of at least three very narrow spikes. To obtain such fine structure requires very slow sweep rates. The predominate spike in Peak 3' has a width at half-height, δ, of only ~ 1 mV. Peak 3 shows none of this structure and has a δ value of ~ 5mV. Another interesting feature of the curve in Figure 5.10 is the appearance of a new peak between Peak 2 and 3 which has a nearly reversible counterpart.

Figure 5.11 indicates the effect of expanding the sweep in the cathodic limit at the higher sweep rate of 20mV/s. The decrease in deposition current in the voltage range 0.7 to 0.3 V with increased sweep limit suggests that there is a "memory" effect operative here where the surface "remembers" its prior treatment in the previous sweep. Also, in the next to last sweep a shoulder is obtained on the left side of Peak 2 which disappears in the next sweep.

Additional curves for this surface are shown in Figure 5.12
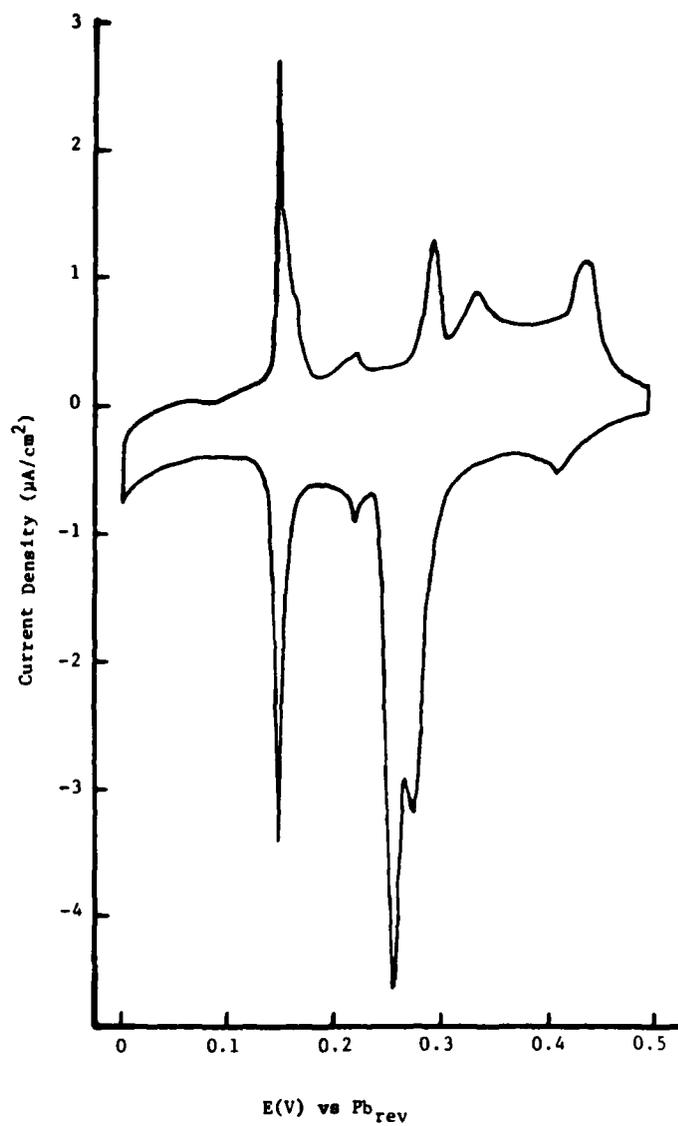
Figure 5.10   Voltammogram for the UPD of Pb on Au(100)-(5x20) in 0.1 M HF + 1mM Pb $(NO_3)_2$. Sweep rate: 2 mV/s. Initial Potential: 0.0V.
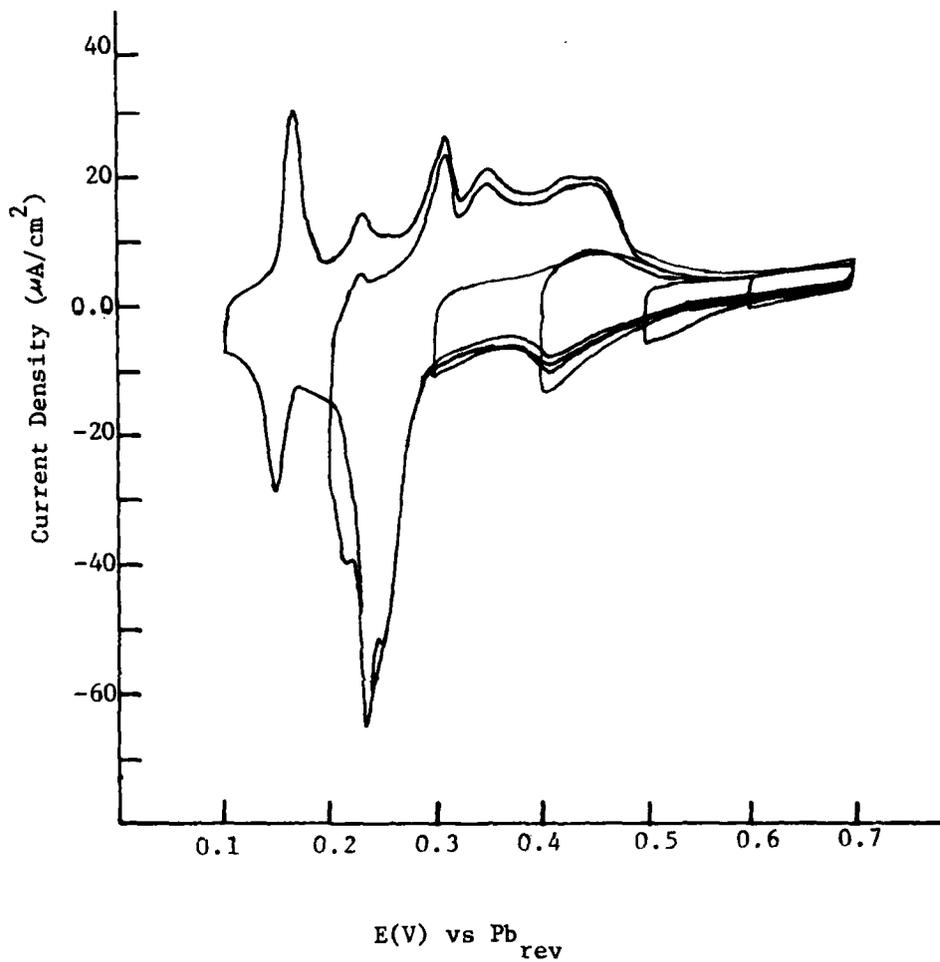
Figure 5.11 Voltammograms for the UPD of Pb on Au(100)-(5x20) in 0.1 M HF + 1mM Pb(NO$_3$)$_2$. Sweep rate: 20 mV/s. Initial potential: 0.7 V. Electrode swept cathodic in 0.1 V steps.
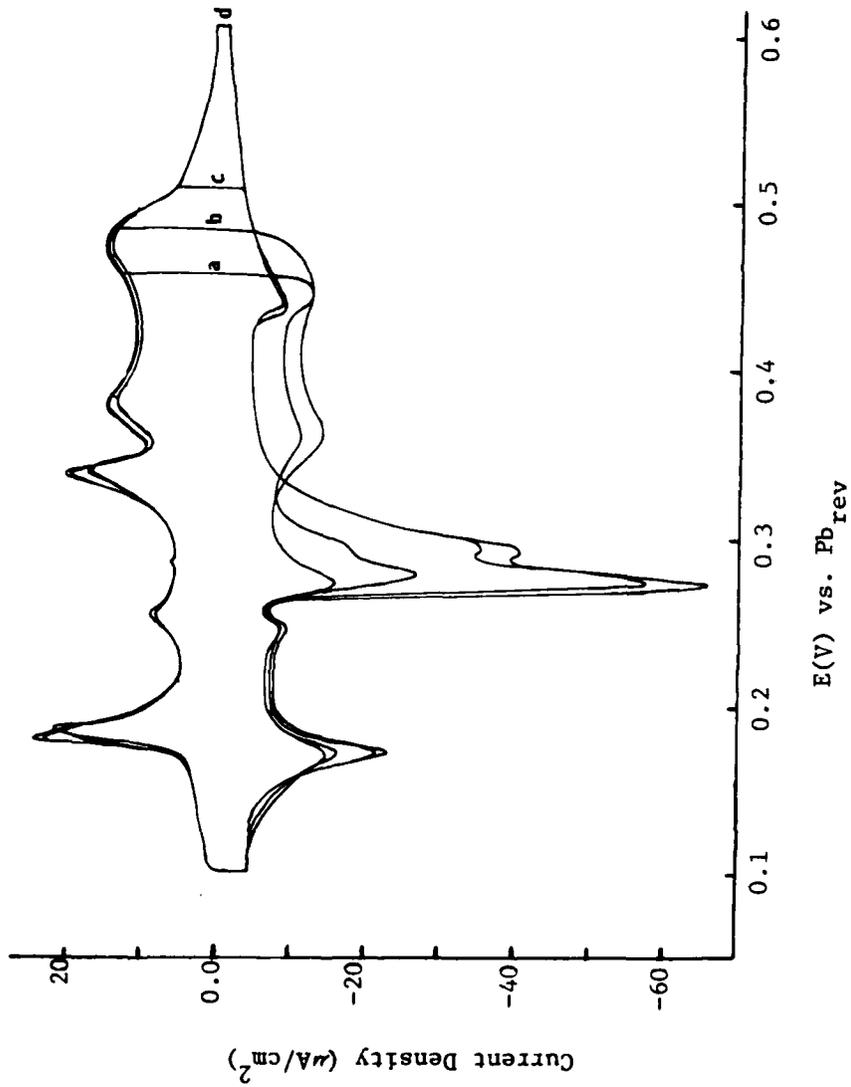
Figure 5.12 Voltammograms for the UPD of Pb on Au(100)-(5x20) in 0.1 M HF + 1mM Pb(NO$_3$)$_2$. Sweep rate: 20 mV/s. Electrode initialized at 0.0 V.

where the anodic limit was varied at 20mV/s. An unusual phenomena
is depicted in sweeps a and b. The incomplete removal of a small
amount of Pb produces an enhanced initial deposition current which
is compensated for by a decrease in Peak 2 and, to a lesser extent,
Peak 1. A new peak between Peaks 1 and 2 also develops. These
peaks are evidently strongly influenced by the structure of the
surface as they are only obtained on the nearly adsorbate-free
Au surface as indicated by curves c and d. More will be said
about this when the LEED results are summarized at the end of this
chapter.

5.3.3 Au(111)

Voltammograms for the UPD of Pb on Au(111) are shown in Figure
5.13 for s=20mV/s and an initial potential of 0.7 V. Curve d
covers the voltage range 0.1 to 0.7 V while curve b was taken
from 0.1 to 0.5 V. Missing from these curves is the broad ad-
sorption region usually seen at $\sim$0.45 V on the other surfaces.
An extremely small amount of Pb adsorption takes place on this
surface until a potential of $\sim$0.24V is reached (Peak a). At
this potential a sharp peak is obtained with δ=10mV for curve
2. Some small "bumps" are visible both in the deposition and
stripping portions of curve d. They are, however, quite real as
shown in curve 2 where the small amount of Pb left on the surface
by terminating the voltage scan at 0.5V has a large effect on
the deposition profile. The anodic profile is not affected by this.
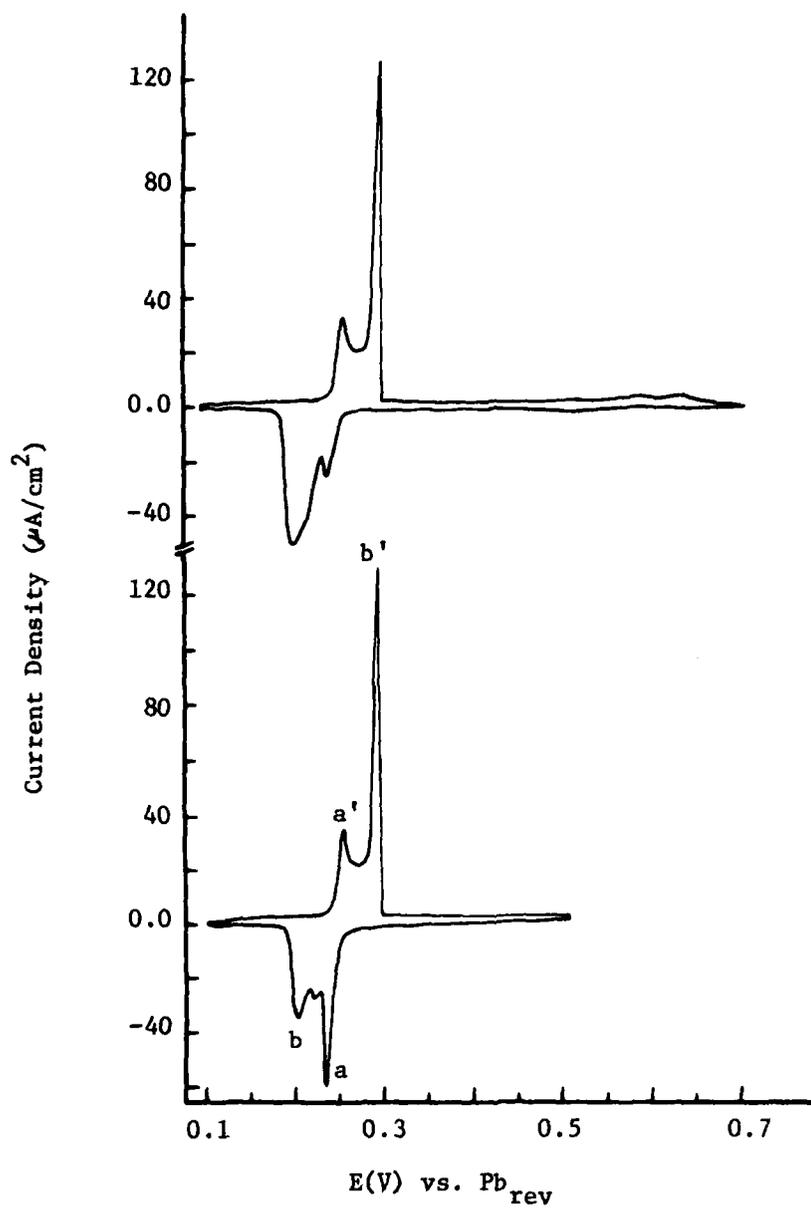
Figure 5.13 Voltammograms for the UPD of Pb on Au (111)-(1x1) in
0.1 M HF + 1mM Pb(NO$_3$)$_2$. Sweep rate: 20 mV/s. Elect-
rode initialized at 0.7 V.

The anodic portion of the curves contains two peaks, a' and b', which are quite sharp. For the case of Peak b', the value of δ is $\sim$7.5 mV. The UPD process occuring on this surface is quite irreversible as indicated by the large voltage shift between the peak structures in the anodic and cathodic sweeps. Out of all four single crystals studied this is the only surface that has no cathodic and anodic peaks that are reversible counterparts.

In an attempt to match each deposition peak with its corresponding stripping peak for the (111)surface, sweep studies which progessively increased the cathodic limit were undertaken (Figure 5.14). As is shown by sweep d Peaks a and a' are associated with each other although there is some contribution from Peak a over the entire stripping potential range. As the potential is swept more cathodic (sweeps e and f) further growth of Peak a' occurs and a third peak between a' and b' becomes visible. This third peak nearly disappears when the voltage is swept to 0.1 V.

The deposition portions of Figure 5.14 for sweeps e-g exhibit unusual behavior. There is a surface "memory effect" at work here where the surface somehow remembers that the previous sweep was not taken through the entire deposition range. Even sweep g has not returned to the normal sweep deposition profile as shown in Figure 5.13 although it covers the range of 0.1 -0.5V. Certainly some type of surface structure change is occurring

The effect of sweep rate is demonstrated in Figure 5.15. The i-E axes apply only to the curve for s=10mv/s. The potential
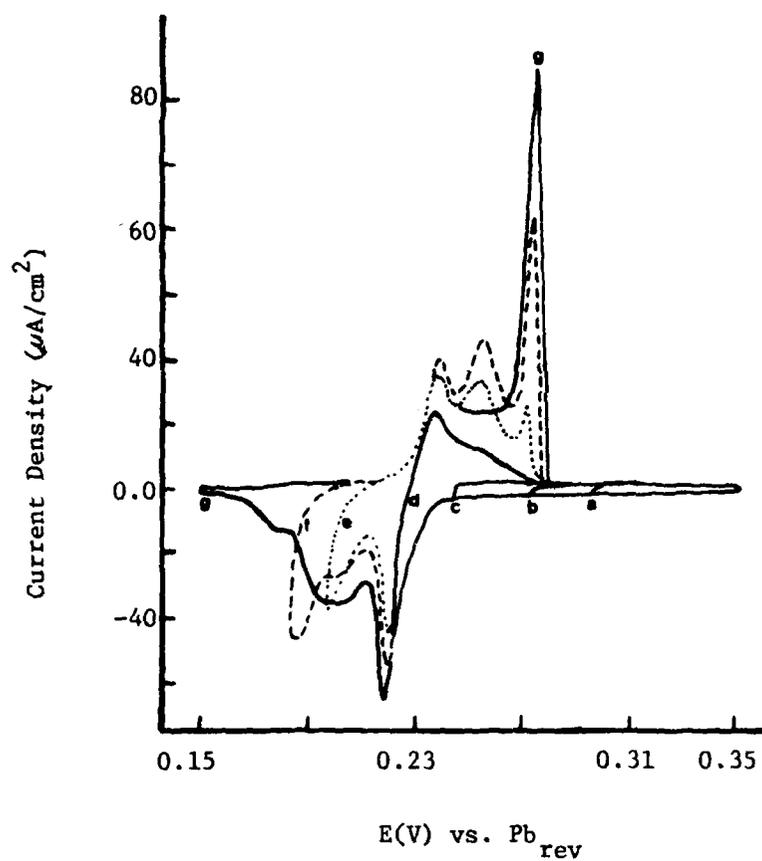
Figure 5.14 Voltammograms for the UPD of Pb on Au (111)-
(1x1) in 0.1 M HF + 1mM $Pb(NO_3)_2$. Sweep rate
20 mV/s. Initial potential: 0.7 V.
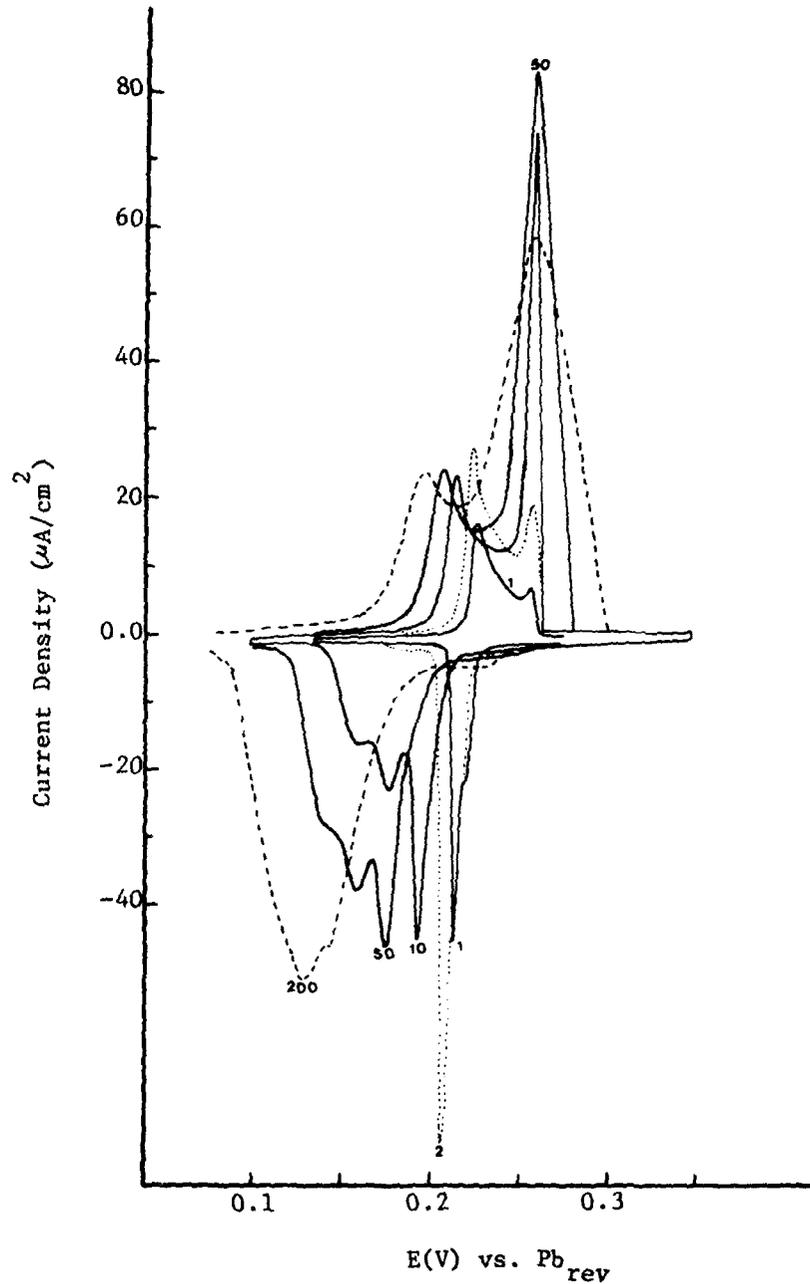
Figure 5.15 Voltammograms for the UPD of Pb on Au(111)-(1x1)
in 0.1 M HF + 1mM Pb(NO$_3$)$_2$ at various sweep rates. All curves
have been adjusted to that for 10mV/s by placing the last anodic
peak at the same potential. X and Y scales apply only to
s=10mV/s. Current scale can be adjusted by multiplying by
the following factors: 0.25 for s=1 and 2mV/s, 2.5 for
s=50mV/s and 5.0 for s=200mV/s.

axis for each has been adjusted so that Peak b' is at the same
absicissa value for all sweeps. At 1mV/s both the anodic and
cathodic sweeps have changed a great deal. The deposition region
has been reduced to one very sharp spike (δ=4mV) with a small
shoulder. The shoulder probably represents part of the structure
that was previously to the left of Peak a'. At s=2mV/s this
structure is almost completely merged with Peak a' causing
an extremely large Peak a' to develop. At s=5mV/s, the sweep
profile returns to that seen in Figure 5.13. In the anodic por-
tion Peak a' is now larger than b' since Peak b has nearly dis-
appeared. Also interesting is the fact that even at this slow
sweep rate the process indicated by Peaks a and a' is still not
reversible.

Increase in sweep speed causes all of the peaks to broaden.
At s=200mV/s Peak b' has a half-width of nearly 50mV while Peak
a' is nearly blended into the other deposition structure causing
a continuous potential range at which the deposition process oc-
curs.

Of particular interest is the sharpness or relatively small
amount of curvature in the transition region for Peak b' (right
side) to the background current. Even at very slow sweep rates
the transition on right side of this peak is still quite abrupt.
The behavior is almost that of a delta function.

5.3.4 Au(410)

This surface was chosen for two reasons. First, since poly-

crystalline samples are composed of mixtures of many different structures, stepped surfaces may be a better approximation of the real structure of a polycrystalline surface than low index planes. Stepped surfaces are known to be more active towards adsorption at least in some instances than their low index counterparts (e.g., see reference 101). Second, the large deposition peak occurring on the (100) surface was thought to be a result of the reconstructed hexagonal overlayer which gives rise to the (5x20) LEED pattern for this crystal. For the Au(410) surface this reconstruction is not possible due to interruption of the (100) structure by steps every four atomic rows. Adsorption on the terraces should be occurring on the square (1x1) primitive mesh of (100) orientation rather than the reconstructed (5x20) mesh.

A voltammetry curve for this surface at s=50mV/s is shown in Figure 5.16. There are no sharp peaks as found on the previous surfaces. It appears that the processes responsible for the sharp spike-like voltammetry peaks on the other surfaces (including well-cycled polycrystalline Au) are greatly hindered on this stepped-surface. Most of the structure found is broad and ill-defined with some of the peaks composed of two or more overlapping peaks. Adsorption commences at ~0.6 V, much earlier than any of the other surfaces. Also structure is found much nearer the Pb reversible potential.
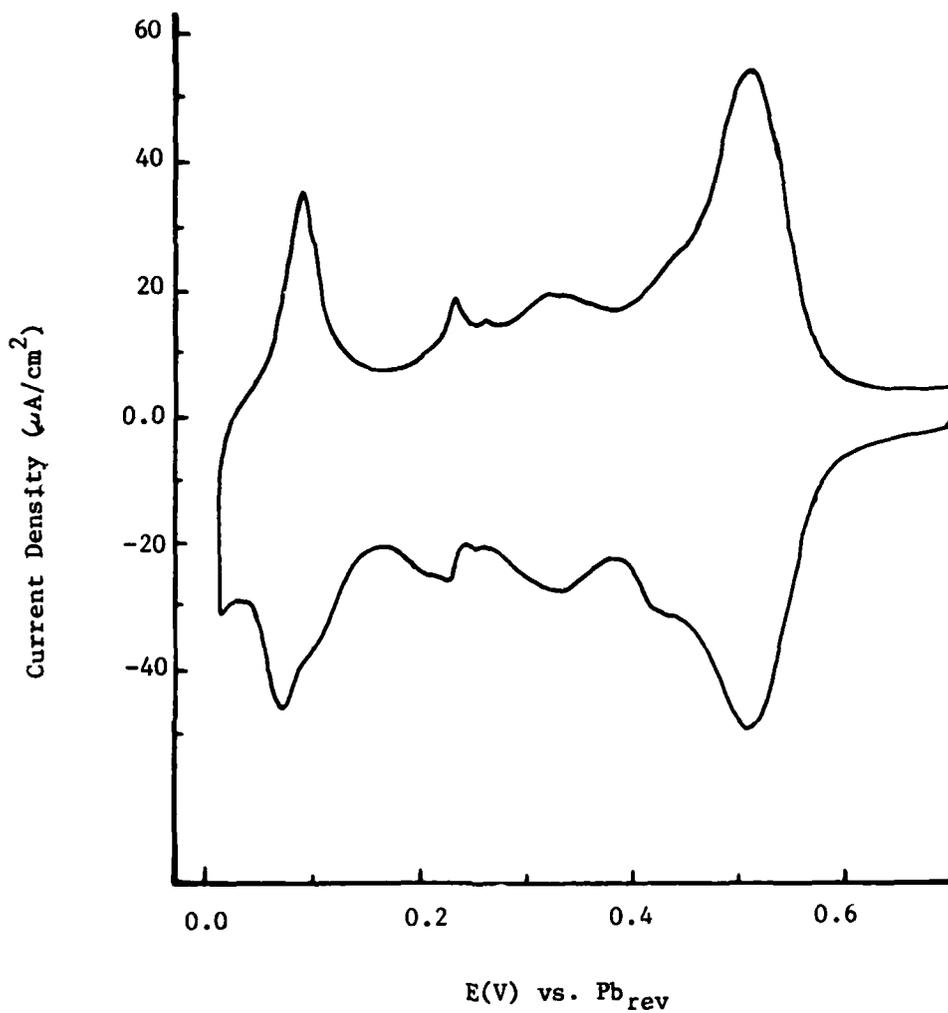
Figure 5.16 Voltammogram for the UPD of Pb on Au (410) in 0.1 M HF + 1mM Pb(NO₃)₂. Sweep rate: 50mV/s. Initial potential 0.7 V. Swept to 50 mV.

Progessive cathodic sweeps from an initial potential of 0.7 V
are shown in Figure 5.17. Comparison of this curve with Figure
5.16 indicates that nothing unusual has occurred by varying the
cathodic limit.

5.4 Post-Examination of the Electrodes With AES and LEED

Before and after Auger spectra for Au(110) are shown in Fig-
ure 5.18a and b. The initial electrochemical potential was potent-
iostated to 0 V $\pm$ 0.001 V for approximately 10s.[1] Electrochemical
experiments consisting of approximately 30 cycles between 0 and
0.70 were then performed on this surface. The cycling was then
finally stopped at 0.050V on the cathodic sweep and the electrode
subsequently removed to the LEED-AES chamber. At this separation
potential approximately 0.6 of a monolayer of Pb (as measured from
the charge under the voltammetry peaks) was on the surface.

Using the minimum in the derivative Auger spectrum as an in-
dication of the species, the "after" spectrum in Figure 5.18 in-
dicates a new "peak" at $\sim$270eV. Two possible species on the

---

[1] Thermodynamically bulk lead is expected to deposit at this
potential. It is rather unlikely that Pb crystals formed because
of the overpotential expected for the nucleation of such crystal-
lites. More likely is the completion of the monolayer or the
formation of a second layer of Pb on the initial monolayer, and
possibly surface alloy formation. The choice of the reversible
bulk Pb potential seemed appropriate at the time of the experi-
ments but in retrospect there are uncertainties as to what to
expect for the surface condition at this potential.
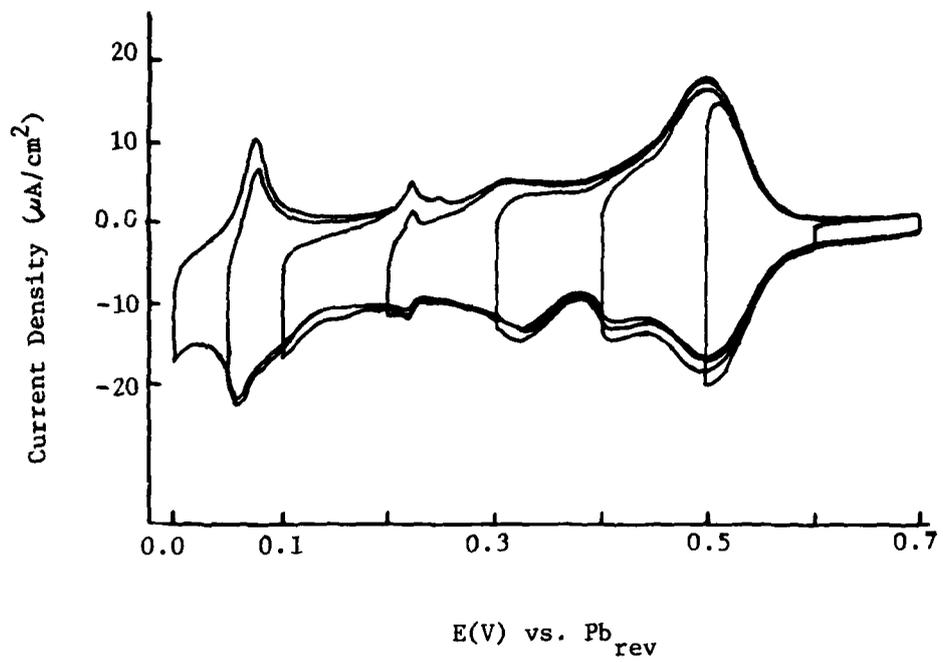
Figure 5.17 Voltammograms for the UPD of Pb on Au(410) in 0.1 M
HF + 1mM Pb(NO$_3$)$_2$. Sweep rate: 20 mV/s. Initial
potential: 0.7 V.
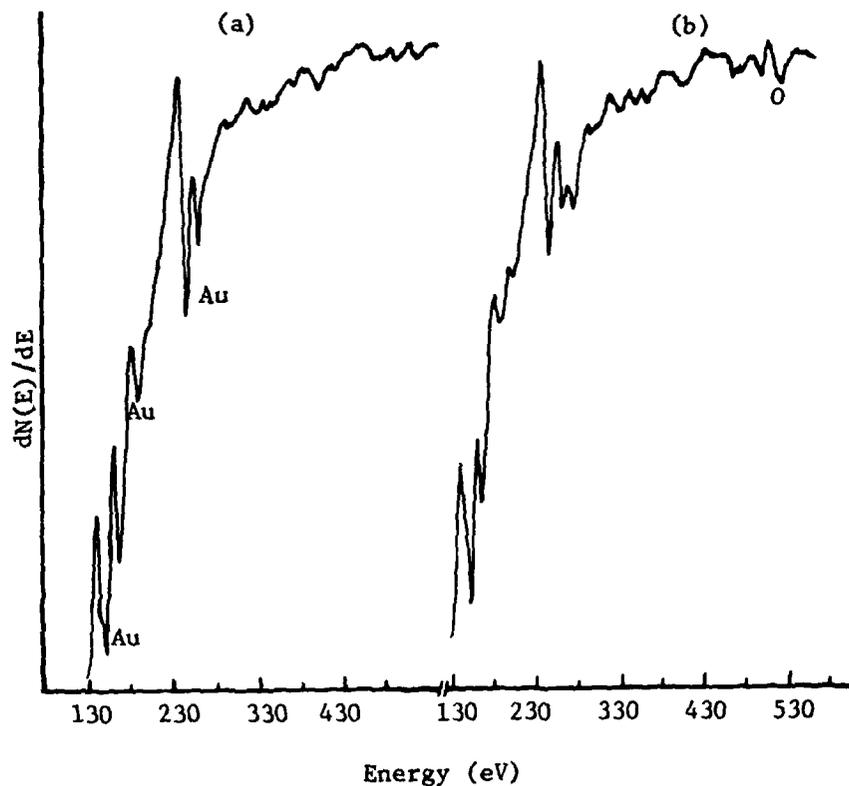
Figure 5.18 a. Auger spectrum of a clean Au(100) single
crystal. Beam energy: 1800 eV. Beam
current: 13μA. Modulation voltage:
10 V.

b. Same surface and conditions as a except
crystal subjected to electrochemical
treatment. The electrode was initialized
at 0.0 V and cycled approximately 20 times
between 0 and 0.7 V. It was removed from
the thin-layer cell at 50 mV on the cath-
odic sweep.
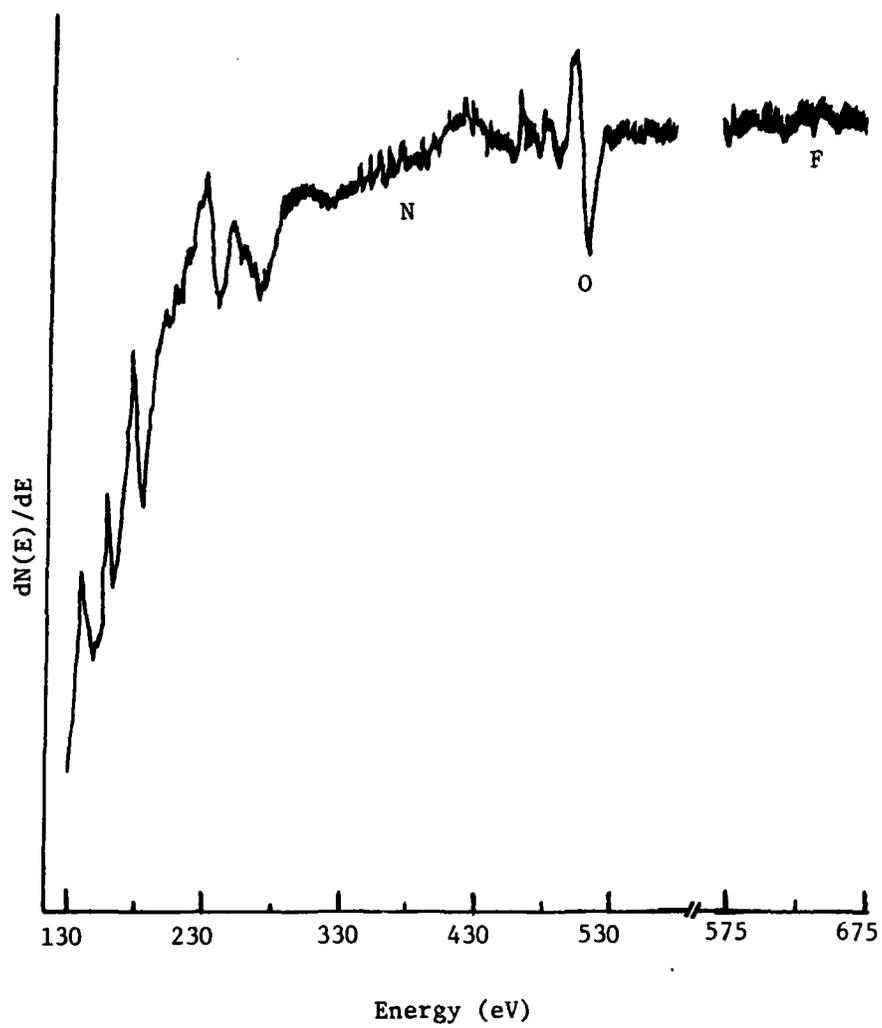
Figure 5.18 c. Au(100) surface with same condition as in b, except electrode was removed from the cell at 0.7 V.

electrode surface could be responsible for this derivative peak:
Pb with a transition at ~267 eV or carbon with an Auger transition
at ~272 eV. Unfortunately the Auger peak intensities for Pb are
low and those peaks of appreciable intensity nearly overlap with
those of gold (see list of Auger transitions below and Figure 5.19).

Pb	Au
90eV	95eV
94	
130	141
181	184
249	239
267	255

The quality of the signal in Figure 5.18b and the intrinsic width
prevent establishing whether lead or carbon is responsible for this
peak. Since it is quite certain that Pb was on the surface near
monolayer level, it is reasonable to assume this peak is due to
Pb.

The peak at ~200 eV is more pronounced in the "after" than
"before" spectrum but it appears to be associated with gold. In
repeat Auger spectral scans on the same crystal surface variability
was observed in the magnitude of this peak equivalent to that evi-
dent in the comparison of the two curves in Figure 5.18 a and b.
The source of this variability is unexplained.

If the new peak at ~270 eV is due to Pb it is shifted some
3 eV from the 267 eV peak for bulk Pb. This is a large shift for
Auger but not improbable as there appears to be some oxygen in the
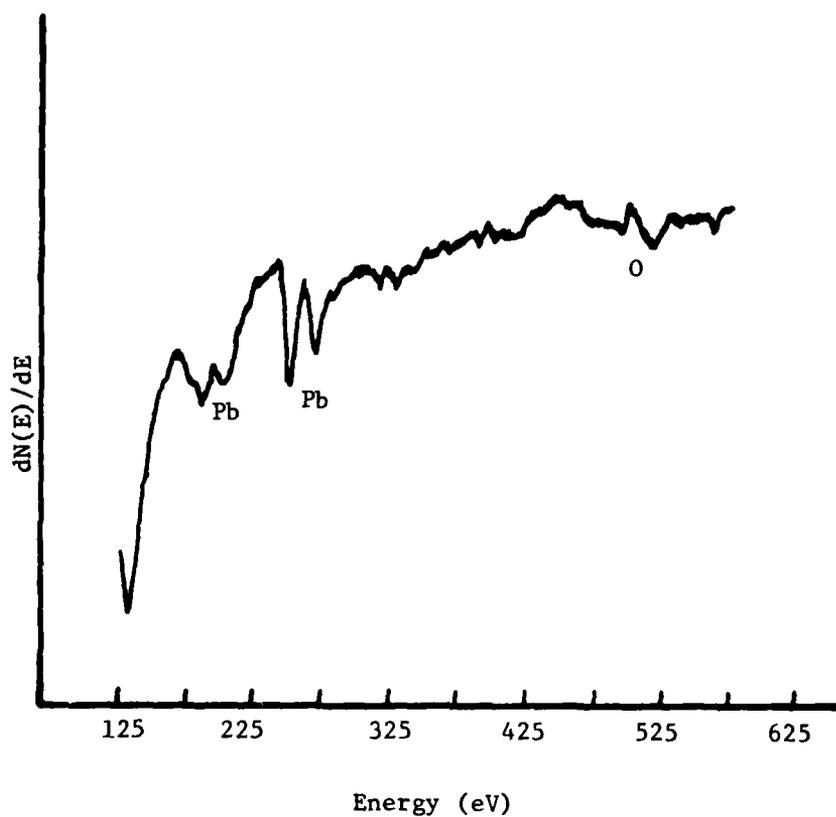
Figure 5.19   Auger spectrum of polycrystalline Pb foil.
             Same conditions as in Figure 5.18a.

overlayer which may be in the form of PbO_x. Often a fairly large

O signal was found especially when the electrodes were pulled

apart in the double layer region (see Figure 5.18c) and the $\sim$270 eV

peak is also present while the intensity of the Au peaks are very

much reduced.[1] Also noticeable in this spectrum is the enhanced

peak over that of Au at 182 eV. There is a Pb but not a carbon

transition near this voltage. Since gold oxide cannot form in

the potential regimes used in this work and water does not re-

act with gold at room temperature to form an oxide layer (68),

it must be assumed that there is residual Pb and O on the surface.

The Auger spectrum never showed the presence of either N (from

$Pb(NO_3)_2$) or F (from HF), suggesting that the layer is composed of

lead oxide produced as a hydrolysis product when HF and HNO_3 were

evaporated off the surface during pump-down. This lead oxide lay-

er is probably patch-like or, possibly, in the form of crystal-

lites blocking only a relatively small fraction of the surface

as a reasonable LEED pattern was obtained from both of the sur-

faces in Figure 5.18 b and c.

---

[1] The spectrum in Figure 5.18c was obtained using a borrow-
ed lock-in amplifier which produced a slightly noisier signal than
the PARC 128A used to obtain Figures 5.18 a and b. The PARC
128A was being repaired at the time thus necessitating the use
of the other lock-in.

The evidence presented above strongly suggests that the ~ 270 eV peak is due to Pb on the Au surface. If, however, the 270 eV peak is due to carbon the quantity present is very small. To calculate the atomic concentration X_i of element i in terms of the measured Auger current I_i Chang's equation(52)

$$X_i = \frac{\alpha_i I_i}{\sum_j \alpha_j I_j} \qquad (5-2)$$

can be used where j runs over all elements present and the α's are inverse sensitivity factors defined by

$$\alpha_i I_i^o = I_s^o \qquad (5-3)$$

The superscript o indicates the pure element and s is an arbitrarily chosen standard element. Using Chang's α-values for C and Au obtained with a CMA provides a value of $X \lesssim 0.1$ monolayer for the curve shown in Figure 5.18b. The use of α-values determined by a CMA is not strictly valid for results obtained with a RFA so that X_i values obtained in this way are only approximate. Since the peak at ~ 270 eV was generally smaller than that shown in Figure 5.18b, the amount of carbon is never much above $\lesssim 0.05$ monolayer. Unfortunately sensitivity factors do not exist for Pb to allow the same type of calculation to be performed.

Several of the LEED patterns obtained after electrochemical treatment are shown in Figures 5.20 through 5.24. A summary of all LEED patterns is presented in Table 5.1. All electrode separation were performed in the cathodic sweep. The potentials
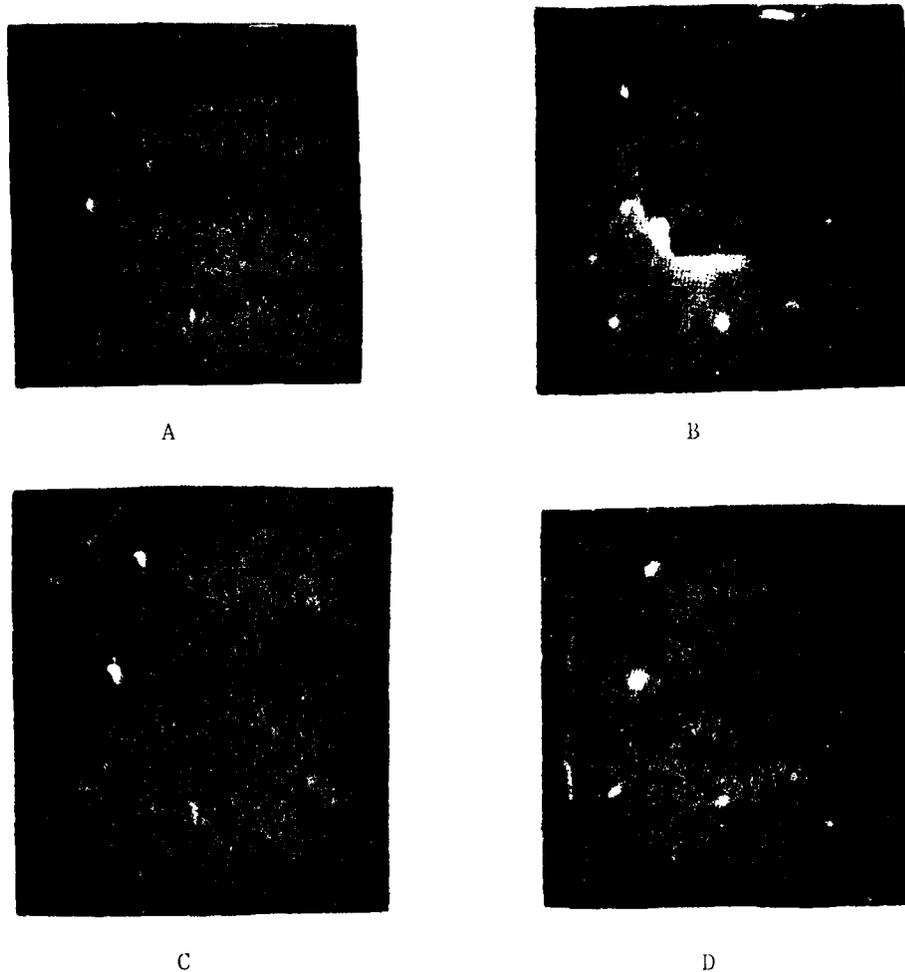
Figure 5.20. LEED patterns obtained for the Au(100) surface after electrochemical treatment in 0.1 $\underline{M}$ HF+1 mM Pb(NO$_3$)$_2$.

A. Electrodes separated after contact only at 0.6 V vs. Pb$_{rev}$. LEED at 61 eV.

B. Initial potential: 0.7 V vs. Pb$_{rev}$; potential swept to 0.1 V and cycled out to 0.7 V and removed. LEED at 54 eV.

C. Same as B except swept to 0.3 V and removed.

D. Initial potential: 0.0 V; potential swept to 0.7 V and removed. LEED at 57 eV.

Same photographic conditions as in Figure 5.4.
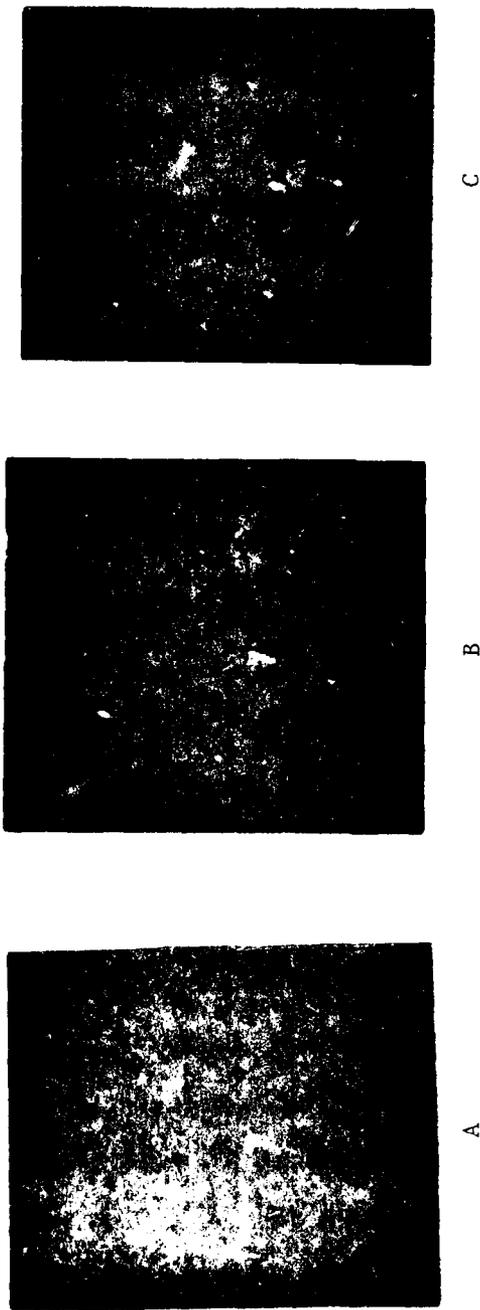
Au(110)

Figure 5.21. LEED patterns obtained after electrochemical treatment in 0.1 M HF + 1 mM Pb(NO$_3$)$_2$.

A. Electrodes separated after contact only at 0.6 V vs. Pb$_{rev}$. LEED at 61 eV.

B. Initial potential: 0.7 V vs. Pb$_{rev}$; potential swept to 0.3 V and removed. LEED at 60 eV.

C. Same as B except potential swept to 0.1 V and cycled out to 0.7V and removed. Same photographic conditions as in Figure 5.4. The two spots at the bottom of the outer rows of spots in B are not seen in A or C due to the finite dimensions of the screen.

Au(110)

Figure 5.22. Square LEED pattern obtained after electrochemical treatment in 0.1 $\underline{M}$ HF + 1 mM $Pb(NO_3)_2$. Initial potential: 0.0 V vs. Pb_{rev}; potential cycled to 0.7 V and removed at 0.3 V. LEED at 64 eV. Film: Kodak 2475. f-setting: 8. Exposure time: 30 s.
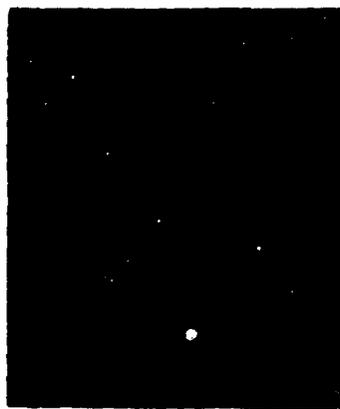
A. Au(111)   B. Au(410)

Figure 5.23.   LEED patterns obtained after electrochemical
               treatment in 0.1 $\underline{M}$ HF + 1 mM $Pb(NO_3)_2$.

       A.   Initial potential: 0.7 V vs. Pb_{rev}; potential
            swept to 0.1 V and cycled out to 0.7 V and re-
            moved. LEED at 57 eV.

       B.   Same as A except potential swept to 0.05 V.
            LEED at 48 eV.

       Same photographic conditions as in Firure 5.4.

A   B
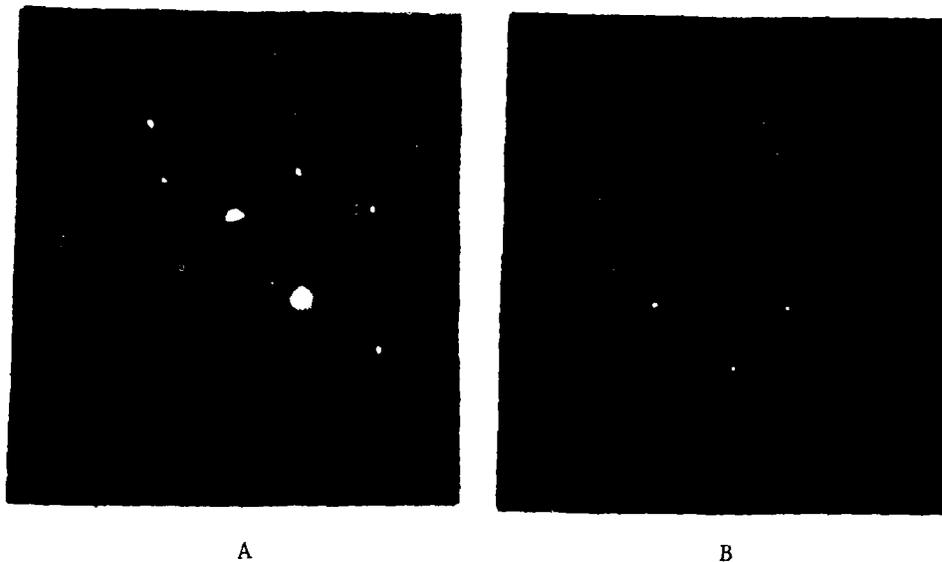
Figure 5.24   A.   LEED pattern for clean Au(410).   68 eV

                   B.   LEED pattern obtained for Au(410) after electro-
chemical treatment in 0.1 M HF + 1 mM $Pb(NO_3)_2$.
Initial potential: 0.7 V. Cycled 5 times be-
tween 0.7 V and 50 mV and removed at 50 mV.   68 eV.

Photographic conditions same as in Figure 5.4.

Table 5.1 Summary of LEED Patterns Obtained After Electrochemical Treatment

Single Crystal	Initial E(V)	Final E(V)	Separation E(V)	Electrochem. Treatment	LEED Pattern
Au(100)	0.0	0.7	50 mV	30 cycles from 0-0.7	(1x1)
	0.0	0.7	0.7	10 cycles from 0-0.7	(1x1) Figure 5.20 D
	0.6	0.6	0.6	No cycling	weak (5x20) Figure 5.20 A
	0.7	0.1	0.7	1 cycle	(1x1) Figure 5.20 B
	0.7	0.3	0.3	No cycling	(1x1) and (5x20)
Au(110)	0.0	0.7	0.3	10 cycles from 0-0.7	square Figure 5.22
	0.0	0.7	50 mV	30 cycles from 0-0.7	square
	0.0	1.8	0.7	50 cycles	(1x2) weak (1x3) and split spots Figure 5.21 A
	0.6	0.6	0.6	No cycling	Figure 5.21 A
	0.7	0.1	0.7	1 cycle	(1x1) Figure 5.21 C
	0.7	0.3	0.3	No cycling	(1x1) and faint (1x2) Figure 5.21 B
Au(111)	0.7	0.1	0.7	30 cycles from 0.1 to 0.7	(1x1) Figure 5.23
	0.0	0.7	0.7	20 cycles from 0.0 to 0.7	Very weak (1x1)
Au(410)	0.7	50mV	0.7	5 cycles	Weak (1x1) Figure 5.23
	0.7	50mV	0.1	5 cycles	Weak (1x1) Figure 5.24

All separation potentials correspond to the cathodic sweep. Approximate coverage when separated at 0.3 V: 0.31 (85µC/cm²) for Au(110) and 0.12 (45µC/cm²) for Au(100). Separations at 50mV are nealy at full coverage (see Table 5.2) while those at 0.7 V are at zero coverage.

Table 5.2 Estimate of Total Charge Due to the Pb UPD Layer and the Fraction of Au Surface Covered

Surface	Atom Density (per cm^2)	Charge for Complete Coverage ($\mu C/cm^2$) [1]	Measured Charge ($\mu C/cm^2$) [2]	Fraction of Surface Covered by Pb
Au(110)	8.50 x 10^{14}	272	174	0.64
Au(100)	1.20 x 10^{15}	384	176	0.46
Au(111)	1.39 x 10^{15}	445	100	0.22
Au(410)			245	
Polycryst. Au			310	

1 Assuming ideal (1x1) surfaces

2 Measured from beginning of UPD to just before onset of bulk deposition.

Calculations assume Pb is totally discharged on the Au surface.

used are given in the Table and Figure legends. Also listed in
the footnotes of Table 5.1 are the charges associated with UPD
layer formation and the estimated coverage based on an electro-
sorption valence of 2. The charge corresponding to complete cov-
erage for each surface is included in Table 5.2 Present indica-
tions are that the electrosorption valence is close to 2 at mod-
erate and high coverages. The deviation from low coverage is
probably less than 50% and hence qualitatively the coverages
calculated are an indication of the behavior.

Much time was spent working with the (100) surface because
of the large cathodic peak obtained in the voltammetry studies
(see Figure 5.8). Forming and separating the thin-layer cell in
the double layer region produced a weak (5x20) pattern. Retention
of the (5x20) pattern indicates that there is probably less than
0.15 monolayer of uniformally distributed Pb or any other substance
on the surface(40). This is quite an interesting result consider-
ing that no rinsing of the electrode prior to pumping down in the
ultra-high vacuum chamber was performed. Cycling the electrode
from 0.70 to 0.30V (just where the sharp cathodic peak occurs)
and separating the electrode at 0.30V produced either a (1x1)
(Figure 5.20c) or weak (5x20) LEED patterns as the electron beam
was moved around on the surface. The (1x1) pattern contained very
diffuse and somewhat split spots suggesting that the pattern had
not completely reverted to (1x1) or that a defect structure was
present on the surface. The Pb coverage at 0.3V was approximate-

ly 0.12. All other experiments conducted with this (100) surface always produced a sharp (1x1) LEED pattern. Even a (1x1) pattern was obtained when the sweep was stopped at 0.050 V, just short of the onset of bulk deposition. There should be near ½ monolayer of UPD Pb on the surface at this potential but no change in LEED pattern was found.

These results for the (100) surface agree very well with the work of Rhead et al. (39,40). From the progression of LEED patterns found for the vapor deposition of Pb on Au(100), (see Table 3.1) these workers estimated that approximately 0.15 monolayer of Pb was needed to cause the LEED transformation (5x20) to (1x1) and that the (1x1) pattern persisted until 0.6 monolayer of Pb was adsorbed. For their estimation of coverages the c(6x6) pattern was taken as being a representation of a dense compact monolayer of Pb on Au(100).

In the present work the transformation from (5x20) to (1x1) occurred at an estimated coverage of 0.1 and persisted through a coverage of 0.5, the limit for the UPD potential region (i.e., 0V). Thus the UPD results are similar to those for the gas phase studies.

The (110) surface behaved in a somewhat similar manner. Contact and separation of the electrode in the double layer region at 0.60 V without cycling produced a faint (1x3) LEED pattern (clearly evident in the original pattern but difficult to observe

in the reproduced copy in Figure 5.21A). The third order spots
are very weak and have in some places merged to form a nearly
(1x2) pattern. Of interest is the spot-splitting which occurs
for every other pair of vertical spots. The direction of spot-
splitting indicates that there is some type of surface disorder
occurring in a direction along the open channels or troughs of
the (110) surface (104). Surface disorder in this direction is not
usually found in gas phase studies on face-centered-cubic (110)
crystals; instead, spot-splitting and streaking are usully ob-
tained in the opposite direction indicating the presence of sur-
face defects across the open channels (e.g., as would be found
for a kinked surface) (see reference 104).

Separating the Au(110) electrode at 0.30 V after initial-
izing at 0.70 V with no potential cycling produced the LEED pat-
tern in Figure 5.21B. The separation potential of 0.30 V lies
between the broad peak in the deposition sweep and the sharp peak
(see Figure 5.6) and corresponds to a Pb coverage of about 0.31
monolayer. The pattern is basically (1x1) although some of the
spots are not very intense. There is also a trace of some spots
from the clean (1x2) pattern but these are faint. Some spot
streaking is seen indicating defects across the (110) open channels.
Cycling the electrode between 0.70 and 0.10 V once and removing at
0.7 V produced a similar LEED pattern (Figure 5.21c) except the
spots are not quite as sharp and no streaking is evident.

The above results again agree with the gas phase results of Rhead et al. (40). The (1x3) pattern was obtained by the initial Pb deposition on the (1x2) surface. No coverage or suggested surface structure was given for the (1x3) pattern. The coverage, however, must have been low as this pattern was obtained almost immediately after the start of deposition. After the (1x3) pattern a (1x1) pattern was obtained. Similar behavior was found electrochemically. The (1x1) pattern was then transformed to a (7x1) pattern after further Pb vapor deposition which, according to the suggested surface structure, was equivalent to a coverage of over 0.8 monolayer. Since the total electrochemical coverage did not exceed 0.64 monolayer (Table 5.2), this pattern was never observed.

When the (110) surface was contacted with the electrolyte at 0 V, cycled between 0 and 0.70 V, and then removed at either 0.30 V or .050 V a square LEED pattern was obtained (see Figure 5.22). Comparison of the distances between spots with those obtained from the Au(100)-(1x1) surface indicate the surface has a nearly (100) like overlayer. The surface, however, contains defects in both unit cell directions as is indicated by the streaking in the LEED pattern. (It is possible that similar streaking occurred in some of the other LEED patterns but that the photographic conditions did not show it up as well as in Figure 5.22). Indications are that streaking of this type on

surfaces with four-fold symmetry is due to the presence or do-
main boundaries (104). Since starting the sweeps at 0.70 V and
cycling only to 0.01 V did not produce the square LEED pattern,
the excursions to the bulk reversible potential with the (110)
surface caused the surface to grossly reconstruct. The over-
layer must consist of both Pb and Au from the AES results and may
have formed some type of alloy or surface compound.

As an exploratory effort, the (110) surface was also cycled
well out into the oxide potential region for Au. Cycling the
electrode between 0 and 1.80 V with separation at 0.70 V produced
a faint (1x2) rather than a square LEED pattern. The only reason-
able explanation for this occurrence is that oxide formation and
subsequent removal has the same effect as annealing in ultra-high
vacuum. Oxide formation and reduction, however, was not the ob-
ject of study in this work and thus, no other comments will be
made about this result.

Only a few experiments were performed with the other two sur-
faces (111) and (410) . Cycling the (111) surface between 0.10
and 0.70 V with removal at 0.70 V yielded a (1x1) LEED pattern
(Figure 5.23A). The spots are almost of the same quality as the
originals. They are not broad or split as in the pattern for the
initial surface (Figure 5.4) suggesting that this "after" surface
is very near a perfect (1x1) rather than a reconstructed surface.
Holding the (111) surface at 0 V for about 10s and cycling (20

cycles between 0.10 and 0.70V with removal at 0.70V produced a much sharper (1x1) LEED pattern than in Figure 5.32A. The pattern, however, was barely visible due to the large amount of background intensity. (Reproduction problems prevents its inclusion in this thesis). The surface was apparently roughened by the excursion to the reversible bulk potential. The defects, however, were not periodic in nature as would be indicated by split or streaked spots.

The Au(111) surface was not separated at any potentials other than 0.7 V. At this potential the UPD Pb should be completely removed from the Au surface. It is unlikely, however, that any other separation voltages would have produced a LEED pattern other than (1x1) on the Au(111) surface at the coverages accessible in the UPD potential range. At 0 V, the coverage calculated from this charge is only 0.22 monolayer Pb. On the other hand, Rhead et al. (40) found for Pb vapor deposited on this surface that the reconstructed Au(111) surface reverts to a pure (1x1) pattern at low coverages and then to a $\sqrt{3} \times \sqrt{3}$ R30° pattern at higher coverages. Using their suggested structure for this pattern, one obtains a Pb coverage of 0.33. Thus, at the maximum coverage (0.22) in the UPD potential range, the surface would still be expected to be predominantly (1x1).

For the (410) surface cycling between 0.70 V and 0.050 V with separation at either 0.10 or 0.70 V produced basically a (1x1) pattern (Figure 5.23B and 5.24). The after patterns are not of the best quality since they were photographed with the camera locat-

ed off the principle axis in an attempt to record spots otherwise
blocked by the annealing oven. This provided enough spots visible
on the "after" photographs to enable the comparison to be made with
the clean surface patterns. The spot distances are correct for
a (1x1) surface but the spot intensities are very much diminished
over those for a clean surface. Some spots appear to be missing.
This may have resulted from Pb adsorption at some of the step
sites but this is only speculation as very little adsorption and
LEED work has been performed on stepped surfaces of this type.

The fraction of the surface covered by UPD Pb cannot be
estimated for the (410) surface due to the difficulty in calculat-
ing surface atom density with the presence of steps. The measured
charge, however, of 245 C/cm^2 (Table 5.2) for complete coverage
is somewhat higher than that for the (100) surface due to increas-
ed surface area caused by the introduction of steps. This suggests
that the coverage of 0.46 monolayer for the (100) surface is near-
ly the same for the (410) surface.

CHAPTER 6

DISCUSSION AND CONCLUSIONS

Before proceeding with the discussion of specific points this author considers that the characteristic voltammetry curves obtained for the UPD of Pb on Au single crystals are representative of the cleanest and most defect-free Au electrodes used to date to study an electrochemical process. Problems associated with surface heterogeneity are minimized by annealing in ultra-high vacuum followed by examination with LEED. Cleanliness of the surface is insured through use of cycles of argon-ion sputtering and annealing followed by examination with AES. The first voltammetry sweeps are recorded with these surfaces without the need for electrochemical cleaning which almost certainly produces a roughened surface with a structure different from that begun with initially.

6.1 Summary of Results

A brief description of the results presented in Chapter 5 will be given here. The four single crystal Au surfaces studied, (111), (100), (110) and (410), all show characteristic voltammetry curves for the UPD of Pb. Except for the case of the stripping of Pb from the (100) surface the curves are unlike those obtained previously for the low index faces by other workers using less vigorous techniques (compare Figures in Chapter 5 with Figure 2.5). The (110) surface behaves nearly the same as poly-

crystalline Au which was not prepared in ultra-high vacuum (com-
pare Figures 5.1 and 5.7). The (100) surface like the (110)
surface also has a set of sharp, reversible voltammetry peaks
but they are shifted some 60 mV cathodic to where the peaks are
on the (110) surface (Figure 5.9). Also, the (100) surface has a
very large deposition peak which has a very large deposition
peak which has no reversible counterpart. The (111) surface
shows a very narrow adsorption and desorption voltage region
as shown in Figure 5.13. Very little adsorption or desorption is
seen before this voltage region is reached. Several sharp voltam-
metry peaks are obtained which are extremely irreversible even
at slow sweep rates. Unlike the other three surfaces, the (410)
surface exhibits fairly broad adsorption and desorption voltammetry
peaks (Figure 5.16).

After the electrochemical experiments were completed the
electrodes were re-examined with LEED and AES. The (100) and (110)
surfaces were given the most study. Although no quantitative
analysis for Pb was performed the Auger transitions for Au were
always strong while those for Pb were weak. Part of the reason for
the weak Pb signal is the low sensitivity Auger has for Pb in
comparison to Au. LEED results for the (100) surface indicated
that when the crystal was touched to electrolyte at 0.60 V (where
no electrosorption of Pb occurs) and removed the reconstructed
(5x20) surface still remained. Removal at potentials of 0.30 and
0.05V in the deposition sweep produced a (1x1) pattern. The (110)

surface produced essentially a (1x3) pattern when contacted with electrolyte at 0.60 V and removed. Removal at 0.30 and 0.050 V in the deposition sweep produced a (1x1) pattern except when the electrodes were brought together at 0.00 V. A LEED pattern with square symmetry was obtained in this case. If the electrodes were contacted at 0.00 V, cycled into the oxide region and removed at 0.7 V the (1x2) pattern was retained.

The progression (5x20) → (1x1) for the (100) surface and (1x2) → (1x3) → (1x1) for the (110) surface as the amount of Pb is increased was shown to agree well with the gas phase results of Rhead et al. (40) at low coverage. Higher order LEED patterns for these surfaces were not found by Rhead until the gas phase coverage exceeded the maximum electrochemical UPD coverage shown in Table 5.2. The gas phase coverages were estimated from proposed structures for the sequence of LEED patterns obtained in the experiment.

Few experiments were performed using the (410) and (111) surfaces. The (410) surface produced a (1x1) pattern (i.e., the normal pattern for this surface) whether it was removed at 0.050 V or 0.70 V. The (111) surface retained its (1x1) surface structure when cycled between 0.10 and 0.70 V and removed at 0.70 V.

6.2 Influence of Crystal Structure

Clearly from the voltammetry curves presented in Chapter 5 each Au single Crystal surface behaves differently toward the adsorption of Pb. These curves also indicate polycrystalline Au does

not exhibit voltammetry peaks which are a composite of those
for the low index single crystal surfaces. In fact, the curve for
well-cycled polycrystalline Au is nearly the same as that obtained
on the clean (110) surface and drastically different from that for
(111) or (100). Polycrystalline Au must upon potential cycling
become nearly (110)-like in structure with regard to UPD Pb. Despite
the similarity of the voltammetry curves the charge calculated for
formation of the Pb UPD layer at a potential just short of that
for bulk Pb on Au(110) is only about 60% of that for the poly-
crystalline sample even though both samples are presumably very
clean. The polycrystalline sample probably differed in the true-
to-apparent surface area ratio since it had been etched in
dilute aqua rega and had not been high temperature annealed.

Knowing the true structure of the (110)-(1x2) surface might
provide some insight into the similiarity in voltammetry curves.
As mentioned in Chapter 3 analysis of LEED intensity results has
been unsuccessful in determining the structure using simple sur-
face models. The complicated structure of the (110) surface is
reflected by some of the results in the present work. Even though
starting the voltammetry experiments at a potential where bulk
deposition begins produced a grossly reconstructed surface with
four-fold rather than two-fold symmetry (see Figure 5.22) the
voltammetry curve shows no change over those recorded when the
sweep was started in the double layer region. This type of change
should have strongly influenced the adsorption characterisitics if

the surface possessed long-range ordering.

6.3 Comment on UPD Coverages

The total coverages of the UPD Pb layer calculated from the charge were listed in Table 5.2 for each of the low index Au single crystals. An electrosorption valency of 2 for Pb and one Pb per Au atom in the monolayer were assumed in the calculations. The latter assumption may introduce some inaccuracy in the calculation as the lattice parameter for bulk Pb is nearly 20% larger than that for bulk Au. The error is not likely to be very great at low coverage. Gas phase results, however, indicate that contraction of the lattice parameter probably occurs at high Pb coverage (40).

The total charge for the UPD monolayer formation [$\sim$175 $\mu C/cm^2$ for the (100) and (110) surfaces and $\sim$100 $\mu C/cm^2$ for the (111) surface] is lower than those obtained from earlier work [$\sim$300 $\mu C/cm^2$ by Schultze and Dickertmann (29) and $\sim$230 $\mu C/cm^2$ by Adzic et al. (19) with orientations corresponding to the low index surfaces]. The techniques used in preparing the surfaces in the earlier work, however, leave uncertain the actual surfaces obtained in their studies. It is unlikely that the simple low index surfaces were used. The differences in coverages are most likely a result of the difference in pretreatment of the surfaces. In both of the previous studies the crystals were electropolished. Schultze and Dickertmann also annealed the samples in vacuum for 6 h after electropolishing. Although this annealing would have helped in ob-

taining an unroughened surface, each surface was undoubtedly re-roughened by cycling many times into the oxide region for cleaning purposes. The crystals used in the present study were not sub-jected to this type of treatment after the LEED and Auger exami-nation had indicated the quality of the surface. Thus, the higher charge obtained in the earlier single crystal studies is believed to have occurred because of higher area, rather imperfect surfaces, not even necessarilly corresponding to the expected low index planes.

An alternate explanation of the lower coverages in the present work is the possibility that the very clean surfaces involved in the thin-layer cell electrochemical measurements were not en-tirely covered by the drop due to problems in wetting the surface by the electrolyte. The gap of the thin-layer cell was examined with a long focal length magnifying microscope during the bringing together of the single crystal and counter/reference electrode. The gap did appear fully filled in all of the successful experi-ments. Even so, the side view might be desceptive in that there could be unwetted areas not detected by this procedure. Such seems unlikely, however, Furthermore, the post-LEED examination indicated the surface to be uniform even out to the edge of the single crystal.

6.3.1 Formation of Ordered Low-Coverage Pb Overlayers

Schultze and Dickertmann (29) have attempted to correlate their own data for the coverages at which the two pronounced peaks occur in the anodic stripping voltammetry curves with the structural changes noted by Rhead et al. (40) in their LEED studies of Pb/Au

in vacuo (see Table 2.3). They infer that the structural changes are the same at the electrochemical and the solid-vacuum interface. A problem exists with this interpretation as the coverages obtained in the present work and by Adzic et al. (19) for these peaks are too low to infer these same structures. Evidence as to whether the principal voltammetry peaks found for each surface are due to various ordered Pb structures or to random adsorption is found in the post-LEED and -Auger results of the present work.

The LEED transitions (5x20) → (1x1) for the (100) surface and (1x2) → (1x3) → (1x1) for the (110) surface in the gas phase work of Rhead et al. (40) at low Pb Coverages are the same sequence found in the present work. The (1x1) surface is retained even if the electrodes are pulled apart 50 mV positive to the beginning of bulk deposition. Higher order LEED patterns were obtained in the gas phase studies but coverages calculated from the proposed structures indicate that these structures are not formed electrochemically as the electrochemical coverage for complete UPD layer formation is too low. The (111) surface was never separated at a potential with a full Pb UPD layer on it. The (410) surface was separated at +50 mV and the (1x1) surface was retained. This is in agreement with the low Pb charge found for UPD layer formation. For the case of the (100) and (110) surfaces the results indicate that the total amount of UPD Pb on the surface is probably small, even at the potential just before bulk deposition and that this Pb is adsorbed at positions which do not give long-range order to the crystal sur-

face and are undetected by LEED. The same is likely to be correct for the other two surfaces.

6.4 Interpretation of the Voltammetry Curves

No attempt here will be made to explain every peak in the voltammetry curve for each surface. Enough evidence exists, however, to draw certain conclusions about the mechanisms of Pb adsorption on each single crystal examined. Specific points to be discussed include phase transitions, the mechanism of adsorption-desorption on the (111) surface, and the explanation for the large, irreversible peak obtained on the adsorption sweep for the (100) surface.

6.4.1 Phase Transitions

As mentioned in Chapter 2 the very sharp, nearly reversible peaks found on polycrystalline Au are thought to be due to a phase transition where the previously deposited Pb in mainly ionic form condenses into islands or patches with metallic-like properties. The existance of phase transitions, however, has been questioned by Schmidt et al. (20). Evidence obtained in the present work indicates that these peaks for the (100) and (110) surfaces are indeed indicative of a phase transition.

Examination of the voltammetry curve for the stepped (410) surface reveals that no sharp peaks are obtained for this surface. If a phase transition is occurring on the other surfaces, this result is not surprising since the introduction of steps is ex-

pected to hinder a process of this type. The somewhat broadened peak found near the reversible potential may be due to a phase transition on this surface. The occurrence of this peak at a more cathodic potential and its much larger width than the same peaks found for the (100) and (110) surfaces fit in with a phase transition-type of explanation. Surface heterogeneity provided by the steps would cause both of the above to occur.

Other evidence is provided in the voltammetry curve for the (100) surface where one of the peaks in question (peak 3', Figure 5.8) has an extremely narrow half-width of ∿1mV at s=2 mV/s. A phase transition within a two-dimensional layer should occur at a single potential but a non-uniform surface and lack of reversibility of the process can broaden the peak.

Final evidence is found in the post-LEED results. As mentioned in the last section the lack of ordered surface structures except the (1x1) structure obtained for the (100) and (110) surfaces when the electrodes were pulled apart cathodic to the sharp peaks can be taken as an indication that the Pb is located at a few positions on the surface. The UPD Pb could easily exist as patches, formed by the phase transition, which go undetected by LEED because of their location and dimensions.

6.4.2 Mechanism on the Au(111) Surface

The deposition and removal of Pb from the Au(111) surface probably involves a condensation (i.e., nucleation) mechanism where

the very small amount (<0.01 monolayer) of initially adsorbed Pb
condenses into growth centers (i.e., nuclei) where further Pb depo-
sition can occur (see Figure 5.13). Evidence for this is found in
the adsorption and desorption isotherms shown for this and the
other single crystal surfaces in Figures 6.1 and 6.2[1]. Only for
the (111) surface are the isotherms essentially step-like. This
is especially evident for the desorption isotherm where a dis-
continuity is observed. All the adsorption and desorption occurs
in a very narrow range of potentials and both processes are highly
irreversible. The same mechanism has been postulated by Bewick and
Thomas (22) for Pb deposition on Ag(111).

These isotherms are very much similar to the step-shaped
isotherms predicted for gas condensation onto a solid surface(106).
In practice the gas phase isotherms are not nearly as ideally shaped
as that for the (111) surface due to surface heterogeneity effects.
Often, however, these isotherms show hysterisis between the adsorp-
tion and desorption processes as is also found for the case of Pb
adsorbed on Au(111). Also, at slow sweep speeds nearly all the Pb
adsorption occurs at a very narrow range of potentials thus providing

---

[1] The charge calculated for the isotherms was obtained by estimating
the number of chart paper squares in the voltammetry curves every
50 mV. A constant double layer charge was subtracted from this
quantity. The shapes of the isotherms are correct but the final
charges obtained in each differ somewhat from those in Table 5.2
due to the approximate procedure used.
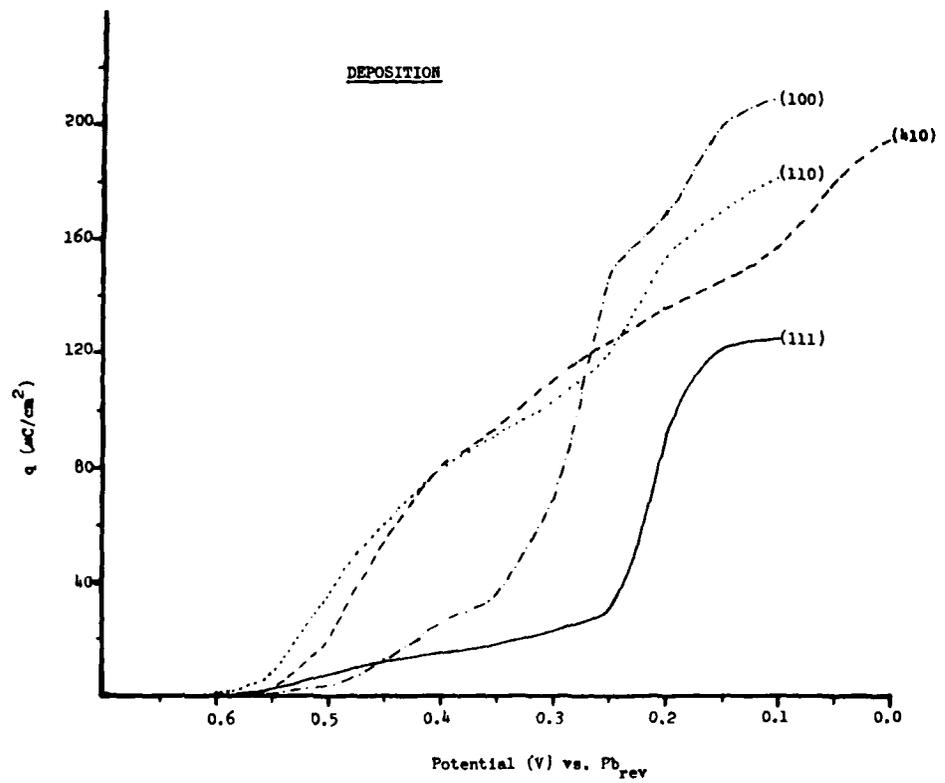
Figure 6.1   Deposition branch of the charge density vs. potential
curves for the UPD of Pb on Au single crystals.
All curves calculated from voltammetry traces for
$s = 20$ mV/s.
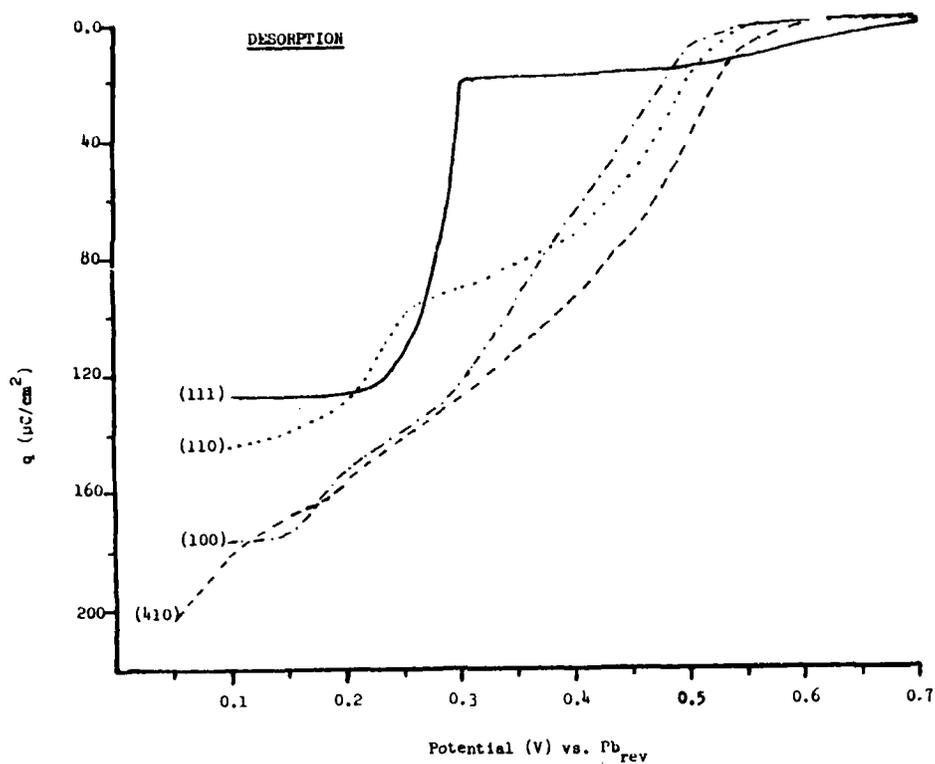
Figure 6.2   Desorption branch of the charge density vs. potential
             curves for the UPD of Pb on Au single crystals.
             All curves calculated from voltammetry traces for
             s = 20 mV/s.

an almost perfect step-shaped adsorption isotherm. On the close-packed (111) surface apparently the interaction of the Pb atoms with the gold orbitals is relatively weak requiring more cathodic potential prior to the condensation.

6.4.3 Origin of the Large Deposition Peak for Au(100)

This peak was not found in the work of Adzic et al.(19). Schultze and Dickertmann (29) did not report the cathodic adsorption currents on the single crystal surfaces. In this work the peak is extremely large and contains much charge under it (see Figure 5.8). At slow sweep speeds the peak actually separates into two sharp peaks (see Figur 5.10). From the results obtained here the peak appears to involve a surface transformation from that indicated by the (5x20) LEED pattern to the square (1x1) surface induced by adsorption of Pb. The process is extremely irreversible even at very slow sweep rates.

The results provide evidnce for this transformation. The large deposition peak on the (100) surface is not found on the (410) surface although the (410) surface is composed of large areas of (100) orientation. The clean (410) surface, however, does not have a reconstructed LEED pattern. The steps prevent the occurrence of massive reconstruction of the surface such as occurs in the case of the (100) surface.

Post-LEED analysis of the electrochemically treated surface indicates that when the electrodes are separated in the double layer region a (5x20) pattern is obtained. Separation of the electrode

at a point nearly midway between the large deposition peak, however, produces mostly a (1x1) surface but some traces of the (5x20) surface can be seen. Separation near the reversible potential of bulk Pb produces a (1x1) LEED pattern over the whole surface. It is interesting that cycling the electrode between 0.70 and 0.10 V with removal at 0.70 V does not produce a (5x20) pattern. A rather large amount of oxygen on the surface as indicated by Auger was found when the electrodes were separated in the double layer region (0.70 V) while very little oxygen was observed at potentials in the UPD region. The oxygen may have arisen from the adsorbed nitrate which in turn then decomposed to leave some gold oxide.

When a very small amount of Pb is left on the surface and the potential scan is reversed the large deposition peak is greatly diminished and a broad initial adsorption region is obtained (see Figure 5.12). This broad adsorption region resembles somewhat that found by Adzic et al. (19) (see Figure 2.5) which could at best have been obtained on a (1x1) (100) surface for reasons discussed earlier. In the present work a small amount of Pb left on the surface does not allow the surface to revert to the (5x20) configuration thus giving a broad adsorption region on the return sweep which is due to the presence of the (1x1) surface.

6.5 Suggestions for Future Work

To add more validity to the post-LEED results an experiment

should be run where the electrode is removed at a potential near
the reversible potential for bulk Pb. After examination with LEED
and AES the electrode would be transferred back to the electro-
chemical cell and the Pb stripped off. If the desorption part of
the voltammetry curve resembles that obtained in the previous
electrochemical curve, it is unlikely that any surface reconstruc-
tion has occured due to the removal of electrolyte.

Another interesting experiment would be to examine the UPD of
a metal such as Cu on Au single crystals. Copper has a lattice
parameter smaller than Au in contrast to Pb whose unit cell distance
is some 20% larger. Ordered structures similar to those seen by
Beckmann et al. (28) using RHEED may be found with LEED. The ob-
tainment of ordered structures for Cu on Au would suggest that the
mechanism of UPD is much different between the Cu/Au and Pb/Au
systems and that the difference is partially due to the size
of the adsorbate.

In the near future the LEED-AES vacuum chamber will also con-
tain a source and analyzer for performing XPS (X-ray Photoelectron
Spectroscopy) measurements. This capability will be helpful in
the UPD studies since the energy of the core electrons ejected from
the UPD overlayer and the substrate will be very sensitive to
their chemical environment (i.e., valence state). Information
oncerning the chemical state of the surface can be obtained
from binding energy shifts with respect to the bulk material.

REFERENCES

1. D. M. Kolb, M. Przasnyski and H. Gerischer, J. Electroanal.
    Chem. 54, 25 (1974)

2. Ibid., Surf. Sci., 43, 662 (1974)

3. R. S. Mulliken, J.Chem Phys., 2, 782 (1934)

4. Dieter M. Kolb, "Advances in Electrochemistry and Electro-
    chemical Engineering", H. Gerischer and C. W. Tobias, eds.,
    John Wiley and Sons, N.Y., Vol. II, (1978), p.125.

5. K. J. Velter and J. W. Schultze, Ber Bunserges. Phys. Chem.,
    76, 920, 927 (1972)

6. Ibid., J. Electroanal. Chem., 44, 63 (1973)

7. J. W. Schultze and F. D. Koppitz, Electrochim. Acta, 21,
    327, 337 (1976)

8. E. Schmidt, P. Beutler and W. J. Lorenz, Ber Bunserges. Phys.
    Chem., 75, 71 (1971)

9. E. Schmidt and H. R. Gygax, J. Electroanal. Chem., 12, 300
    (1966)

10. G. W. Tindall and S. Bruckenstein, Anal. Chem., 40, 1051
    (1968)

11. L. S. Melnicki, T. M. Reidhammer and Stanley Bruckenstein,
    To be published in "Prodeedings of the Symposium on Elect-
    rode Materials and Processes for Energy Conversion and Stor-
    age", Electrochem Soc. Meeting, May, 1979 Boston

12. J. W. Schultze, Ber. Bunserger. Phys. Chem., 74, 705 (1970)

13. Radoslav Adzic, Ernest Yeager and B. D. Cahan, J. Electro-
    anal. Chem., 85, 267 (1977)

14. B. J. Bowles, Electrochim. Acta, 10, 717, 731 (1965)

15. W. Lorenz and G. Salie, Z. Phys. Chem. NF, 29, 390, 408
    (1961). Z. Phys. Chem., 218, 259 (1962)

16. A. Bewick and B. Thomas, J. Electoanal. Chem., 65, 911 (1975)

17. W. J. Lorenz, H. D. Hermann, N. Wuthrich and F. Hilbert, J. Electrochem. Soc., 121, 1167 (1974)

18. W. J. Lorenz, E. Schmidt, G. Staikov and H. Bort, "Faraday Symposia of the Chemical Society", No. 12, Electrocrystallization, Nucleation and Phase Formation, 1977, p. 14.

19. Radoslav Adzic, Ernest Yeager and B. D. Cahan, J. Electrochem. Soc., 121, 474 (1974)

20. E. Schmidt and N. Wurthrich, J. Electroanal. Chem., 34, 377 (1972)

21. A. Bewick and B. Thomas, J. Electroanal. Chem., 70, 239 (1976).

22. Ibid., 85, 329 (1977)

23. Ibid., 84, 127 (1977)

24. D. Dickertmann, F. D. Koppitz and J. W. Schultze, Electrochim. Acta, 21, 967 (1976)

25. Alan Bewick, Jovan Jovićević and Brian Thomas, "Faraday Symposia of the Chemical Society", No. 12, Electrosorption, Nucleartion and Phase Formation, 1977, p. 24.

26. J. Walter Schultze and Dirk Dickertmann, Ibid., p. 36. Ber Bunsenges. Phys. Chem., 82, 528 (1978)

27. D. Dickertmann and J. W. Schultze, Electrochim. Acta, 22., 117 (1977)

28. Hans O. Beckmann, Heinz Gerischer, Dieter M. Kolb and Gunter Lehmpfohl, "Faraday Symposia of the Chemical Society", No. 12, Electrosorption, Nucleation and Phase Formation, 1977 p. 51

29. J. W. Schultze, D. Dickertmann, Surf. Sci., 54, 489 (1976)

30. D. J. Astley, J. A. Harrison and H. R. Thirsk, J. Electroanal. Chem., 19, 325 (1968)

Elizabeth A. Wood, J. Appl. Phys., 35, 1306 (1964)

B. D. Cahan and Ernest Yeager, J. Electrochem.

33. T. Mills and G. M. Willis, J. Electrochem. Soc., 100, 452 (1953)

34. E. Schmidt and H. R. Gygax, J. Electroanal. Chem., 14, 126 (1967)

35. Ibid., 13, 378 (1967)

36. N. A. Vicente and Stanley Bruckenstein, Anal. Chem., 45, 2036 (1973)

37. E. Schmidt and N. Wuthrich, J. Electrochem. Soc., 121, 1610 (1974)

38. R. Adzic, E. Yeager and B. D. Cahan, Ibid., 1611.

39. J. P. Biberian and G. E. Rhead, J. Phys. F: Metal Phys., 3, 675 (1973)

40. J. Perdereau, J.P. Biberian, and G. E. Rhead, Ibid., 4, 798 (1974)

41. W. E. O'Grady, M.Y.C. Woo, P. L. Hagans, and E. Yeager, J. Vac Sci. Technol., 14, (1977)

42. Ibid., J. Electrochem.Soc., 125, 346 (1978)

43. A. T. Hubbard, "CRC Critical Review. Analytical Chem.", 3, 201, (1973)

44. A. T. Hubbard and F. C. Anson, Electroanalytical Chem., Vol. IV, A. J. Bard, ed., Marcel Dekker, N.Y., 1971, p. 129 ff.

45. Ronald G. Musket and John Ferrante, NASA Technical Note TN D-6399, Washington, D.C., 1971 34pp

46. Chuan C. Chang, "Characterization of Solid Surfaces", P.F. Kane and G. B. Larrabee, Eds., Plenun Press, N.Y., 1974, p. 509

47. Ibid., Surf. Sci., 25, 53(1971)

48. L. A. Harris, J. Appl. Phys., 39, 1419 (1968)

49. F. J. Szalkowski and G. A. Somorjai, J. Chem. Phys., 56, 6097 (1972); J. Chem.Phys. 61, 2064 (1974

50. E. N. Sickafus, J. Vac. Sci. Technol., 11, 299 (1974)

51. N.J. Taylor, Rev. Sci. Instr., 40, 792 (1969)

52. C. C. Chang, Surf. Sci., 48, 9 (1975)

53. T. W. Haas, J. T. Grant and G. J. Dooley, "Adsorption-Desorption Phenomena", Ricca, ed., Academic, N.Y., 1972, p.359.

54. G. E. Rhead, J. Vac. Sci. Technol., 13, 603 (1976)

55. F. Dalamare and G. E. Rhead, Surf. Sci., 35, 172 (1973)

56. J. Henrion and G. E. Rhead, Surf. Sci., 29, 20 (1972)

57. A. Sepulveda and G. E. Rhead, Surf. Sci., 66, 436 (1977)

58. C. B. Duke, "Advances in Chemical Physics", Vol. 27, I. Prigogine and Stuart A. Rice, eds., Viley Interscience, N.Y. 1974, p.1

59. G. A. Somorjai and H. H. Farrell, Ibid., Vol. 20, 1971, p.215

60. J. B. Pendry, "Low Energy Electron Diffraction", Academic Press, N.Y., 1974, 407pp

61. J. A. Strozier, D. W. Jepsen and F. Jona, "Surface Physics of Materials", Vol. 1, J. M. Blakely, ed., Academic Press, N.Y., 1975, p.1

62. John W. May, "Advances in Catalysis", Vol. 21, D.D. Eley, Herman Pines and Paul B. Weisz, eds., Academic Press, N.Y., 1970, p. 151.

63. P. J. Estrups and E. G. McRae, Surf. Sci., 25, 1 (1971).

64. G. A Somorjai, "Treatise on Solid State Chemistry", Vol. 6A, Surfaces I, N. B. Hanray, ed., Plenum, N.Y., 1976,p.1

65. M. Henzler, "Electron Spectroscopy for Surface Analysis", H. Ibach, ed., Springer-Verlag, N.Y., 1977, p.117

66. W. E. O'Grady, M. Y. C. Woo, P. L. Hagans and E. Yeager, "Proceedings of the Symposium on Materials and Processes for Energy Conversion and Storage", Vol. 77-6, J.D.E. McIntyre, S. Srinivasan and F. G. Will, eds., Electrochem. Soc., Princeton N.J. 1977 p.172

67. D. G. Fedak and N. A. Gjostein, _Acta Metallurgica_, 15, 827 (1967)

68. M. A. Chesters and G. A. Somorjai, _Surf. Sci._, 52, 21(1975)

69. Private Communication, David Zehner, Solid State Division, Oak Ridge National Laboratory, Oak Ridge, Tenn.

70. P. N. J. Dennis and P. J. Dobson, _Surf. Sci._, 33, 187 (1972)

71. M. Kostelitz, Thesis, Universite´ de Paris VI, 1973.

72. F. Grǿnlund and P. E. H. Nielsen, _J. Appl. Phys._, 43, 3919 (1972)

73. P. W. Palmberg and T. N. Rhodin, _Phys. Rev._, 161, 586 (1967); _J. Chem. Phys._, 49, 134 and 147 (1968)

74. G. A. Somorjai, "Principles of Surface Chemistry", Chap. 1, Prentice-Hall, N. J. (1972)

75. Gert Broden, Thos Rhodin and Weston Capehart, _Surf. Sci._, 61, 143 (1976)

76. B. R. Appleton, D. M. Zehner, T. S. Noggle, J. W. Miller, O. E. Schow III, L. H. Jenkins and J. H. Barrett, "Ion Beam Surface Layer Analysis", Vol. 2, O. Meyer, G. Lenker and F. Kappeler, eds., Plenum, N.Y., 1976, p.607

77. J. F. Wendelken and D. M. Zehner, _Surf. Sci._, 71, 178 (1978)

78. H. P. Bonzel, C. R. Helms and S. Keleman, _Phys. Rev. Letters_, 35, 1237 (1975)

79. T. N. Rhodin and G. Broden, _Surf. Sci._, 60, 466 (1976)

80. R. Ducros and R. P. Merrill, _Surf. Sci._, 55, 227 (1976)

81. B. E. Nieuwenhoys and G. A. Somorjai, _Surf. Sci._ 72, 8 (1978)

82. C. -M Chan, K. L. Luke, M. A. Van Hove, W. H. Weinberg and E. D. Williams, _J. Vac. Sci. Technol._, 16, 642 (1979).

83. J. R. Noonan and H. L. Davis, Ibid, 587

84. D. Wolf, H. Jagodzinski and W. Mority, _Surf. Sci._, 77, 265 and 283 (1978)

85. H. C. Snyman and F. W. Boswell, _Surf. Sci._, 41, 21 (1974)

86. J. S. Hammond and N. Winograd, J. Electrochem. Soc., 123
    80 (1977); Ibid., 124, 826 (1977)

87. Arthur T. Hubbard, Roy M. Ishikawa and James Katekaru, J.
    Electroanal Chem., 86, 271 (1978)

88. R. N. Ross, J. Electroanal. Chem., 76, 139 (1977)

89. Ibid, "Proceedings of the Symposium on Electrode Materials
    and Processes for Energy Conversion and Storage", Vol. 77-6,
    J. D. E. McKintyre, S. Srinivasan and F. G. Will, eds.,
    Electrochem. Soc. Princeton, N. J. 1977, 290

90. Ibid, J. Electrochem. Soc., 126, 67 (1979)

91. Ibid., 126, 78 (1979)

92. Roy M. Ishikawa and Arthur T. Hubbard, J. Electroanal Chem.,
    69, 317 (1976)

93. K. S. Kim, N. Winograd and R. E. Davis, J. Am. Chem. Soc., 93

94. R. W. Revie, B. G. Baker and J. O'M. Bockris, J. Electrochem.
    Soc., 122, 1460 (1975); Surf. Sci., 52, 664 (1975)

95. W. E. O'Grady and J. O'M. Bockris, Surf. Sci., 38, 249 (1973)

96. Theodore Tom, Physics Today, Aug., 32 (1972)

97. Elizabeth A. Wood, "Crystal Orientation Manual", Columbia
    Univ. Press, N. Y., 1963, 75pp

98. C. M. Ferro, A. J. Calandra and A. J. Arvia, J. Electroanal.
    Chem., 59 239 (1975)

99. S. Srinivasan and E. Gileadi, Electrochim, Acta, II, 321
    (1966)

100. J. Perdereau and G. E. Rhead, Surf. Sci., 24, 55 (1971

101. B. Lang, R. W. Joyner and G. A. Somorjai, Surf. Sci., 30
     454 (1972); D. W. Blaxely and G. A. Somorjai, J. Catalysis,
     42, 181 (1976)

102. B. E. Conway and H. Angerstein-Kozlowska, "Electrocatalysis
     on Non-Metallic Surfaces", NBS Special Publ. 455, Proceed-
     ings of Workshop held at NBS, Dec. 9-12, 1975, pp. 107-124

103. G. E. Rhead, _J. Phys. F: Metal Phys._, $\underline{3}$, L53 (1973).

104. C. S. McKee, M. W. Roberts and M. L. Williams, _Advances in Colloid and Interface Sci._, $\underline{8}$, 29 (1977).

105. R. R. Adzic and A. R. Despic, presented at the 25th meeting of the ISE, Brighton, England, 1975.

106. Stephen Brunauer, "The Adsorption of Gases and Vapors", Vol. 1, Princeton Univ. Press, Princeton, N.J., 1943, Chap. 6.

TECHNICAL REPORT DISTRIBUTION LIST, GEN

<table>
<tr><td></td><td>No.
Copies</td><td></td><td>No.
Copies</td></tr>
<tr>
<td>Office of Naval Research
Attn: Code 472
800 North Quincy Street
Arlington, Virginia 22217</td>
<td>2</td>
<td>U.S. Army Research Office
Attn: CRD-AA-IP
P.O. Box 1211
Research Triangle Park, N.C. 27709</td>
<td>1</td>
</tr>
<tr>
<td>ONR Branch Office
Attn: Dr. George Sandoz
536 S. Clark Street
Chicago, Illinois 60605</td>
<td>1</td>
<td>Naval Ocean Systems Center
Attn: Mr. Joe McCartney
San Diego, California 92152</td>
<td>1</td>
</tr>
<tr>
<td>ONR Branch Office
Attn: Scientific Dept.
715 Broadway
New York, New York 10003</td>
<td>1</td>
<td>Naval Weapons Center
Attn: Dr. A. B. Amster,
  Chemistry Division
China Lake, California 93555</td>
<td>1</td>
</tr>
<tr>
<td>ONR Branch Office
1030 East Green Street
Pasadena, California 91106</td>
<td>1</td>
<td>Naval Civil Engineering Laboratory
Attn: Dr. R. W. Drisko
Port Hueneme, California 93401</td>
<td></td>
</tr>
<tr>
<td>ONR Branch Office
Attn: Dr. L. H. Peebles
Building 114, Section D
666 Summer Street
Boston, Massachusetts 02210</td>
<td>1</td>
<td>Department of Physics & Chemistry
Naval Postgraduate School
Monterey, California 93940</td>
<td></td>
</tr>
<tr>
<td>Director, Naval Research Laboratory
Attn: Code 6100
Washington, D.C. 20390</td>
<td>1</td>
<td>Dr. A. L. Slafkosky
Scientific Advisor
Commandant of the Marine Corps
  (Code RD-1)
Washington, D.C. 20380</td>
<td>1</td>
</tr>
<tr>
<td>The Assistant Secretary
  of the Navy (R,E&S)
Department of the Navy
Room 4E736, Pentagon
Washington, D.C. 20350</td>
<td>1</td>
<td>Office of Naval Research
Attn: Dr. Richard S. Miller
800 N. Quincy Street
Arlington, Virginia 22217</td>
<td>1</td>
</tr>
<tr>
<td>Commander, Naval Air Systems Command
Attn: Code 310C (H. Rosenwasser)
Department of the Navy
Washington, D.C. 20360</td>
<td>1</td>
<td>Naval Ship Research and Development
  Center
Attn: Dr. G. Bosmajian, Applied
  Chemistry Division
Annapolis, Maryland 21401</td>
<td>1</td>
</tr>
<tr>
<td>Defense Documentation Center
Building 5, Cameron Station
Alexandria, Virginia 22314</td>
<td>12</td>
<td>Naval Ocean Systems Center
Attn: Dr. S. Yamamoto, Marine
  Sciences Division
San Diego, California 91232</td>
<td>1</td>
</tr>
<tr>
<td>Dr. Fred Saalfeld
Chemistry Division
Naval Research Laboratory
Washington, D.C. 20375</td>
<td>1</td>
<td>Mr. John Boyle
Materials Branch
Naval Ship Engineering Center
Philadelphia, Pennsylvania 19112</td>
<td></td>
</tr>
</table>

TECHNICAL REPORT DISTRIBUTION LIST, GEN

<u>No.</u>
<u>Copies</u>

Dr. Rudolph J. Marcus
Office of Naval Research
Scientific Liaison Group
American Embassy
APO San Francisco 96503   1

Mr. James Kelley
DTNSRDC Code 2803
Annapolis, Maryland   21402   1

P4-2/B1

TECHNICAL REPORT DISTRIBUTION LIST, 359

	No. Copies		No. Copies
Dr. Paul Delahay Department of Chemistry New York University New York, New York 10003	1	Dr. P. J. Hendra Department of Chemistry University of Southhampton Southhampton SO9 5NH United Kingdom	1
Dr. E. Yeager Department of Chemistry Case Western Reserve University Cleveland, OH 44106	1	Dr. Sam Perone Department of Chemistry Purdue University West Lafayette, Indiana 47907	1
Dr. D. N. Bennion Chemical Engineering Department University of California Los Angeles, California 90024	1	Dr. Royce W. Murray Department of Chemistry University of North Carolina Chapel Hill, North Carolina 27514	1
Dr. R. A. Marcus Department of Chemistry California Institute of Technology Pasadena, California 91125	1	Naval Ocean Systems Center Attn: Technical Library San Diego, California 92152	
Dr. J. J. Auborn Bell Laboratories Murray Hill, New Jersey 07974	1	Dr. C. E. Mueller The Electrochemistry Branch Materials Division, Research & Technology Department Naval Surface Weapons Center White Oak Laboratory Silver Spring, Maryland 20910	1
Dr. Adam Heller Bell Laboratories Murray Hill, New Jersey 07974	1		
Dr. T. Katan Lockheed Missiles & Space Co, Inc. P.O. Box 504 Sunnyvale, California 94088	1	Dr. G. Goodman Globe-Union Incorporated 5757 North Green Bay Avenue Milwaukee, Wisconsin 53201	1
Dr. Joseph Singer, Code 302-1 NASA-Lewis 21000 Brookpark Road Cleveland, Ohio 44135	1	Dr. J. Boechler Electrochimica Corporation Attention: Technical Library 2485 Charleston Road Mountain View, California 94040	1
Dr. B. Brummer EIC Incorporated 55 Chapel Street Newton, Massachusetts 02158	1	Dr. P. P. Schmidt Department of Chemistry Oakland University Rochester, Michigan 48063	1
Library P. R. Mallory and Company, Inc. Northwest Industrial Park Burlington, Massachusetts 01803	1	Dr. H. Richtol Chemistry Department Rensselaer Polytechnic Institute Troy, New York 12181	1

TECHNICAL REPORT DISTRIBUTION LIST, 359

	No. Copies		No. Copies
Dr. A. B. Ellis Chemistry Department University of Wisconsin Madison, Wisconsin 53706	1	Dr. R. P. Van Duyne Department of Chemistry Northwestern University Evanston, Illinois 60201	1
Dr. M. Wrighton Chemistry Department Massachusetts Institute of Technology Cambridge, Massachusetts 02139	1	Dr. B. Stanley Pons Department of Chemistry Oakland University Rochester, Michigan 48063	1
Larry E. Plew Naval Weapons Support Center Code 30736, Building 2906 Crane, Indiana 47522	1	Dr. Michael J. Weaver Department of Chemistry Michigan State University East Lansing, Michigan 48824	1
S. Ruby DOE (STOR) 600 E Street Washington, D.C. 20545	1	Dr. R. David Rauh EIC Corporation 55 Chapel Street Newton, Massachusetts 02158	'
Dr. Aaron Wold Brown University Department of Chemistry Providence, Rhode Island 02192	1	Dr. J. David Margerum Research Laboratories Division Hughes Aircraft Company 3011 Malibu Canyon Road Malibu, California 90265	1
Dr. R. C. Chudacek McGraw-Edison Company Edison Battery Division Post Office Box 28 Bloomfield, New Jersey 07003	1	Dr. Martin Fleischmann Department of Chemistry University of Southampton Southampton 509 5NH England	1
Dr. A. J. Bard University of Texas Department of Chemistry Austin, Texas 78712	1	Dr. Janet Osteryoung Department of Chemistry State University of New York at Buffalo Buffalo, New York 14214	1
Dr. M. M. Nicholson Electronics Research Center Rockwell International 3370 Miraloma Avenue Anaheim, California	1	Dr. R. A. Osteryoung Department of Chemistry State University of New York at Buffalo Buffalo, New York 14214	1
Dr. Donald W. Ernst Naval Surface Weapons Center Code R-33 White Oak Laboratory Silver Spring, Maryland 20910	1	Mr. James R. Moden Naval Underwater Systems Center Code 3632 Newport, Rhode Island 02840	1

TECHNICAL REPORT DISTRIBUTION LIST, 359

<u>No.</u>
<u>Copies</u>

Dr. R. Nowak
Naval Research Laboratory
Code 6130
Washington, D.C.   20375

Dr. John F. Houlihan
Shenango Valley Campus
Penn. State University
Sharon, PA   16146